PLASTIC DESIGN CAPABILITIES
OF HOLLOW STRUCTURAL SECTIONS

PLASTIC DESIGN CAPABILITIES
OF HOLLOW STRUCTURAL SECTIONS

By

JAN HUDOBA, Dipl. Ing.

A Thesis
Submitted to the School of Graduate Studies
in Partial Fulfilment of the Requirements
for the Degree
Master of Engineering

McMaster University

January, 1971

MASTER OF ENGINEERING (1971)
(Civil Engineering)

McMASTER UNIVERSITY
Hamilton, Ontario.

TITLE: Plastic Design Capabilities of Hollow Structural Sections

AUTHOR: Jan Hudoba, Dipl. Ing. (Bratislava)

SUPERVISOR: Dr. R. M. Korol

NUMBER OF PAGES: x, 157

SCOPE AND CONTENTS:

A research programme is presented for assessing the capability of Hollow Structural Sections in Plastic Design. This investigation attempts to relate the flange slenderness and yield stress to the rotation capacity of Hollow Structural Sections subjected to both constant moment regions and to moment gradients.

An experimental programme was performed on 31 different cross sections to evaluate the moment-curvature relationship which is of fundamental importance in Plastic Methods. The occurrence of local buckling for some sections in the compression flange and the consequent reduction in moment resistance is the critical factor which separates members into compact and non compact categories.

The moment-curvature relations from tests are compared with analytical predictions. The plastic hinge rotations delivered by the present test sections are compared with the maximum practical requirements for plastically designed continuous beams. Theoretical elastic and inelastic buckling

solutions of plate elements are also presented to relate to possible local buckling of the flats of square and rectangular hollow structural sections.

Plate ratios of compression flanges are then selected for use in plastic design of hollow structural sections. Such a separation permits segregation into compact and non compact categories and can be used in working stress or elastic design methods.

ACKNOWLEDGEMENTS

I wish to express my deepest gratitude to Dr. R. M. Korol for his advice and patience during the course of this thesis work. Also, I would like to thank Mr. James Cran and Mr. Larry Ife for their time spent in discussions concerning this problem.

This investigation was made possible through the financial assistance of Comite International pour le Developpement et l'etude de la Construction Tubulaire (CIDECT) with direct motivation of the Steel Company of Canada, to whom I extend my sincere thanks.

TABLE OF CONTENTS

LIST OF FIGURES

LIST OF TABLES

CHAPTER 1

INTRODUCTION

The elastic design of steel structures is based on the concept of a specified safety factor against nominal yielding of the most highly stressed fibers. This method is therefore satisfactory provided that the yield stress is reached without premature buckling. This approach is not strictly rational however since virtually all structural members have some residual stress locked in before they are subjected to any external loads. Allowable stress based solely on a yield point criterion does not give a consistent margin of safety against failure. Present-day codes such as CSA Standards S16 attempt in part to take into account properties of the cross-section and continuity of the structure but still fall short of complete consistency.

Plastic design takes advantage of the ductile property of a material of which the structure is made and proposes to base the design on the actual load-carrying capacity of the structure. The working loads are determined as a specified percentage of the ultimate load, which will be realized only if the members undergo plastic deformations at a number of sections without local buckling, producing a consequent fall-off in bending moment resistance. This process is generally referred to as the redistribution of moments and formation of plastic hinges.

Thus two necessary conditions must be satisfied in plastic design

a) redistribution of moments in an indeterminate structure when the plastic moment M_p is reached at the section of the first and subsequent hinges before collapse,

b) maintenance of the resisting moment M_p at a critical section until sufficient additional sections have yielded to produce a "mechanism".

When the plastic moment M_p is reached at the first hinge of an indeterminate structure it is assumed that relative rotation of the segments meeting the hinge can occur until sufficient additional sections have yielded to form a mechanism. This rotation for which the plastic moment is maintained is called the "rotation capacity".

The rotation capacity at a plastic hinge may be reduced by local buckling at a rotation smaller than that required to form a mechanism in the structure. Cross-sections which satisfy the minimum rotation requirements are classified as "<u>Compact Sections for Plastic Design</u>". These sections are capable of developing their computed plastic moments to the minimum rotation requirements without the presence of local buckling.

<u>In structures designed by the allowable stress method the "compact sections"</u> are capable of reaching only the

computed plastic moments without the presence of local buckling. They do not need to satisfy the minimum rotation requirement.

Those which are capable of reaching only the computed yield moment prior to local buckling are termed "Non-Compact".

Reduced stress sections are those which will buckle locally before they reach the computed yield moment M_y which is defined as that moment at which yielding of the outer fibers is initiated.

The initial position of an idealized stress-strain (σ-ε) curve for cold-formed steel in tension or compression is shown in Figure 1.1. For strains below the yield strain, ε_y, the material is elastic, with the slope of the stress-strain curve defined as the elastic modulus, E. As the strain is increased beyond ε_y, the stress again begins to increase with the slope of the curve in this range, E_{st}, the strain-hardening modulus. A strain of ε_y represents the onset of strain-hardening.

In "simple plastic" theory, it is assumed that all elements of a given cross-section in a member subjected to flexure remain elastic up to the attainment of the "plastic moment", M_p, which is the moment corresponding to a stress of $\pm F_y$ in all elements of the section. This state corresponds to $E_{st}/E \to 0$. It is further assumed that, once the plastic moment has been reached, the moment at that cross-section remains constant for all further increases in curvature. This assumed behaviour neglects the additional moment capacity due to the effects of strain-hardening, and assumes that the shape factor M_p/M_y is approximately unity.

Figure 1.2 shows a plot of moment, M, non-dimensionalized as M/M_p, vs curvature for a simple-supported HSS beam. The curvature is equivalent to a ratio of the maximum strain in the outside fibers to half of the depth of the HSS. $K_p = M_p/EI$ is the curvature which would correspond to a moment, M_p, if the beam were to remain completely elastic. The symbol I denotes the moment of inertia about the neutral axis of the beam. The dashed curve represents the behaviour assumed in simple plastic theory. The dot-and-dashed curve includes the penetration of yielding through the cross-section and the effects of strain-hardening. This more exactly predicted curve does not take into account any residual stresses that might exist in HSS. The actual behaviour of a typical beam with residual stresses is shown by the solid curve in the figure. This curve departs from the predicted curve at the proportional limit of yielding and shows the influence of residual stresses of HSS. This feature will be described more fully in Section IV in Figures from 4.1 to 4.31.

In some cases local buckling can occur within the yielded portion of the compression flange and this can precipitate a drop-off in moment capacity. This behaviour is typical of beams subjected to loads producing moment gradients primarily. The "rotation capacity" of the beam is defined as $\Theta = K/K_p - 1$, where K is the rotation at which M drops below M_p. The absolute inelastic hinge rotation, $K-K_p$, of the full span will be denoted by the term "hinge capacity".

Wide-flange beams subjected to moment gradient have been the subject of both analytical and experimental investigations(3,6,7). The present investigation attempts to define the effect of moment gradient and constant moment on the rotation capacity for HSS. An attempt will be made to relate the flange slenderness ratio, b/t, to the hinge capacity of HSS beams.

Because HSS beams subjected to moment gradient are influenced greatly by residual stresses, there is a definite need for more experimental studies in this area.

The ASCE "Comentary on Plastic Design in Steel"(15) assumes for A36 steel beams designed by plastic-design methods that unloading does not occur until the plastic rotation (the total rotation minus the rotation at M_p) is at least three times the hypothetical rotation calculated by an elastic analysis with $M=M_p$. This is equivalent to saying that unloading does not occur until the maximum plastic strain is at least three times the strain calculated by an elastic analysis with $M=M_p$.

The paper by Jombock and Clark(16) was prepared for a report summarizing information on the post buckling strength of flat plates in edge compression which would serve as background material for the preparation of a guide to design criteria for metal compression members. This paper examines the effect of local buckling of square tubes in compression.

In the paper by Thurlimann[17], the aspects concerning inelastic instability of steel structures are presented. For plates, a solution for determining the beginning of strain-hardening has been derived using the theory of orthotropic plates with appropriate moduli developed from theoretical and experimental considerations with respect to the effect of residual stresses.

An investigation into the structural behaviour of stainless steel columns and beams is described by Johnson and Winter[18]. The mechanical properties are discussed including different stress strain curves in tension and compression, the pronounced effect of cold working, and the low proportional limit. An important problem in light gage metal construction is the post buckling behaviour of thin compression elements.

A study at the U.S. Steel Applied Research Laboratory by McDermott[19] was aimed at determining the requirements and capabilities of ASTM A514 steel in plastically designed structures. The curve for A514 steel has a linear elastic portion which is usually followed immediately by an approximately linear strain-hardening portion. For cold-formed steel of HSS, the stress-strain curve has the same shape. In conclusion of this paper regarding the required rotation capacity in plastically designed structures, it was indicated that a value of hinge rotation H=0.5 should be satisfactory for A514 steel beams which are generally designed for uniform loads rather than for concentrated loads and H=1 would presumably be satisfactory for steel columns in building frames and for other steel beam-columns subject to nearly linear variation of moment.* Because the derivations of H are not sensitive to the shape of the material stress-strain curve, these values of H should be applicable to structures of any steel.

Lukey and Adams[6] reported the results of an experimental investigation of the influence of the flange slenderness ratio on the rotation capacity of members subjected to moment gradient. The tests were performed on rolled wide-flange beams, simply supported and subjected to a concentrated load at midspan.

Analytical and experimental investigations, by Smith and Adams[7], have been attempted to define the effect of moment gradient on the rotation capacity and to separate the influence of moment gradient from that of the unbraced slenderness ratio. The tests were performed on simply supported, wide-flange beams subjected to a concentrated load at midspan. The results provide a design recommendation

---

*Hinge rotation $H = K_p.L$ (Figure 2.11).

for the limiting flange slenderness ratio for compact sections used in structures designed by the allowable stress method.

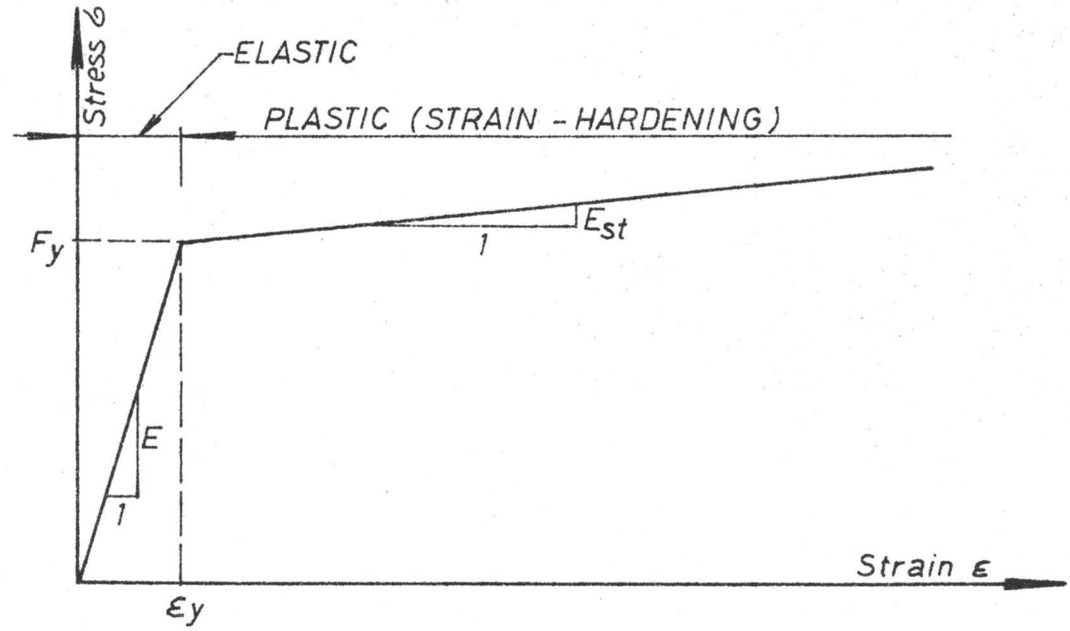

FIGURE 1·1 Stress - Strain Relationship

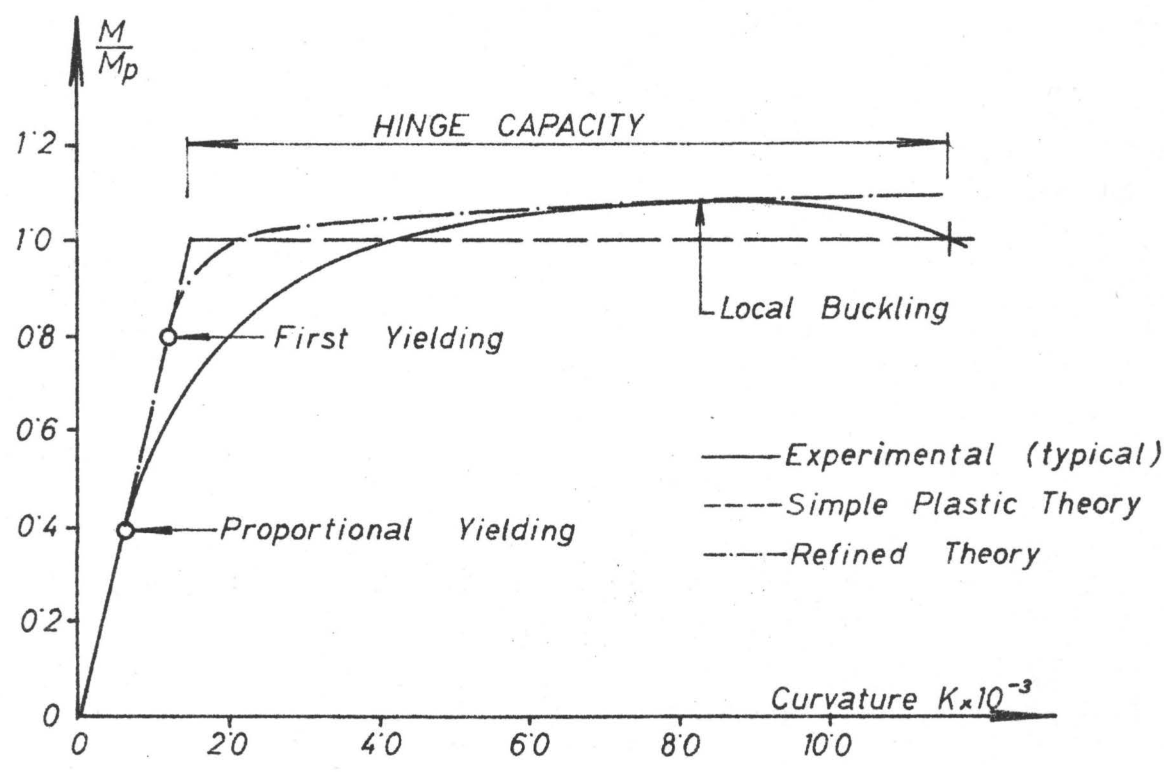

FIGURE 1·2 Moment - Curvature Relationship

CHAPTER II

ANALYTICAL FORMULATION OF BEAM BEHAVIOUR

2.1 Methods of Analysis

A brief outline of the theoretical work associated with HSS beam behaviour follows. Two types of beams are studied: a simple span type and a three span statically indeterminate type.

For the three span beam the distribution of moments shows the formation of plastic hinges. Maximum loads associated with the collapse mechanism are computed which were of value in designing the loading system. Deflections are computed using conventional slope-deflection equations. Permissible hinge rotation is evaluated and a rotation requirement for plastic design is recommended.

A brief review of earlier work in terms of plastic hinge rotation requirements is included. This information is used to complement the limited structural forms that are considered in this work.

For the case of the simple span, the calculated expression for deflection is used in a computer programme to predict the load-deflection behaviour. This information is later compared with test results in Chapter 4.

2.11 Elastic Analysis

The elastic moments were calculated for a designed loading condition for a simply-supported beam in Figure 2.1 and three span beam in Figure 2.2a. The total load on the beam was P[kips] to simulate 2-point loading on a beam. For the three span beam, the negative moments at the interior supports were computed to have the value equal to 9.73 P[inch-kips] and the positive moments equal to 5.28 P[inch-kips]. The elastic distribution of moments shows the formation of the first plastic hinges at the interior supports.

2.12 Plastic Analysis

The work described herein is divided into 5 parts. The first pertains to the conventional plastic analysis to evaluate the collapse load. The second is associated with deflections at critical points which can become important for some structures. Thirdly, the hinge rotation requirement is computed for the beam described in Figure 2.2a. The fourth recommends the required rotation capacity of plastically designed structures from analytical studies which are performed in this part.

The last part pertains to the comparison of measured and predicted curvature at the interior support.

(A) Calculation of Maximum Loads

These have been calculated on the assumption that mechanisms will develop at collapse. Figure 2.2(c,d) shows the bending moment distribution at collapse and the collapse mechanism for the three span beam. For the type of loading shown, the computed ultimate load $P_u = M_p/7.5$[kips], where M_p is in kips-inch.

(B) Calculation of Deflection

This part presents a method for computing the predicted deflections of a simple beam and the three span beam. These computed values are compared to test results in Chapter 4. For the simple span, the deflections were calculated by assuming the nondimensional moment-curvature relationship in the computer program for the determination of the shape of load-deflection curve. For the three span beam, the idealized moment-curvature relation is assumed and the shape of the load-deflection curve is determined by the two points of deflection, at yield load and at ultimate load.

(a) Simple Beam Case

By assuming that the plastic hinge occurs at midspan, the conventional slope deflection equations are used to determine midspan deflection just at ultimate load.

The following form of the slope deflection equations will be used, the nomenclature being as shown in Figure 2.3a with clockwise moment and angle change being positive

$$\phi_{AB} = \phi_{AB}{}^{F} + \frac{\delta}{\ell} + \frac{\ell}{3EI}\,(M_{AB} - \frac{M_{BA}}{2}) \ .$$

The quantity $\phi_{AB}{}^{F}$ is the slope at end A due to a similar loading of a simply-supported beam.

The equation for member 2-1 in Figure 2.3b is

$$\phi_{21} = \phi_{21}{}^{F} + \frac{\delta}{\ell} + \frac{\ell}{3EI}\,(M_{21} - \frac{M_{12}}{2}) \ .$$

Now

$$\phi_{21}{}^{F} = -\frac{1}{6}\,\frac{(\frac{P}{2})}{EI}\,(2b\ell + \frac{b^3}{\ell} - 3b^2) \qquad \text{(From Reference 10, pp. 102).}$$

When $M_p = (\frac{P}{2})a$ the expression of $\phi_{21}{}^{F}$ is then given by

$$\phi_{21}{}^{F} = -\frac{M_p}{6EI}\,\frac{1}{a}(2b\ell + \frac{b^3}{\ell} - 3b^2) \ .$$

Substituting this expression of $\phi_{21}{}^{F}$ and using the condition that $\phi_{21} = 0$, the solution can be expressed as follows

$$\phi_{21} = -\frac{M_p}{6EI}\,\frac{1}{a}(2b\ell + \frac{b^3}{\ell} - 3b^2) + \frac{\delta}{\ell} + \frac{\ell}{3EI}(-M_p) = 0$$

$$\delta = \frac{M_p}{EI}[\frac{\ell^2}{3} + \frac{\ell}{6a}(2b\ell + \frac{b^3}{\ell} - 3b^2)] = \frac{M_p}{EI}[\frac{a^2}{3} + ab + \frac{b^2}{2}] \ .$$

Using this expression and assuming the nondimensional moment-curvature relationship, the deflection can be expressed at any step in loading. This is done in the computer program in

Appendix 1.

For the beam of the dimensions a=30" and b=38"

$$\delta = \frac{2160\ M_p}{EI}\ .$$

(b) Three Span Beam Case

It is shown in Figure 2.2 that the first hinge is at 1. The nomenclature of the slope-deflection equations is as shown in Figure 2.3a with clockwise moment and angle change. The expression below takes this into account and for member 2-1 in Figure 2-4

$$\phi_{21} = -\ \phi_{21}{}^{F} + \frac{1}{2}\phi_{12}{}^{F} + \frac{\delta_u}{\ell} + \frac{\ell}{3EI}(M_{21} - \frac{1}{2}M_{12})\ .$$

Using the condition that $\phi_{21}=0$, the solution can be expressed as follows

$$0 = -\ \frac{M_p}{6EI}\ \frac{1}{a}(2b\ell + \frac{b^3}{\ell} - 3b^2) - \frac{1}{2a}\ \frac{M_p}{6EI}(b\ell - \frac{b^3}{\ell}) + \frac{\delta_u}{\ell} + \frac{\ell}{3EI}(-M_p + \frac{M_p}{2})$$

$$\delta_u = \frac{M_p}{EI}[\frac{\ell^2}{6} + \frac{\ell}{6a}(2.5b\ell + \frac{b^3}{2\ell} - 3b^2)]\ .$$

To give quantitative values to the above dimensions as chosen which are representative of tests described in Figure 2.2

$$\delta_u = 1724\ \frac{M_p}{EI}\ .$$

<u>Load-Deflection Curve for Three Span Beam</u>

Above the yield load, P_y, the slope of the load-deflection curve is the same as that of a simple beam (Figure 2.5). For deflection purposes the approximation can be used that at point 1 $M_y \approx M_p$.

For the type of loading shown in Figure 2.2

$$\delta_{AB} = \frac{2160\ M_p}{EI} \left(\frac{\Delta P}{P_y{}'}\right)$$

where $P_y{}' \approx P_y$ with the approximation that $M_y \approx M_p$.

The quantity ΔP may be obtained as

$$\Delta P = P_u - P_y' = (4-3.08)\ \frac{M_p}{\ell} = 0.92\ \frac{M_p}{\ell}\ .$$

Thus

$$\delta_{AB} = 2160\ \frac{M_p}{EI}\left(\frac{0.92}{3.08}\right) = 645\ \frac{M_p}{EI}\ ;$$

$$\delta_y' = \delta_u - \delta_{AB} = (1724-645)\frac{M_p}{EI} = 1079\ \frac{M_p}{EI}$$

and the corresponding approximate yield load

$$P_y' = \frac{P_u - \Delta P}{P_u}\ P_u = \frac{3.08}{4}\ P_u = 0.77\ P_u\ .$$

It is of interest to see whether or not the method given herein will predict actual load-deflection relationship with a sufficient degree of accuracy. Although the agreement between the theory based on idealized behaviour and the tests is by no means exact, it is considered adequate in view of the fact that the effect of residual stresses, stress-concentrations, and the gradual plastification of the cross-section have been neglected in the theory.

(C) Calculation of Permissible Hinge Rotation

The rotation capacity characterizes the ability of a member to absorb rotations of near-maximum plastic moment. This capability is necessary for redistribution of moment in the continuous beam. The transfer of moment to point 2 is only possible if the plastic moment is maintained at the first hinge to form at 1 while hinge 2 is developing in the beam.

Local buckling may limit the rotation capacity of a section in which case the beam would be classified as non-compact. Only compact sections are those in which no such loss in moment resisting capacity results during build-up of moments at other sections.

The rotation capacity requirement is a function of the applied loading and the geometry. The plastic hinges at the supports will require a considerable amount of rotation -- enough to allow the load to increase. The hinge that will form at the center span of the beam requires no rotation capacity requirement since that hinge is the last to develop in forming a mechanism.

The maximum rotation requirement for the three span beam loaded as shown in Figure 2.2 is obtained from the angle change $\phi_{12}-\phi_{10}$ at support 1.

The hinge angle H, will be equal to the change in slope at that section as shown in Figure 2.4.

The slope-deflection equation for member 1-2 in Figure 2.4 is

$$\phi_{12} = -\phi_{12}^{F} + \frac{1}{2}\phi_{21}^{F} + \frac{\delta_u}{\ell} + \frac{\ell}{3EI}(M_{12}-\frac{1}{2}M_{21})$$

$$= \frac{M_p}{6EI}\,\frac{1}{a}[(b\ell-\frac{b^3}{\ell})+\frac{1}{2}(2b\ell+\frac{b^3}{\ell}-3b^2)] + \frac{\delta_u}{\ell} + \frac{\ell}{3EI}(-M_p+\frac{M_p}{2})$$

$$\phi_{12} = \frac{\delta_u}{\ell} - \frac{M_p\,\ell}{6EI} + \frac{M_p}{6EI}\,\frac{1}{a}(2b\ell-\frac{b^3}{2\ell}-\frac{3}{2}b^2) \ .$$

The quantity δ_u is known

$$\delta_u = \frac{M_p}{EI}[\frac{\ell^2}{6} + \frac{\ell}{6a}(2.5b\ell+\frac{b^3}{2\ell}-3b^2)] \ .$$

Therefore,

$$\phi_{12} = \frac{3}{4}\,\frac{M_p\,b}{EI} \ .$$

The angle change $\phi_{10} = \frac{M_p\,c}{3EI}$ and the hinge angle

$$H_1 = \phi_{12}-\phi_{10} = \frac{(.75b-.33c)M_p}{EI} \ .$$

For the three span beam loaded as shown in Figure 2.2

$$H_1 = 14.5\,\frac{M_p}{EI} \ .$$

This equation may be nondimensionalized by dividing both sides by $K_p\ell$, giving

$$\frac{H_1}{K_p\ell} = .213 \ .$$

This cannot be compared with the criterion that the section can be capable of rotating to the rotation capacity requirement, because all of the rotation occured at a point. The yield zone is distributed along the beam with strains varying all the way from the elastic limit and further beyond this limit into the plastic region. An approximate comparison may be made by computing the average unit rotation K_A, on the basis that the total rotation is divided by the hinge length -- the length along the beam in which the moment is greater than the yield moment.

Computation of the Hinge Length for H.S.S.

The hinge length for a simple supported beam (Figure 2.6) applied to a solid rectangular cross-section is L/3, where L is the beam length. This length results from the shape factor being 1.5. For a wide-flange beam possessing a shape factor of 1.14 the hinge length is $\frac{1.14-1}{1.14}L = 0.12L$.

For HSS the average shape factor is about 1.25 and thus $M_y=0.8\ M_p$. It follows then that the hinge length becomes 0.20 L.

For the 3 span beam of Figure 2.2 the hinge length must be computed in the neighbourhood of the interior support. Since the moment changes are so rapid the value employed for a simple supported beam is not applicable. Figure 2.7 shows that the hinge length is 0.2c+0.1a at incipient collapse.

Thus $\qquad \Delta L = 0.2c+0.1a = 11.4$ inches .

The average rotation

$$K_A = \frac{H_1}{\Delta L} = 1.27\ \frac{M_p}{EI}$$

or

$$\frac{K_A}{K_p} = 1.27\ .$$

The yield zone must absorb a subsequent average rotation that is 1.27 times the value at the elastic limit for this loading and this geometry.

(D) Recommended Rotation Requirement in Plastic Design

In order to determine whether the delivered hinge capacity of a given member is adequate, it is first necessary to know the hinge capacity required to form a mechanism in a particular structural situation. Analytical studies have been performed to determine maximum plastic rotation requirements for practical structures.

Kerfoot(12) has analyzed the symmetrical 3-span beam subjected to point loadings shown in Figure 2.10. The length ratio, α, and the load ratio, β, were varied in this study to provide a range of situations in which plastic hinge rotations were required both in regions of constant moment and of moment gradient. This study indicated that, only for very extreme values of α and β would the required hinge capacity at any point exceed K_pL, where $K_p = M_p/EI$ and L is shown in Figure 2.10.

Driscoll(13) has presented the symmetrical 3-span beam subjected to distributed load. Figure 2.11 presents some of the limiting values of H/K_pL obtained as a result of that study. The largest required plastic hinge rotation is $0.425\ K_pL$ for this structure.

An analysis of frames[12] has indicated that the largest required plastic hinge rotation for a single span rigid frame such as that shown in Figure 2.12a is $0.475\ K_pL$ when $a=0.2$ and the value of C is in range $0 < C < 1.0$. For a gable frame in Figure 2.12b, this rotation is $1.05\ K_pL$ in the rafter for $0 < C < 0.5$. In more complex structures the theoretical hinge angle required to form a mechanism may be rather large[13]. However, it has been shown that, for such structures, a load close to the ultimate can be attained with much smaller hinge rotations. This is illustrated in Figure 2.13, taken from Reference (15). The load, P, non-dimensionalized as P/P_u, is plotted against the plastic rotation, Θ_H, of the first hinge to form, represented non-dimensionally as $\Theta_H\ EI/M_pL$. The structure considered is the two-span portal frame shown in the inset. The hinge angle at formation of a mechanism is $1.52\ M_pL/EI$, but 98% of the ultimate load is reached at a rotation of $0.54\ M_pL/EI$. Since the attainment of 98% of the calculated ultimate load would be considered satisfactory for design purposes, it is concluded that practical rotation capacity requirements need not be related to the large theoretical rotations encountered in highly redundant frames[15].

These analyses can be used to estimate the required rotation capacity of plastically designed structures. The recommended value of 4 for plastic rotation requirement in plastic design would be considered satisfactory to form a mechanism.

(E) Comparison of Measured and Predicted Curvature

A comparison of measured curvature K at the support ① agrees with the average K_A over the hinge length and with the value of $\Theta=4$ as proposed is shown in Figure 2.9 for cold formed HSS-6.x4.x.437 of test No. 12. The assumptions for test comparisons are shown in Figure 2.8 and the explanation of this is given below.

Curve ⓐ of Figure 2.9 does not take into account the influence of residual stresses for reaching M_p at the last formed hinge. The curvature $K_p=920\times10^{-6}$ in^{-1} at point ② of Figure 2.7 assumes the predicted M-K relation (simple plastic theory) and the corresponding measured curvature K at point ① has a value about 2200×10^{-6} in^{-1} which is 2.4 times of K_p. The change of curvature over the hinge length is shown by the dot-and-dashed curve in Figure 2.9.

A more realistic curve for comparison is the one labelled ⓑ which takes into account the influence of residual stresses. With the curvature $\overline{K}_p=1100\times10^{-6}$ in^{-1} at ② M_p calculated by the simple plastic theiry is reached. The corresponding measured curvature K at point ① reaches a value about 3500×10^{-6} in^{-1} which is 3.8 times K_p.

In Figure 2.9 this curve is shown by the full line.

The standard calculation omitting residual stresses is computed in Section 2.12(C) by the average rotation method and the recommended rotation requirement in plastic design is also shown in Figure 2.9 as lines ⓓ.

This example shows that the actual curvature at a support is about twice that of the average curvature over the hinge length. The higher peak of curvature is due to residual stresses in the HSS since these stresses flatten the M-K relation earlier than anticipated. The plastic moment M_p at point ②, the last hinge to form is reached with this higher curvature than in the section free of residual stresses.

2.2 Instability of Fully Plastic Square or Rectangular Beams

Failure due to plastic instability is considerably more likely when the average strains are in the strain-hardening range since the buckling stress is a function of the tangent modulus.

The performance of such a beam can be illustrated by a load-deflection curve or by a moment-curvature relationship such as in Figures 2.14 and 2.15. Both of these curves are typical of properly behaved beams in terms of plastic design.

The plastic moment M_p is reached and maintained through a considerable deformation. The moment M_p is maintained by the beam for an average plastic rotation of about 4 times K_p before the plastic hinge behaviour is terminated by unloading. The cause of unloading in this beam was due to the formation of a local buckle in the compression flange. The mechanism of failure so described is typical of HSS beams with a high plate ratio of compression flange.

2.21 Description of Behaviour Related to M-K Relationship

The behaviour of a typical rectangular HSS beam in the plane of bending is shown in Figure 2.14 where the moment M is plotted against the curvature at the center of the beam. A standard test description follows.

At first the response of the beam was elastic, as can be seen by the linear M-K relationship. Elastic behaviour was terminated when the sum of the bending stress and the residual stress first reached the yield stress. If no residual stress were present in the beam linearity would have been extended to M_y, the yield moment. As more and more of the material in the constant moment region yields, the resistance of the beam to further load increases was reduced, so that finally no additional load could be carried. This load occurredwhen the tangent to the M-K curve became horizontal at a moment equal to M_{max}, slightly larger than the plastic moment. The curvature corresponding to this ultimate load is a few times larger than the curvature at initial yielding.

As soon as M_{max} was attained, local buckling of the compression flange was initiated. During this deformation the initial shape of the cross-section was distorted as shown in the photograph in Fig. 4.38. Unloading became significant when local buckling in the most strained compression flange was clearly observed.

The photograph in Fig. 4.38 shows the final deformed shapes and local buckles in the compression flanges of a number of beams.

The test just described represents a fairly typical beam history. A number of other possibilities will be described below.

2.22 Possible Load-Deformation Curves

Some idealized load-deflection curves are shown in Figure 2.15.

The solid curve OAB corresponds to the case of a compact section where no local buckling occurs. This is an ideal condition seldom reached with compact sections. The situation described above for the test beam is given by curve OAC. Load-deflection curves are often idealized by the elastic portion OAD and a plastic hinge region DB.

Curves OAEF and OAGH represent situations in which local buckling influences are more significant and occur after some portions of the beam have yielded. To classify a section as compact sufficient deformation must be attained at a load greater than or equal to that causing M_p. When the load decreases below that value the section is carrying a moment less than M_p. Thus, the curve OAEF may represent a section which is compact or non-compact depending on the rotation criteria specified to transfer moment for the formation of another plastic hinge. The curve OAGH is the typical load-deflection curve of a non-compact section and the curve OIJ is typical of local elastic buckling. In Figure 2.15 we have shown the best possible performance of beams (curve OAB) and we also have shown how actual beams fall short of this ideal.

2.3 Elastic and Inelastic Buckling of Plate Elements

2.31 Beam Behaviour

Three major ranges of beam behaviour are shown schematically in Figure 2.16:

i) the range in which full plastification is possible,

ii) the range in which the resistance to buckling is impaired by partial yielding and

iii) the range in which the capacity is controlled by elastic buckling.

The three ranges of moment capacity for HSS are dependent on the plate slenderness, which controls local buckling.

In the first range, local instability of the fully plastified section limits the deformability but permits attainment of the full plastic moment. Beams suitable for use in plastic design are therefore selected from this category. In the other ranges neither full moment capacity nor adequate deformability exists, and those members can only be used in allowable stress design.

The important fact for design are the relationships between the moment capacity and the geometry of the section. These relationships are entirely a function of instability and they cover the geometric requirements for behaviour which are needed for plastic design. Thus, the problem is to find for compact sections the maximum permissible ratio b/t of plate elements of the compression flange.

2.32 Local Buckling of Plate Element of Beam

The fundamental differential equation expressing equilibrium of a plate under the action of forces in its median plane is[2]

$$\frac{EI}{(1-\nu^2)}\left(\frac{\partial^4 w}{\partial x^4} + 2\frac{\partial^4 w}{\partial x^2 \partial y^2} + \frac{\partial^4 w}{\partial y^4}\right) + t\left(\sigma_x \frac{\partial^2 w}{\partial x^2} + \sigma_y \frac{\partial^2 w}{\partial y^2} + 2\upsilon_{xy}\frac{\partial^2 w}{\partial x\, \partial y}\right) = 0 \qquad (1)$$

where w is the transverse deflection

σ_x and σ_y are the normal stresses

υ_{xy} is the shear stress

t is the thickness of the plate

ν is Poisson's ratio, assumed 0.3

and $I = t^3/12$ is the moment of inertia .

If only a uniformly distributed compressive stress σ_x exists and σ_y and υ_{xy} vanish then eq. (1) assumes the simplified homogeneous form

$$\frac{EI}{(1-\nu^2)} \left(\frac{\partial^4 w}{\partial x^4} + 2 \frac{\partial^4 w}{\partial x^2 \partial y^2} + \frac{\partial^4 w}{\partial y^4}\right) + \sigma_x t \frac{\partial^2 w}{\partial x^2} = 0 . \qquad (2)$$

This equation is valid only within the range of Hooke's law and has to be revised when σ_x exceeds the proportional limit. Beyond this point the effective tangent-modulus E_{st} is assumed to apply in the x-direction while in the y-direction Young's modulus E remains valid. We thus assume anisotropic behaviour of the plate when the critical stress σ_c lies above the elastic limit.

Let $\tau = E_{st}/E$ and the factor $E\tau$ must be substituted for E when σ_c exceeds the proportional limit.

Thus equation (2) becomes

$$\frac{EI}{1-\nu^2}\left(\tau \frac{\partial^4 w}{\partial x^4} + 2\sqrt{\tau} \frac{\partial^4 w}{\partial x^2 \partial y^2} + \frac{\partial^4 w}{\partial y^4}\right) + \sigma_x t \frac{\partial^2 w}{\partial x^2} = 0 . \qquad (3)$$

The appropriate expressions for the moments are

$$M_x = - \frac{EI}{1-\nu^2}\left(\tau \frac{\partial^2 w}{\partial x^2} + \nu\sqrt{\tau} \frac{\partial^2 w}{\partial y^2}\right)$$

$$(4)$$

$$M_y = - \frac{EI}{1-\nu^2}\left(\nu\sqrt{\tau} \frac{\partial^2 w}{\partial x^2} + \frac{\partial^2 w}{\partial y^2}\right) .*$$

---

* M_y in this section only relates to the y-axis as shown in Fig. 2.17 to avoid confusion with the yield moment.

General Solution of the Differential Equation

The solution of the partial differential equation (3) must satisfy the boundary conditions on all four edges.

Now we will consider initially only B.C. on the loaded edges. The condition of simple support on the loaded edges is assumed and requires

$$w = 0$$

$$M_x = -\frac{EI}{1-\nu^2}\left(\tau \frac{\partial^2 w}{\partial x^2} + \nu\sqrt{\tau}\,\frac{\partial^2 w}{\partial y^2}\right) = 0 \ .$$

The former condition necessitates that $\partial^2 w/\partial y^2$ must be zero, and the boundary conditions become

$$w = 0 \qquad \text{and} \qquad \frac{\partial^2 w}{\partial x^2} = 0 \ . \tag{5}$$

The differential equation (3) and the boundary condition (5) are satisfied by the expression

$$w = Y \sin\frac{n\pi x}{a} \qquad (n = 1,\ 2,\ 3\ \ldots)$$

where Y is a function of y to be determined.

Upon introducing this expression into the differential equation (3) and concelling $\sin\frac{n\pi x}{a}$ we obtain the ordinary differential of the fourth order

$$\frac{d^4Y}{dy^4} - 2\sqrt{\tau}\left(\frac{n\pi}{a}\right)^2\frac{d^2Y}{dy^2} + \left[\tau\left(\frac{n\pi}{a}\right)^4 - \frac{\sigma_c t}{D}\left(\frac{n\pi}{a}\right)^2\right]Y = 0 \tag{6}$$

where σ_x is replaced by σ_c, the unknown critical longitudinal stress at which the plate buckles and

$$D = \frac{EI}{1-\nu^2} .$$

Introducing the dimensionless parameter

$$\mu^2 = \frac{\sigma_c t}{D\tau} \left(\frac{a}{n\pi}\right)^2 \tag{7}$$

the differential equation (6) assumes the form

$$\frac{d^4Y}{dy^4} - 2\sqrt{\tau}\left(\frac{n\pi}{a}\right)^2 \frac{d^2Y}{dy^2} + \tau\left(\frac{n\pi}{a}\right)^4(1-\mu^2)Y = 0 . \tag{8}$$

The solution of this differential equation together with the boundary conditions determines the parameter μ which by (7) leads to the formula for the critical stress

$$\sigma_c = \left(\frac{n\pi}{a}\right)^2 \frac{D\tau}{t} \mu^2 . \tag{8a}$$

The general solution of equation (8) is

$$Y = C_1 \cosh k_1 y + C_2 \sinh k_1 y + C_3 \cos k_2 y + C_4 \sin k_2 y$$

where k_1 and k_2 are defined by

$$k_1 = \frac{n\pi}{a} \sqrt[4]{\tau} \sqrt{\mu+1} \text{ and } k_2 = \frac{n\pi}{a} \sqrt[4]{\tau} \sqrt{\mu-1} . \tag{8b}$$

The general solution of equation (3) is

$$w = \sin \frac{n\pi x}{a}(C_1 \cosh k_1 y + C_2 \sinh k_1 y + C_3 \cos k_2 y + C_4 \sin k_2 y) . \tag{9}$$

The constants C_1 to C_4 are to be determined such that the boundary conditions at all edges will be satisfied. The physical features pertinent to the above mathematical formulation are shown in Figure 2.17.

If we assume equal elastic restraint by both web support edges, the deflection w corresponding to the smallest value of σ_c is a symmetric function of y, and the terms $C_2 \sinh k_1 y$ and $C_4 \sin k_2 y$ in equation (9) vanish.

Thus equation (9) simplifies to

$$w = \sin \frac{n\pi x}{a}(C_1 \cosh k_1 y + C_3 \cos k_2 y) \quad . \tag{10}$$

To determine the constants C_1 and C_3 we invoke the boundary conditions at the unloaded edges

$$\begin{aligned} [w]_{y=\pm\frac{b}{2}} &= 0 \\ \psi &= \overline{\psi} \;. \end{aligned} \tag{11}$$

The first condition expresses the assumption that the edges $y=\pm\frac{b}{2}$ remain straight when the plate buckles. The second one is a condition of continuity which indicates that the angle of rotation ψ at the edge of the buckling plate is equal to the angle of rotation $\overline{\psi}$ of the restraining web plate which is rigidly connected.

Now ψ and $\overline{\psi}$ must be expressed in terms of the deflection w. The bending moment M_y per unit length is proportional to the angle $\overline{\psi}$.

This elastic restraining condition can be expressed by

$$M_y = -\,\overline{\xi}\,\overline{\psi} \tag{12}$$

where $\overline{\xi}$ is a factor depending upon the dimensions of the restraining plates, assumed constant along the edge.

From equations (4) we have

$$M_y = -D\left[\frac{\partial^2 w}{\partial y^2} + \nu\sqrt{\tau}\,\frac{\partial^2 w}{\partial x^2}\right]_{y=\pm\frac{b}{2}} .$$

Since $\frac{\partial^2 w}{\partial x^2} = 0$ this equation reduces to

$$M_y = -D\left[\frac{\partial^2 w}{\partial y^2}\right]_{y=\pm\frac{b}{2}} . \tag{13}$$

Substituting into equation (12)

$$\overline{\psi} = \frac{D}{\overline{\xi}}\left[\frac{\partial^2 w}{\partial y^2}\right]_{y=\pm\frac{b}{2}} .$$

But $$\psi = \pm\left[\frac{\partial w}{\partial y}\right]_{y=\pm\frac{b}{2}} .$$

Therefore the second boundary condition (11) takes the form

$$\left[\frac{\partial w}{\partial y} \pm \frac{D}{\overline{\xi}}\,\frac{\partial^2 w}{\partial y^2}\right]_{y=\pm\frac{b}{2}} = 0 .$$

It is convenient to introduce ξ a dimensionless number defined by

$$\xi = \frac{2}{b}\frac{D}{\bar{\xi}} . \tag{13a}$$

Thus
$$\left[\frac{\partial w}{\partial y} \pm \frac{b}{2}\,\xi\,\frac{\partial^2 w}{\partial y^2}\right]_{y=\pm\frac{b}{2}} = 0 . \tag{14}$$

The parameter ξ is a function of the dimensions of the buckling and restraining plates and can be referred to as the coefficient of restraint. Theoretically ξ can assume values from 0 to ∞. When $\xi=0$ the plate is completely fixed at the edges a, and when $\xi=\infty$, it is free to rotate about these edges. In the case of hollow structural sections this coefficient can be determined from the properties of the section and lies between the extreme values $\xi=0$ and $\xi=\infty$.

Introducing the general form (10) into the boundary conditions (11) and (14) yields two equations

$$C_1 \cosh k_1 \frac{b}{2} + C_3 \cos k_2 \frac{b}{2} = 0$$

$$(C_1 k_1 \sinh k_1 \frac{b}{2} - C_3 k_2 \sin k_2 \frac{b}{2}) + \xi\,\frac{b}{2}(C_1 k_1^2 \cosh k_1 \frac{b}{2} - C_3 k_2^2 \cos k_2 \frac{b}{2}) = 0.$$

Nonzero values, of these homogeneous linear equations, for C_1 and C_3 result only when the determinant $\Delta=0$. This gives rise to the stability condition which leads to the solution for the critical stress, i.e.

$$k_1 \tanh k_1 \frac{b}{2} + k_2 \tan k_2 \frac{b}{2} + \xi\,\frac{b}{2}(k_1^2+k_2^2) = 0 . \tag{14a}$$

To normalize equation (14a) it is convenient to introduce the ratio $\beta=\frac{a}{b}$ into equations (8a) and (8b) to give

$$\sigma_c = \frac{1}{b^2} \left(\frac{n\pi}{\beta}\right) \frac{D\tau}{t} \mu^2 \tag{15}$$

$$k_1 \frac{b}{2} = \frac{n\pi}{2\beta} \sqrt[4]{\tau} \sqrt{\mu+1}$$

$$k_2 \frac{b}{2} = \frac{n\pi}{2\alpha} \sqrt[4]{\tau} \sqrt{\mu-1} \qquad .(16)$$

Consequently, the stability condition (14a) becomes

$$\sqrt{\mu+1} \tanh\left(\frac{\pi}{2} \sqrt{\mu+1} \frac{n\sqrt[4]{\tau}}{\beta}\right) + \sqrt{\mu-1} \tan\left(\frac{\pi}{2} \sqrt{\mu-1} \frac{n\sqrt[4]{\tau}}{\beta}\right)$$

$$+ \pi \xi \mu \frac{n\sqrt[4]{\tau}}{\beta} = 0 \ . \tag{17}$$

This equation defines the relation between the parameter μ and the ratio $n\sqrt[4]{\tau}/\beta$.

Introducing $\xi=\infty$ into (17) we obtain the stability condition for a plate simply supported along its edges. The hyperbolic function assumes values only between +1 and -1 and can simply be added to the absolute term.

Thus $$\tan\left(\frac{\pi}{2} \sqrt{\mu-1} \frac{n\sqrt[4]{\tau}}{\beta}\right) = -\infty \ .$$

The smallest root satisfying this equation is

$$\frac{\pi}{2} \sqrt{\mu-1} \frac{n\sqrt[4]{\tau}}{\beta} = \frac{\pi}{2}$$

and $$\mu^2 = [(\frac{\beta}{n\sqrt[4]{\tau}})^2 + 1]^2 . \qquad (17b)$$

Substituting μ^2 and $D = \frac{Et^3}{12(1-\nu^2)}$ into (15) we get

$$\sigma_c = \frac{\pi^2 E\sqrt{\tau}}{12(1-\nu^2)} (\frac{t}{b})^2 (\frac{\beta}{n\sqrt[4]{\tau}} + \frac{n\sqrt[4]{\tau}}{\beta})^2 . \qquad (18)$$

The only unknown in equation (18) remaining to be found is n, which indicates the number of half waves in which the plate buckles in the x-direction. To find this number of half waves for a given aspect ratio α we proceed as follows: For sufficiently short plates, i.e., for small values of α, buckling will occur in one half wave. Above a certain ratio α two half waves will be formed. For the limiting ratio at which there is the transition from one state of equilibrium to the other, i.e., when both cases are equally possible at the same buckling stress σ_c, equation (18) will yield the same value of σ_c whether we introduce n=1 or n=2. In the same way it will be possible to determine the limiting value of β for buckling in two or three half waves. Thus we can find the limiting ratio $\overline{\beta}$ at which either n or n+1 half waves can occur from the equation

$$\frac{\overline{\beta}}{n\sqrt[4]{\tau}} + \frac{n\sqrt[4]{\tau}}{\overline{\beta}} = \frac{\overline{\beta}}{(n+1)\sqrt[4]{\tau}} + \frac{(n+1)\sqrt[4]{\tau}}{\overline{\beta}} .$$

It follows that $$\overline{\beta} = \sqrt[4]{\tau}\sqrt{n(n+1)} .$$

For n = 1, 2, 3, ... we have $\bar{\beta}/\sqrt[4]{\tau} = \sqrt{2}, \sqrt{6}, \sqrt{12}, \ldots$.

In the elastic range when $\tau=1$, the number of half waves becomes independent of the nature of the material and the buckling occurs in one half wave up to $\beta = \frac{a}{b} = 1.414$ and from $\beta = 1.414$ to $\beta = 2.449$ in two half waves. For long plates the length of the half waves approaches the width b. If $\tau=1$, equation (18) takes the form

$$\sigma_c = \frac{\pi^2 E}{12(1-\nu^2)} \left(\frac{t}{b}\right)^2 \left(\frac{\beta}{n} + \frac{n}{\beta}\right)^2 = \frac{\pi^2 E}{12(1-\nu^2)} \left(\frac{t}{b}\right)^2 k \qquad (18a)$$

where k is defined as the variable part of σ_c in (18a) and is plotted as a function of β in Figure 2.18.

Returning now to the general buckling condition (17) for elastically restrained plates, we find that the transcendental form in which μ depends upon $\beta/n\sqrt[4]{\tau}$ is inconvenient for applications. In the case of the simply supported plate just considered we have found an algebraic expression (17b) for μ^2, namely,

$$\mu^2 = 1 + 2\left(\frac{\beta}{n\sqrt[4]{\tau}}\right)^2 + \left(\frac{\beta}{n\sqrt[4]{\tau}}\right)^4 .$$

It is possible to express the relationship between μ^2 and $\beta/n\sqrt[4]{\tau}$ defined by equation (17) approximately by a similar algebraic expression. With an error of less than 1%, the values μ^2 can be computed for different restrain conditions employing

$$\mu^2 = 1 + p\left(\frac{\beta}{n\sqrt[4]{\tau}}\right)^2 + q\left(\frac{\beta}{n\sqrt[4]{\tau}}\right)^4 \qquad (19)$$

where p and q are factors depending on the coefficient of restraint ξ.

The factors p and q were computed for various values of ξ from the exact stability condition (17). Figure 2.19 shows p and q plotted against ξ.

Substituting the expression (19) into equation (15) and introducing $D = Et^3/12(1-\nu^2)$ and $a = \beta b$ is obtained

$$\sigma_c = \frac{\pi^2 E\sqrt{\tau}}{12(1-\nu^2)} \left(\frac{t}{b}\right)^2 \left[\left(\frac{n\sqrt[4]{\tau}}{\beta}\right)^2 + p + q\left(\frac{\beta}{n\sqrt[4]{\tau}}\right)^2\right] . \qquad (20)$$

This equation for σ_c is valid for all possible values of elastic restraint.

Introducing the notation

$$k = \left(\frac{n\sqrt[4]{\tau}}{\beta}\right) + p + q\left(\frac{\beta}{n\sqrt[4]{\tau}}\right)^2 \qquad (21)$$

the equation (20) assumes the form

$$\sigma_c = \frac{\pi^2 E\sqrt{\tau}}{12(1-\nu^2)} \left(\frac{t}{b}\right)^2 k . \qquad (22)$$

The value β_0 for which σ_c reaches a minimum and upon which the design of long plates can be based is found from condition $\frac{\partial\sigma_c}{\partial\beta} = 0$, namely

$$\beta_0 = n\sqrt[4]{\frac{\tau}{q}} .$$

Substituting β_0 in equation (20) we get

$$\text{Min } \sigma_c = \frac{\pi^2 E \sqrt{\tau}}{12(1-\nu^2)} \left(\frac{t}{b}\right)^2 (p+2q) = \frac{\pi^2 E \sqrt{\tau}}{12(1-\nu^2)} \left(\frac{t}{b}\right)^2 k \qquad (23)$$

an expression independent of n. The plate coefficient

$$k = p + 2\sqrt{q} \qquad (24)$$

becomes independent of τ. This is important since it permits the use of precalculated values for the coefficient k which are applicable in the elastic and inelastic ranges of buckling.

The limiting cases on the unloaded edges are shown in Figure 2.20. Note that the clamped edge case predicts critical stresses 1.74 times the simply supported regardless of the tangent modulus value.

Determination of the Coefficient of Restraint

When the cross-section distorts, it is assumed that the webs remain vertical up to a certain height. It is assumed in this analyses that the webs, between the compressive flange and the neutral axis, are acted upon on both unloaded edges with one edge simply supported and the other fixed. Thus the half wavelength c is assumed for webs to have a value of 0.4 d as indicated in Figure 2.21. Each of the restraining webs of width c is acted on edges by moments M_y per unit length. It can be inferred from equation (9) that M_y must be proportional to $\sin(n\pi x/a)$ where a is the length of the plate and $\lambda = a/n$ the length of a half wave. The distribution of M_y along the edges a is sinusoidal as illustrated by Figure 2.21. Each panel between two straight nodal lines n-n represents a plate simply supported on all four edges and loaded symmetrically on two opposite edges by the variable moment M_y per unit length. Under the assumption that no compressive forces are acting on the restraining plate, it is possible to develop the following expression for the angle of rotation $\bar{\psi}$ as function of M_y.

The deflection $\bar{w}$ of the restraining plate can be determined from the differential equation (3). Due to the assumption $\sigma_x=0$ the last term of this equation vanishes, but we allow for the effect of the anisotropy produced by compressive stresses σ_x above the proportional limit by retaining the coefficients τ and $\sqrt{\tau}$ in the first two terms of the differential equation.

For the loading condition considered here the deflection $\bar{w}$ can be expressed in the general form

$$\bar{w} = (C_1 \sinh \frac{\sqrt[4]{\tau}\ \pi\bar{y}}{\lambda} + C_2 \cosh \frac{\sqrt[4]{\tau}\ \pi\bar{y}}{\lambda} + C_3\ \bar{y} \sinh \frac{\sqrt[4]{\tau}\ \pi\bar{y}}{\lambda}$$

$$+ C_4\ \bar{y} \cosh \frac{\sqrt[4]{\tau}\ \pi\bar{y}}{\lambda})$$

in which C_1 to C_4 are constants which are defined by the given boundary conditions. When the four sides of the plate are simply supported, the expression for $\bar{w}$ becomes

$$\bar{w} = \frac{c\lambda}{2\pi D'\sinh(\sqrt[4]{\tau}\ \pi y/\lambda)} [\frac{\bar{y}}{c} \cosh \frac{\sqrt[4]{\tau}\ \pi(\bar{y}-c)}{\lambda} + (1-\frac{\bar{y}}{c}) \cosh \frac{\sqrt[4]{\tau}\ \pi\bar{y}}{\lambda}$$

$$- \frac{\sinh(\sqrt[4]{\tau}\ \pi\bar{y}/\lambda) + \sinh \frac{\sqrt[4]{\tau}\ \pi(\bar{y}-c)}{\lambda}}{\sinh(\sqrt[4]{\tau}\ \pi y/\lambda)}]\ M_y \ .$$

Using $\bar{\psi} = (\frac{\partial \bar{w}}{\partial \bar{y}})_{\bar{y}=c}$ leads to equation (25)

$$\bar{\psi} = - \frac{\lambda}{2\sqrt[4]{\tau}D'} \frac{1}{\pi} \tanh \frac{\sqrt[4]{\tau}\ \pi c}{2\lambda} [1 + \frac{\sqrt[4]{\tau}\ \pi c/\lambda}{\sinh(\sqrt[4]{\tau}\ \pi c/\lambda)}]\ M_y$$

$$= - \frac{\lambda}{2\sqrt[4]{\tau}D'} \rho_1 (\frac{\sqrt[4]{\tau}\ c}{\lambda})\ M_y \qquad (25)$$

where ρ_1 indicates that the ratio of the moment M_y to the rotation $\bar{\psi}$ is constant along the edges, c and t_c are the inflection point distance and the thickness of the restraining plate, $D' = Et_c^3/12(1-\nu^2)$ the flexural rigidity of the restraining plate and λ the length of the half wave of the buckling plate.

For the sake of simplification we assume $\lambda = \sqrt[4]{\tau}b$ which is for freely supported edges.

Thus, the term (25) simplifies to

$$\bar{\psi} = - \frac{b}{2D'} \rho_1 (\frac{c}{b})\ M_y \ .$$

In Figure 2.22 ρ_1 is plotted as a function of $\sqrt[4]{\tau}c/\lambda = \frac{c}{b}$.

From equation (13a) and (12) the coefficient ξ is obtained

$$\xi = \frac{2D}{b\bar{\xi}} = \frac{2D}{b} \frac{b}{2D'} \rho_1 (\frac{c}{b}) = \frac{t^3}{t_c^{\ 3}} \rho_1 (\frac{c}{b}) \ . \qquad (26)$$

Now we must include the effect of the longitudinal stress σ_x on the stiffness of the effective width c of the restraining plate. It can be done approximately by multiplying expression (26) by the factor

$$r = \frac{1}{1-(t^2c^2/t_c{}^2b^2)} .$$

This expression exactly satisfies the conditions which control the limiting cases on r and therefore ξ becomes infinite when $t/b = t_c/c$, in which case both plates are simply supported without restraint. When, owing to high rigidity of the restraining members, $t^2c^2/t_c{}^2b^2$ is very small, r approaches unity, which is correct, as in this case no modification of equation (26) is required.

Introducing the expression r as a factor in equation (26) finally leads to

$$\xi = \frac{t^3}{t_c{}^3} \frac{\rho_1(\frac{c}{b})}{1-(t^2c^2/t_c{}^2b^2)} . \tag{27}$$

This equation applies when $\frac{c}{b} < 1$ and $t = t_c$.

Thus
$$\xi = \rho_1 \frac{\frac{c}{b}}{1-(\frac{c}{b})^2} = A\rho_1 . \tag{27a}$$

The plate coefficient k can now be determined between the limits indicated in Figure 2.20. It is given with the aid of the diagram for ρ_1 in Figure 2.22, the values of the parameters p and q can be read from Figure 2.19. This permits computation of the factor $k = p + 2\sqrt{q}$, required to determine σ_c from equation (23). Discrete values are tabulated in the last column of Table 2.1. In Figure 2.23a k is plotted as a function of d/b. Some typical examples of the effective restraint provided by the webs of rectangular HSS to top flange buckling is given in Figure 2.23b.

Determination of the Critical Stress in the Inelastic Range of Buckling

The critical stress σ_c of long rectangular plates, loaded longitudinally by compressive forces may be computed from equation (22) where k is independent of τ. In the elastic range of buckling, when $\tau=1$, the critical stress σ_c can be directly computed from (22). In the inelastic range τ, which depends on σ_c, is an unknown quantity. Therefore equation (22) is given in the form

$$\frac{\sigma_c}{\sqrt{\tau}} = \frac{\pi^2 E}{12(1-\nu^2)} \left(\frac{t}{b}\right)^2 k \; . \qquad (28)$$

We can precalculate the values σ_c as function of $\sigma_c/\sqrt{\tau}$ for steel with an assumed proportional limit σ_p and a yield strength F_y. Such functions can be computed from τ-values, which are given by the expression

$$\tau = \frac{(F_y-\sigma_c)\sigma_c}{(F_y-\sigma_p)\sigma_p} \; . \qquad (29)$$

For calculation it is convenient to provide a table of the τ-values computed from equation (29) and the corresponding function of $\sigma_c/\sqrt{\tau}$. For steel take a yield strength

F_y = 55 kips/in^2 and an assumed proportional limit σ_p=48 ksi. This proportional limit was based on results of tensile tests in Chapter 3. Such a table for these values is given as Table 2.2 where the τ-values are computed by the expression (29).

In Table 2.2 it can be seen that for a τ-value of 0.1 the yield stress F_y can be reached at the correct strain of 0.5%. The corresponding buckling stress σ_c is about 0.99 F_y and thus the designed τ-value of 0.1 can be considered reasonable for calculation of the critical b/t ratio for a compact section in allowable stress design. To this τ-value of 0.1 the corresponding value of $\sigma_c/\sqrt{\tau}$ is 200. From equation (28) this critical ratio for b/t can be calculated as

$$\frac{b}{t} = \sqrt{\frac{\pi^2 E\ k}{12(1-\nu^2)}\ (\frac{\sqrt{\tau}}{\sigma_c})} = 28$$

where $E = 29600$ ksi

$\nu = 0.3$

$k = 5.8$ for square section (Figure 2.23b)

and $\frac{\sigma_c}{\sqrt{\tau}} = 200$ ksi.

For a compact section in plastic design the ratio of $E_{st}/E = \frac{1}{40}$ for the required plastic rotation of 4 can be used. To this value of τ the corresponding value of $\sigma_c/\sqrt{\tau}$ is 350 ksi and the critical ratio of b/t using the dimensions above and equation (28) is

$$\frac{b}{t} = \sqrt{\frac{\pi^2 E\ k}{12(1-\nu^2)} \left(\frac{\sqrt{\tau}}{\sigma_c}\right)} = 21$$

where
$$\frac{\sigma_c}{\sqrt{\tau}} = 350 \text{ ksi} .$$

It is expected that the ratio of b/t less than about 21 adequately defines a compact section with a plastic rotation 4 times the elastic rotation and that for a ratio higher than about 28 a compact section in allowable stress design can be defined.

Application of the Plastic Theory to Inelastic Buckling

Plastic design methods assume that local buckling of flanges will not occur during the formation of plastic hinges. Such conditions made the re-examination of the problem of plate buckling in the inelastic range necessary. The flanges must be able to sustain strains considerably larger than the yield strain and can be compressed beyond the yield point and for materials which can be modelled by Figure 2.24 into the strain-hardening range without buckling. For elastic design it is considered sufficient if the yield stress is reached without premature local buckling.

The behaviour of flange-plates that buckle in the intermediate range between the proportional limit and the strain-hardening range is largely governed by the presence and distribution of residual stresses. The sum of the proportional limit stress and the largest residual stress component in the longitudinal direction is then equal to the yield stress. Although no direct solution of this problem has been developed, a reasonable transition curve can be given.

During yielding the material changes its physical properties, so that at strain-hardening the initially isotropic material is assumed to be orthotropic -- that is, the properties are direction-dependent.

Thus

$$\frac{\partial \varepsilon_x}{\partial \sigma_x} = \frac{1}{E_x} \qquad \frac{\partial \varepsilon_x}{\partial \sigma_y} = \frac{1}{E_y}$$
$$\frac{\partial \varepsilon_x}{\partial \sigma_y} = -\frac{\nu_y}{E_y} \qquad \frac{\partial \varepsilon_y}{\partial \sigma_x} = -\frac{\nu_x}{E_x} \tag{29}$$
$$\frac{\partial \gamma_{xy}}{\partial \upsilon_{xy}} = \frac{1}{G_t}$$

where E_x and E_y are the tangent moduli

G_t is the tangent shear modulus

ν_x and ν_y are coefficients of dilatation for increases in σ_x and σ_y

γ is the shear strain

and υ is the shear stress .

The relationships between the increments of strains and stresses can be written as follows

$$d\varepsilon_x = \frac{1}{E_x}\, d\sigma_x - \frac{\nu_y}{E_y}\, d\sigma_y$$
$$d\varepsilon_y = -\frac{\nu_x}{E_x}\, d\sigma_x + \frac{1}{E_y}\, d\sigma_y \tag{30}$$
$$d\gamma_{xy} = \frac{1}{G_t}\, d\upsilon_{xy} .$$

The expressions for the bending moments and twisting moments in terms of the deflection, w, in the direction of the z-axis become

$$M_x = - \frac{E_x I}{1-\nu_x \nu_y} \left(\frac{\partial^2 w}{\partial x^2} + \nu_y \frac{\partial^2 w}{\partial y^2}\right)$$

$$M_y = - \frac{E_y I}{1-\nu_x \nu_y} \left(\frac{\partial^2 w}{\partial y^2} + \nu_x \frac{\partial^2 w}{\partial x^2}\right) \qquad (31)$$

and

$$M_{xy} = - 2G_t \, I \frac{\partial^2 w}{\partial_x \partial_y}$$

in which I is the moment of inertia per unit width of plate and is equal to $t^3/12$, t denoting the thickness of the plate.

The condition that the bent position be in equilibrium can be expressed by

$$D_x \frac{\partial^4 w}{\partial x^4} + 2H \frac{\partial^4 w}{\partial_x^2 \partial_y^2} + D_y \frac{\partial^4 w}{\partial y^4} = - \frac{t\sigma_x}{I} \frac{\partial^2 w}{\partial x^2} \qquad (32)$$

in which

$$D_x = \frac{E_x}{1-\nu_x \nu_y} \qquad D_y = \frac{E_y}{1-\nu_x \nu_y} \qquad D_{xy} = \frac{\nu_y E_x}{1-\nu_x \nu_y}$$

$$D_{yx} = \frac{\nu_x E_y}{1-\nu_x \nu_y} \qquad \text{and } 2H = D_{xy} + D_{yx} + 4G_t .$$

From these relationships can be derived the buckling strength.

Equating internal and external work is more amenable to the solution of σ_x than is equation (32) and therefore

$$\frac{\sigma_x t}{I} \iint \left(\frac{\partial w}{\partial x}\right)^2 dx\, dy = \iint \left[D_x\left(\frac{\partial^2 w}{\partial x^2}\right)^2 + D_y\left(\frac{\partial^2 w}{\partial y^2}\right)^2 + (D_{xy}+D_{yx}) \times \left(\frac{\partial^2 w}{\partial x^2}\right)\left(\frac{\partial^2 w}{\partial y^2}\right) + 4G_t\left(\frac{\partial^2 w}{\partial x \partial y}\right)^2\right] dx\, dy\ . \quad (33)$$

When an appropriate deflection surface is assumed, equation (33) yields an approximate solution.

In Figure 2.25 the plate is assumed supported at all four edges. The loaded edges, $x=0$ and $x=a$, are hinged, and the edges $y=\pm\frac{b}{2}$ have equal restraint against rotation (Figure 2.25). For this case the following deflection surface is used

$$w = \left[B\pi\left(\frac{y}{b} - \frac{1}{4}\right) + (A+B)\cos\frac{\pi y}{b}\right]\sin\frac{\pi x}{\lambda}\ . \quad (34)$$

The ratio B/A depends on the restraint. For elastic restraints, with M_y equaling the moment per unit length required for unit rotation,

$$\xi = \frac{B}{A} = \frac{M_y\ b}{2D_y\ I}\ . \quad (35)$$

Substituting w from equation (34) into equation (33) and integrating yields

$$\sigma_c = \frac{\pi^2 t^2}{12b^2}\left[D_x\left(\frac{b}{\lambda}\right)^2 + D_y\left(\frac{\lambda}{b}\right)^2 \frac{\frac{1}{4} + (C_1 + \frac{2}{\pi^2})\xi + \xi^2 C_3}{\frac{1}{4} + \xi C_1 + \xi^2 C_2} + (D_{xy}+D_{yx}) \times \frac{\frac{1}{4} + \xi C_1 + \xi^2 C_4}{\frac{1}{4} + \xi C_1 + \xi^2 C_2} + 4G_t \frac{\frac{1}{4} + \xi C_1 + \xi^2 C_4}{\frac{1}{4} + \xi C_1 + \xi^2 C_2}\right] \quad (36)$$

in which $C_1 = 0.09472 \quad C_2 = 0.00921$

$C_3 = 0.04736 \quad C_4 = 0.01139$.

In the limiting case when the unloaded edges $y=\pm\frac{b}{2}$ are hinged, the minimum values of σ_c are ($\xi=0$)

$$\sigma_c = \frac{\pi^2}{12} \left(\frac{t}{b}\right)^2 \left(2\sqrt{D_x D_y} + D_{xy} + D_{yx} + 4G_t\right) \tag{37}$$

which is obtained when the half-wave length, λ, satisfying

$$\frac{\lambda}{b} = \sqrt[4]{\frac{D_x}{D_y}} \; . \tag{38}$$

For the determination of the moduli E_x, E_y, ν_x, ν_y and G_t, several theories of plasticity are available. The stress-strain law used by Handelman and Prager satisfies the above assumptions reasonably well. The moduli by this theory simplify to

$$\begin{aligned} E_x &= E_{st} \qquad E_y = \frac{4E\,E_{st}}{E+3E_{st}} \qquad G_t = \frac{E}{2(1+\nu)} \\ \nu_x &= \frac{E_{st}(2\nu-1)+E}{2E} \qquad \nu_y = \frac{2[E_{st}(2\nu-1)+E]}{E+3E_{st}} \; . \end{aligned} \tag{39}$$

The effective values of the moduli can be obtained from an incremental stress-strain relationship. From the average stress-strain curve for the strain-hardening range can be expressed

$$\varepsilon-\varepsilon_y = \frac{\sigma-F_y}{E_{st}} + K\left(\frac{\sigma-F_y}{E_{st}}\right)^m \tag{40}$$

in which $E_{st} = 900$ kips/in^2, K=21 and m=2. Thus the following values of the moduli were found to be applicable

$$D_x = 3000 \text{ kips/in}^2 \qquad D_y = 32800 \text{ kp/in}^2$$
$$D_{xy} = D_{yx} = 8100 \text{ kp/in}^2 \quad \text{and} \quad G_t = 2400 \text{ kp/in}^2 . \tag{40a}$$

The developed expression for the buckling strength of orthotropic plates can be applied only if all material is strained into the strain-hardening range beyond the intermediate range. Figure 2.26 shows a typical stress-strain curve with elastic, intermediate and strain-hardening ranges.

The sections contain residual stress of considerable magnitude in order that partial yielding will set in at an applied stress considerably below the yield stress. The elastic solution is valid only up to a limiting stress σ_p which is determined in order that the sum of the applied stress, σ_p, and the maximum residual compressive stress, σ_R, equals the yield stress F_y. The stress σ_p corresponds to the effective proportional limit of the section.

The elastic buckling stress of a perfectly plane plate of isotropic material is given by

$$\sigma_c = k \frac{\pi^2 E}{12(1-\nu^2)} \left(\frac{t}{b}\right)^2 . \tag{41}$$

It can be written in a dimensionless form

$$\frac{\sigma_c}{F_y} = \frac{1}{\alpha^2} \tag{42}$$

where $$\alpha = \frac{b}{\pi t}\sqrt{\frac{12F_y(1-\nu^2)}{k\ E}} \ . \qquad (43)$$

This is valid for values of α larger than a limiting value α_p as shown in Figure 2.27. In this figure α_y is equal to the value of α at the point of strain-hardening. From the point $(\frac{\sigma_p}{F_y})$ and α_p a transition curve must be followed to the point at which the buckling stress equals the yield stress, $\frac{\sigma_c}{F_y} = 1$ (from 42).

The transition curve can be taken as

$$\frac{\sigma_c}{F_y} = 1 - [1-(\frac{\sigma_p}{F_y})\ (\frac{\alpha-\alpha_y}{\alpha_p-\alpha_y})^n] \qquad (44)$$

and the limiting value of n is suggested

$$n_{max} = \frac{2(\alpha_p-\alpha_y)}{(\alpha_p{}^2-1)} \ . \qquad (45)$$

Now we need to determine the value of α_p and α_y. Equation (42) gives the value of α_p by substituting $\sigma_c=\sigma_p$, in which σ_p is the effective proportional limit. For structural wide-flange shapes it is conservative to take $\frac{\sigma_p}{F_y} = 0.5$ and thus $\alpha_p = \sqrt{2}$. The value of α_y can be obtained for the type of compression element; it is nearly independent of the amount of restraint. For the plate supported along all four edges is $\alpha_y = 0.58$.

The most important consideration is the determination of the corresponding values of b/t for this point of strain-hardening.

We can calculate this value from equation (37) by substituting the given values of the moduli (40a) with the assumption that $\sigma_c = \bar{F}_y$. For calculation of value $\bar{F}_y$ can be used the following consideration: The flanges will now be considered to be compressed 4 times the elastic limiting strain into the strain-hardening range without buckling. Thus for yield stress F_y = 55 ksi can be computed from equation (40) the value of $\bar{F}_y$ = 60.9 where the plastic strain reached 4 times the elastic strain.

Thus $$\sigma_c = \frac{\pi^2}{12} \left(\frac{t}{b}\right)^2 \left(2\sqrt{D_x D_y} + D_{xy} + D_{yx} + 4G_t\right) \geq \bar{F}_y \ . \qquad (46)$$

Introducing the values (40a) and $\bar{F}_y$ = 60.9, equation (46) yields

$$\frac{b}{t} \leqq \sqrt{\frac{31000}{60.9}} = 22.6 \ . \qquad (47)$$

From this analysis, it is expected that the ratio of b/t less than about 23 adequately defines a compact section with a plastic rotation capacity equal to 4 times the elastic rotation i.e. Θ=4.

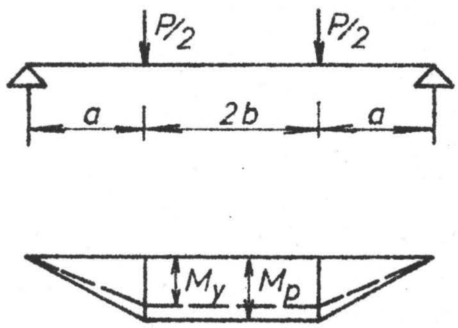

(a) Loading

(b) Bending moment distribution

FIGURE 2·1 Simple Span Beam

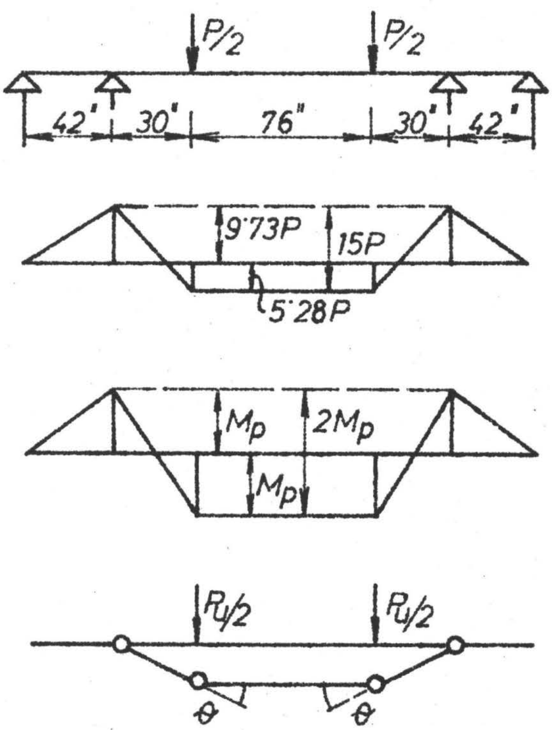

(a) Loading

(b) Elastic bending moment distribution

(c) Bending moment distribution at collapse

(d) Collapse mechanism

FIGURE 2·2 Three Span Beam

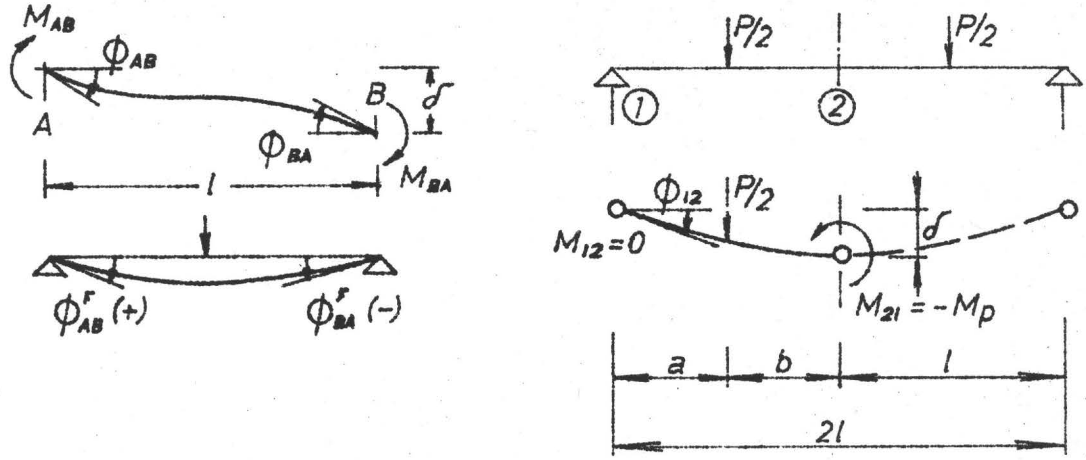

(a) Nomenclature

(b) Deformation of Simple Beam

FIGURE 2.3 Deflection of Simple Beam

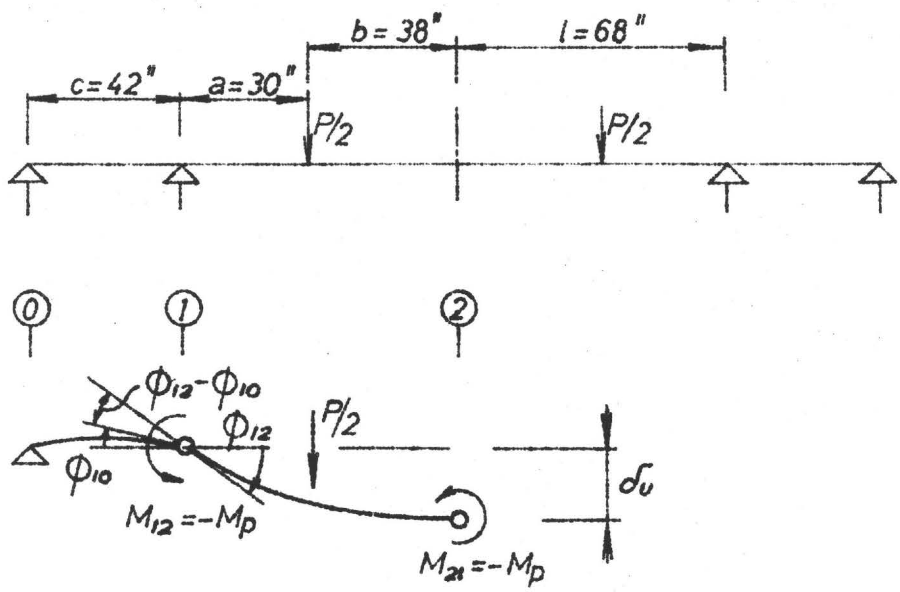

FIGURE 2.4 Deflection of Three Span Beam

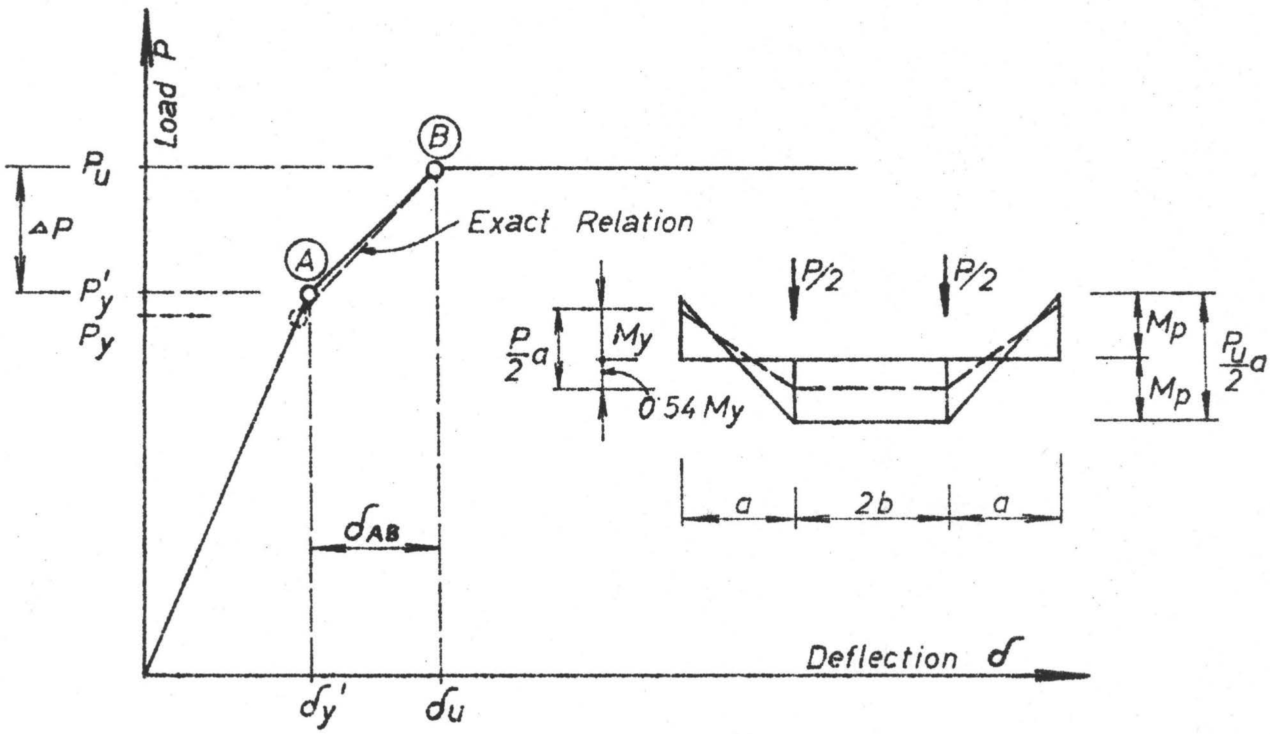

FIGURE 2.5 Load - Deflection Curve of Three Span Beam

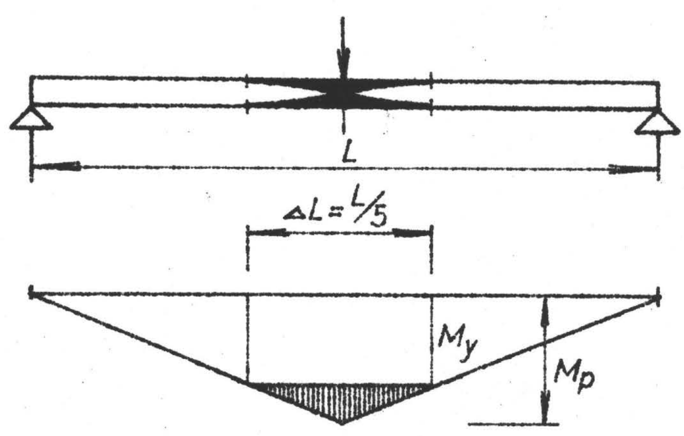

FIGURE 2.6 Hinge Length of Simply Supported H.S.S. under Concentrated Load

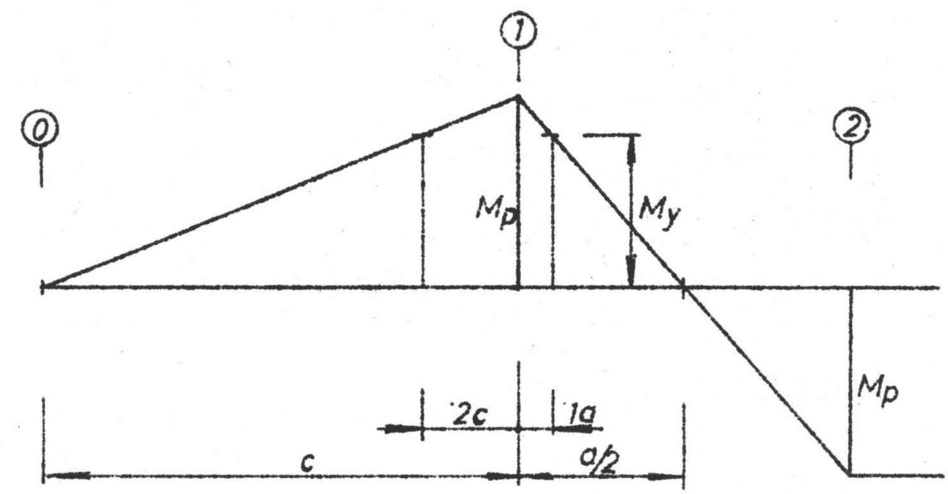

FIGURE 2.7 Hinge Length at Interior Support

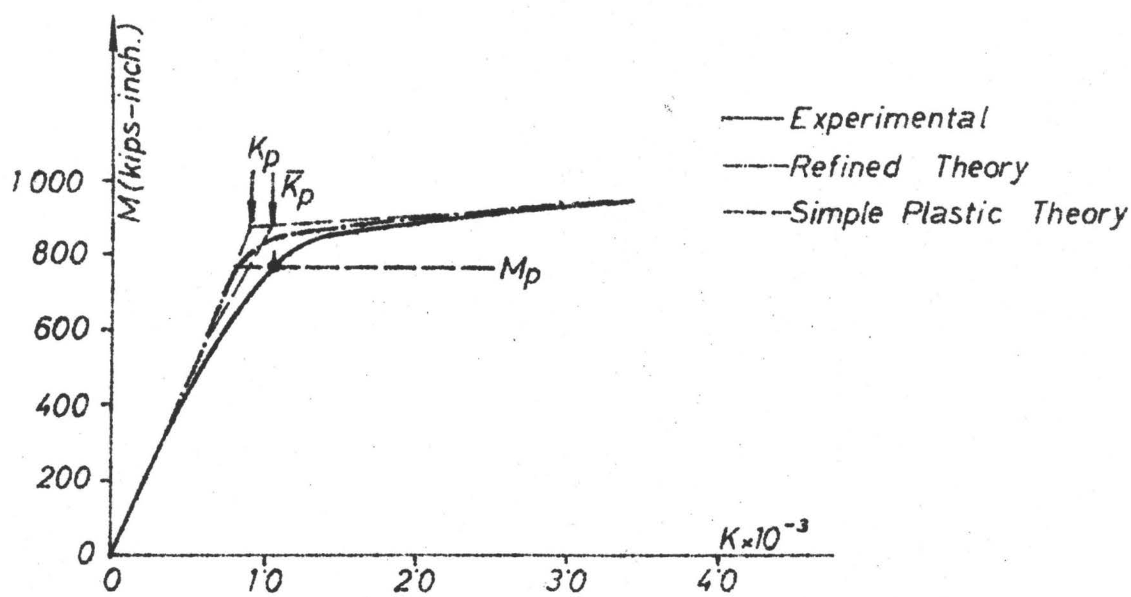

FIGURE 2.8 Assumption of Formed Hinge for Test No. 12

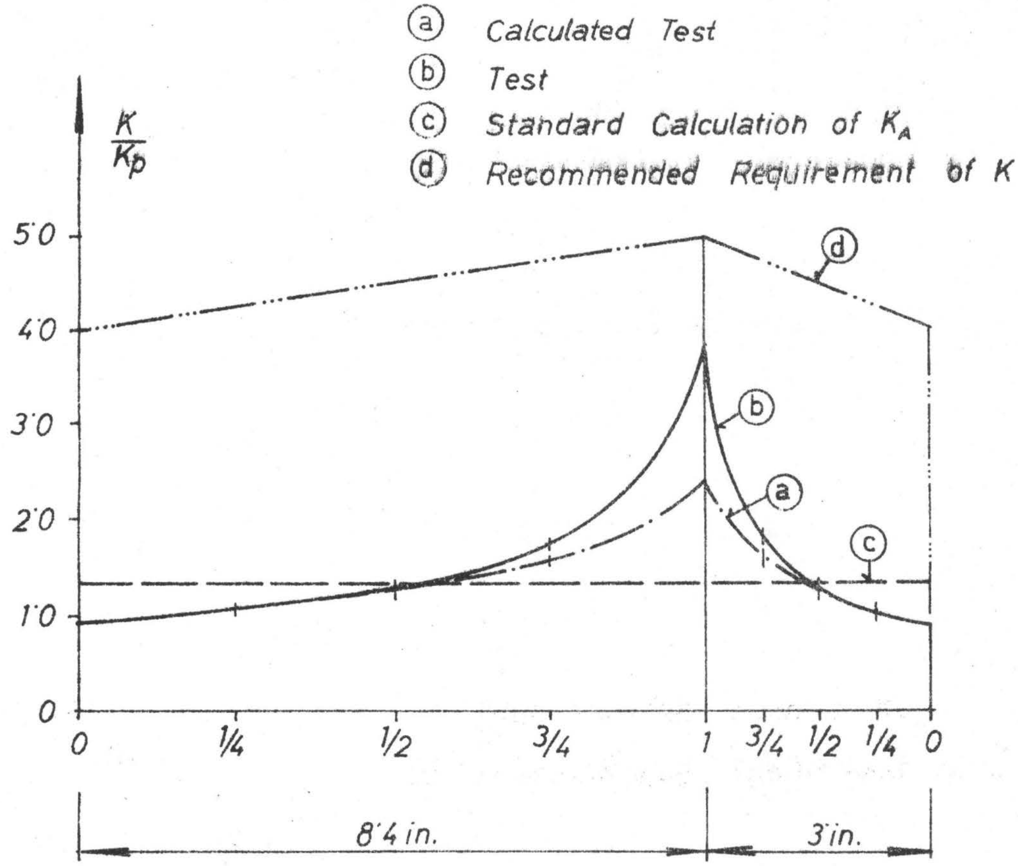

(a) Calculated Test $\frac{K}{K_p} = \frac{2\,200}{920} = 2{\cdot}4$				(b) Test $\frac{K}{K_p} = \frac{3\,500}{920} = 3{\cdot}8$		
Point	M (kp.-in.)	K ($\times 10^{-6}$)	K/K_p	M (kp.-in.)	K ($\times 10^{-6}$)	K/K_p
0	703	830	0·90	703	830	0·90
1/4	753	970	1·05	756	973	1·05
1/2	802	1 150	1·25	808	1 155	1·26
3/4	852	1 440	1·57	864	1 550	1·68
1	902	2 200	2·40	914	3 500	3·80

FIGURE 2·9 Measured and Calculated Curvature at Support for HSS - 6" x 4" x .437 of Test No. 12

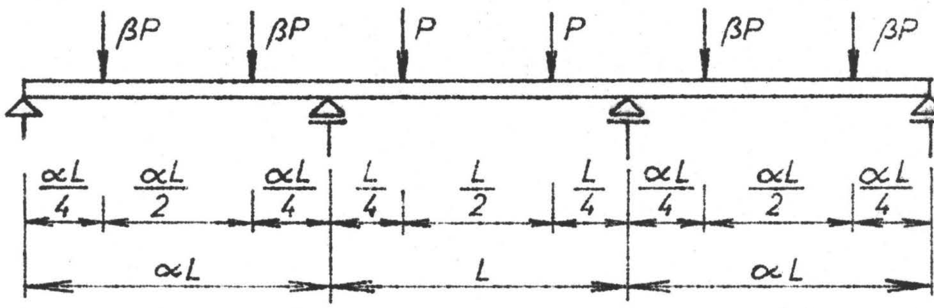

FIGURE 2·10 Three Span Continuous Beam

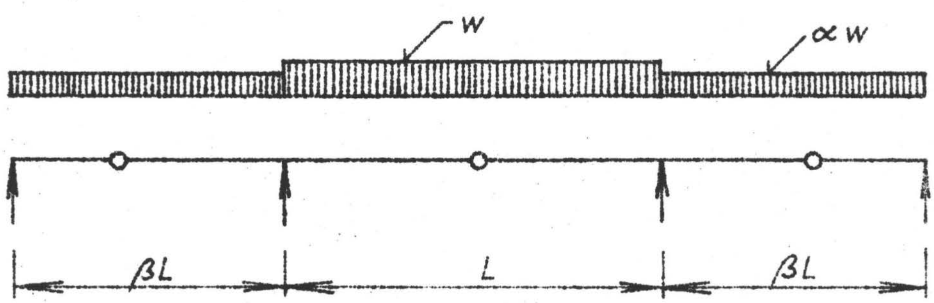

Note : $\alpha_{min} = 0{\cdot}25$

Location of Last Hinge to Form	Maximum "Angles" for Given Geometry	$\left(\frac{H}{LK_p}\right)$
At midspan in all cases except the following :	First hinge at support ($\alpha_{min} = 0{\cdot}25$)	0·425
(1) $0{\cdot}7 < \beta < 1{\cdot}0$ $0{\cdot}25 < \alpha < 0{\cdot}30$	First hinge at midspan ($\alpha_{min} = 0{\cdot}25$)	0·050
(2) $1{\cdot}3 < \beta < 2{\cdot}9$ $0{\cdot}6 < \alpha < 1{\cdot}0$	First hinge in side span	0·186

FIGURE 2·11 Values of H/LK_p

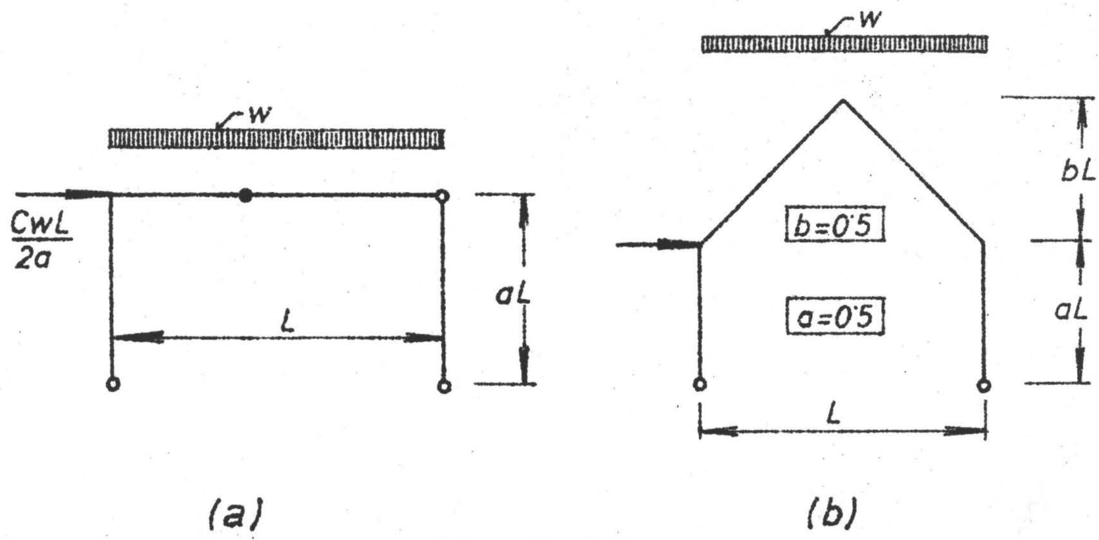

FIGURE 2·12 Single Span Rigid Frames

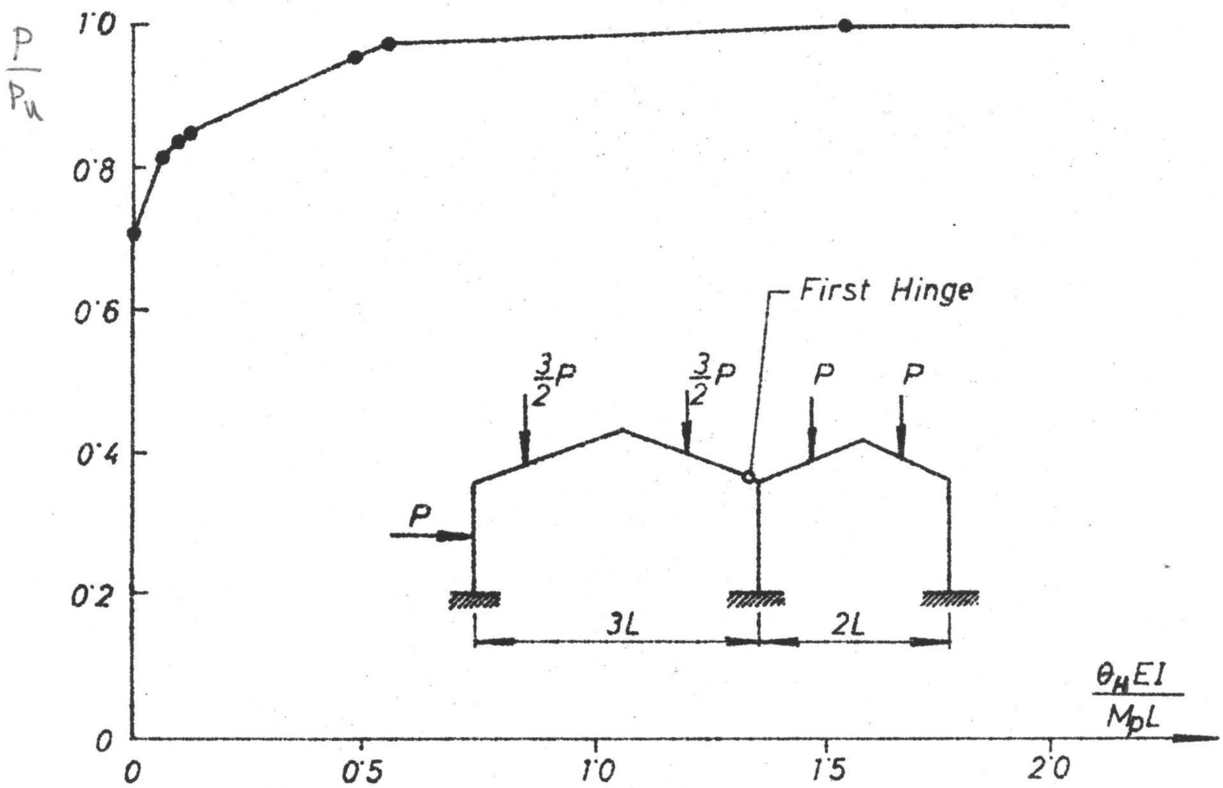

FIGURE 2·13 Two-Bay Gable Frame

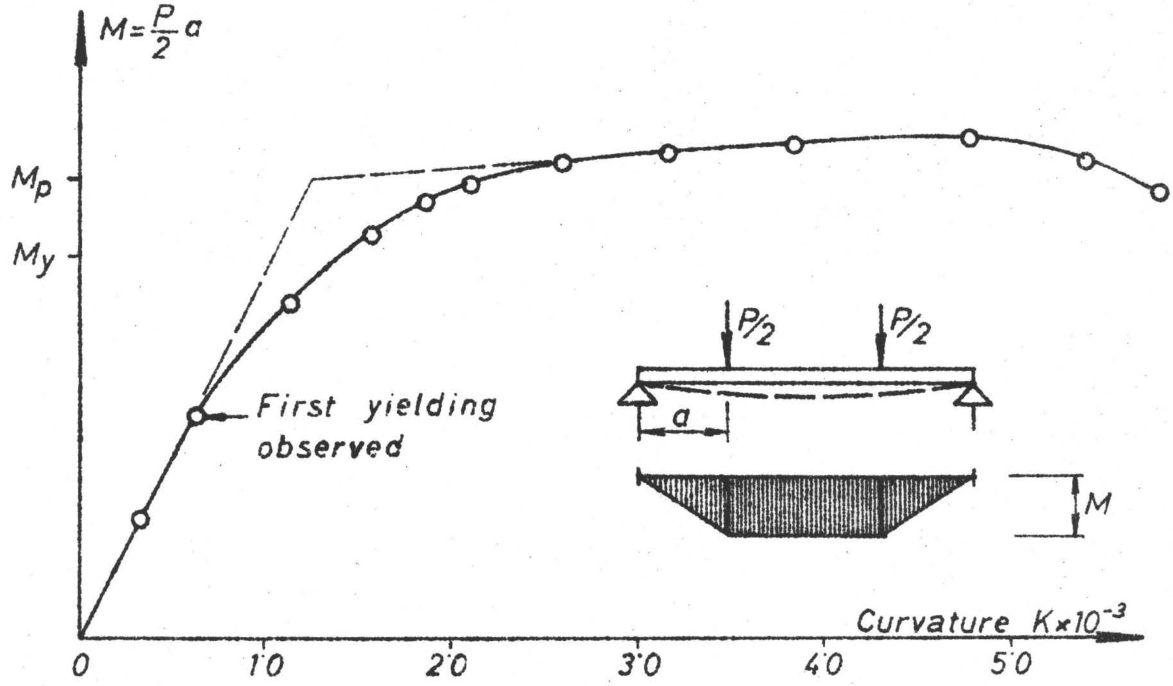

FIGURE 2·14 Typical Experimental Moment - Curvature Relationship

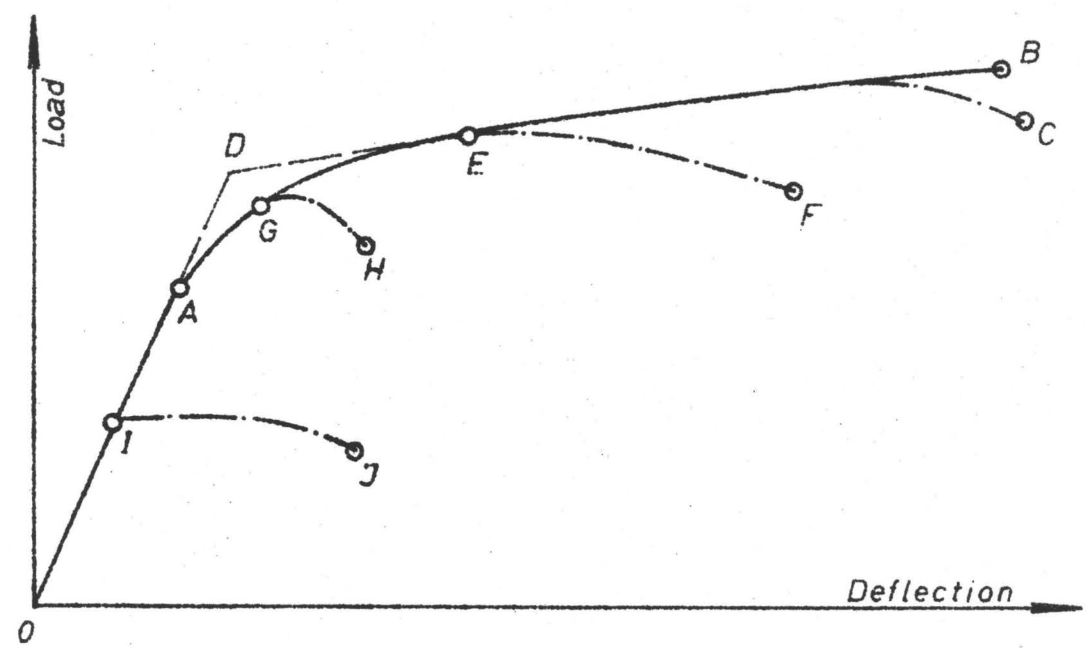

FIGURE 2·15 Possible Load - Deflection Curves for Beams

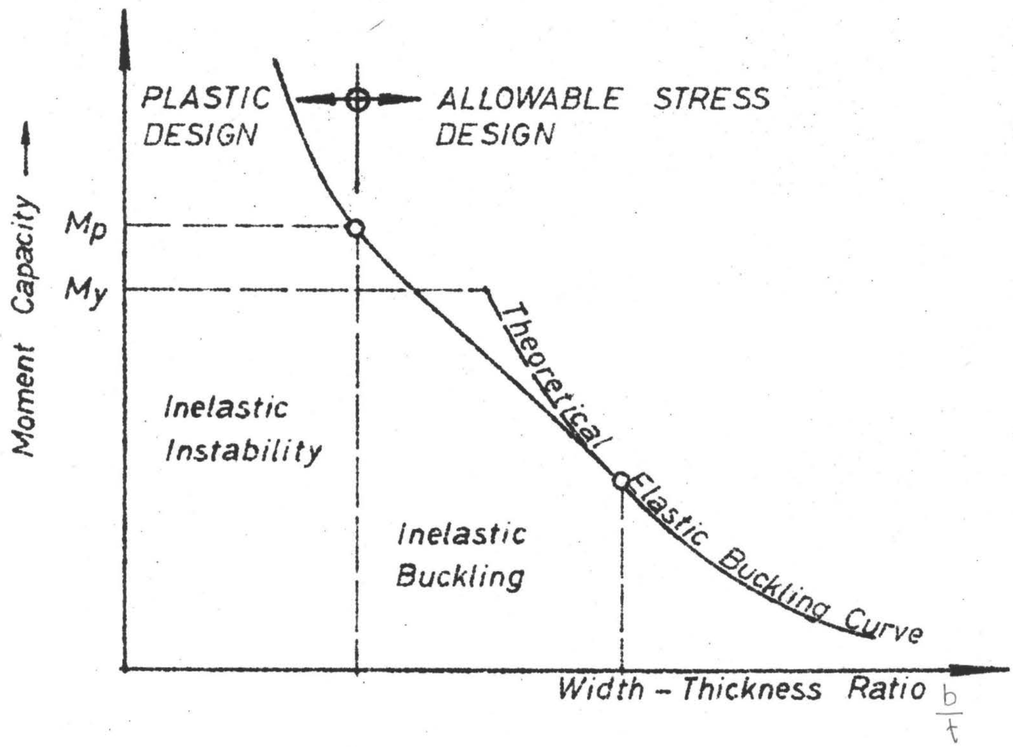

FIGURE 2.16 Ranges of Beam Behaviour

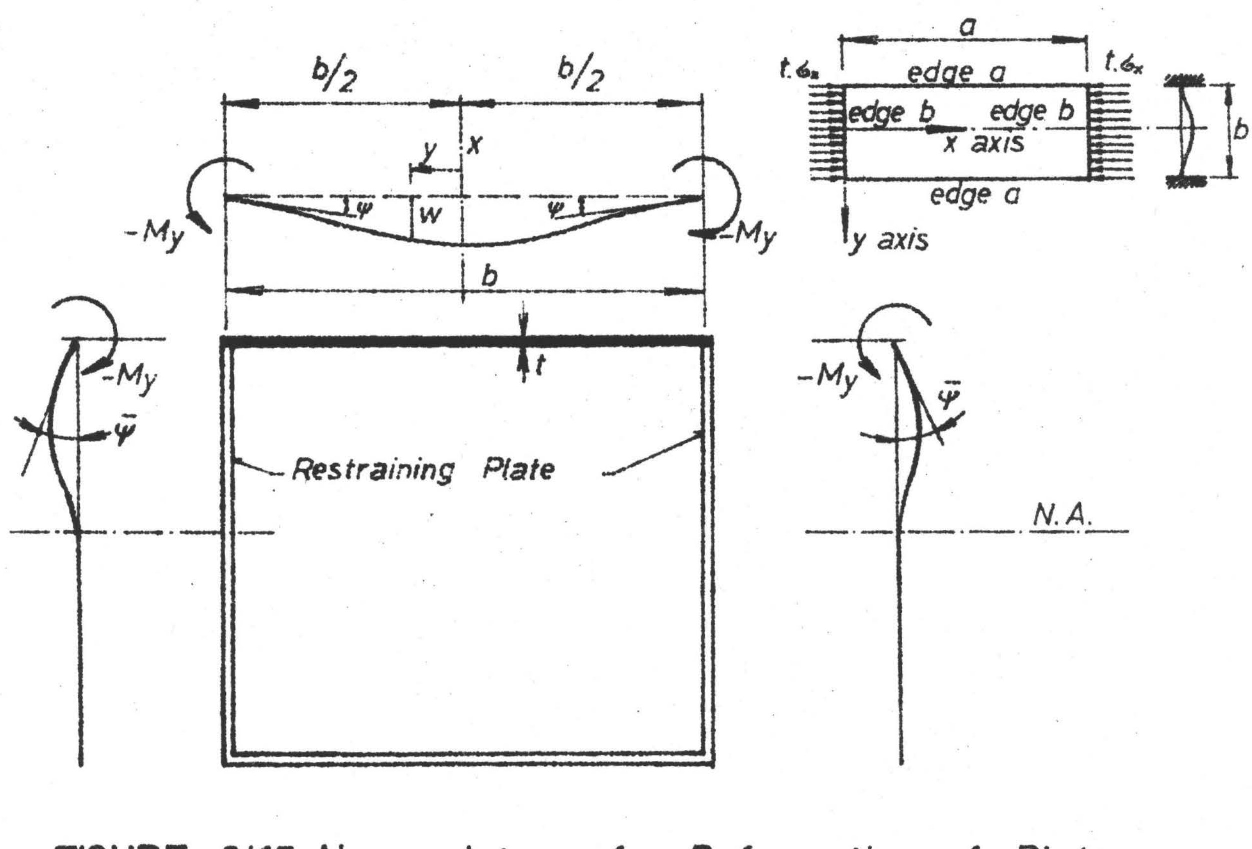

FIGURE 2.17 Nomenclature for Deformation of Plate

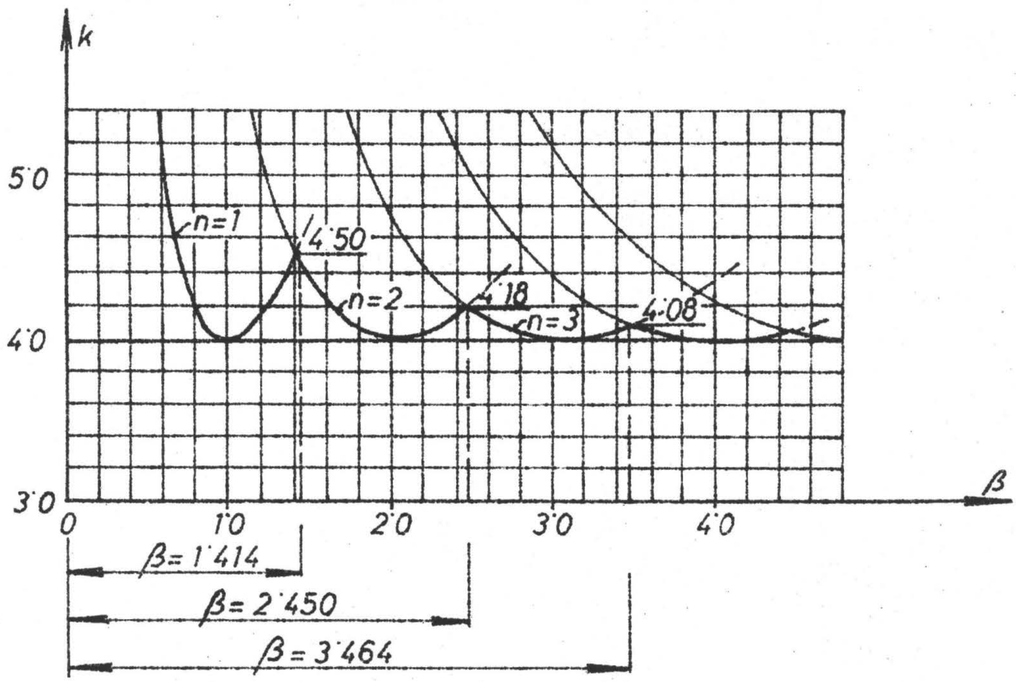

FIGURE 2'18 Dependence of σ_c on the Aspect Ratio β

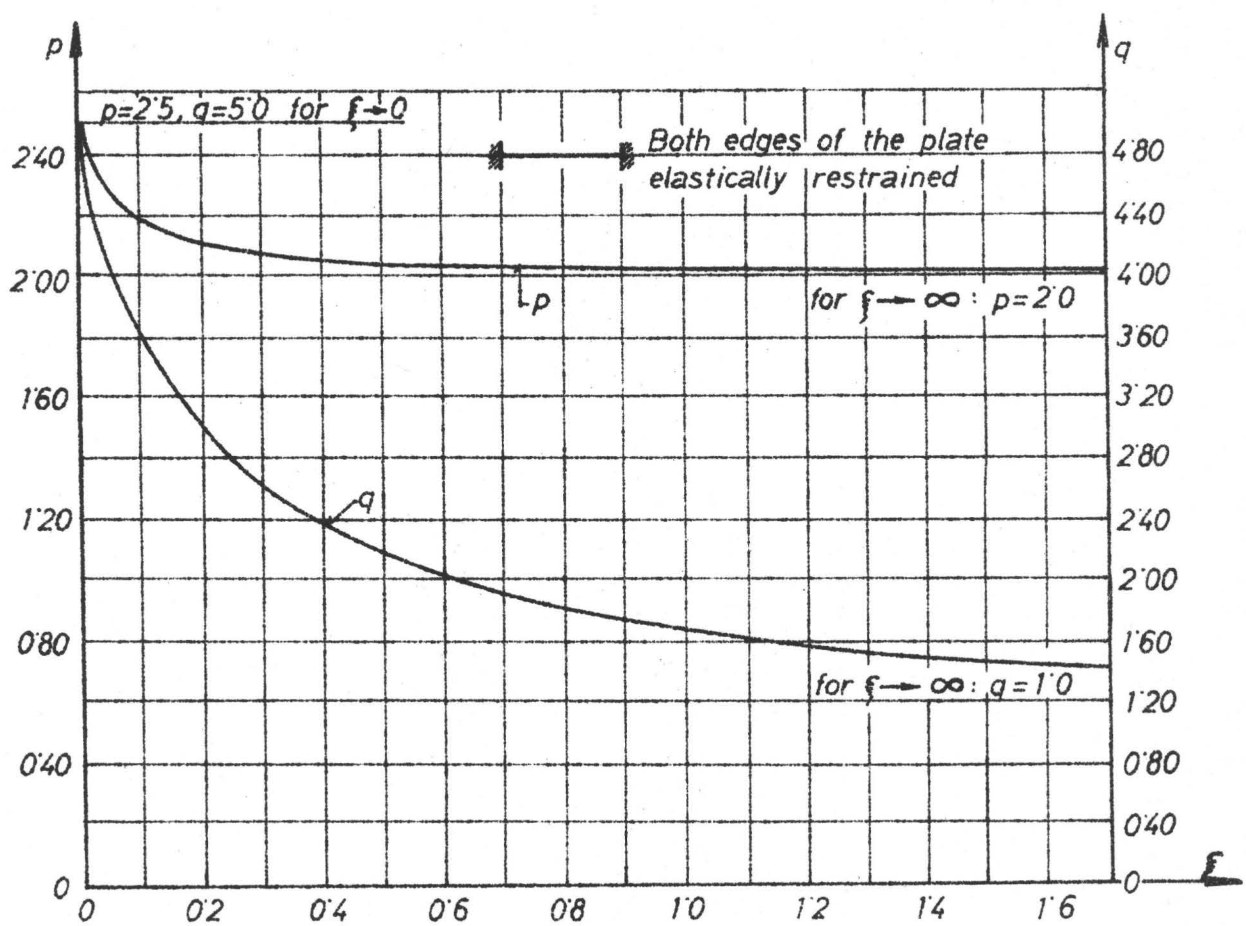

FIGUR 2'19 Factors Depending on the Coefficient of Restraint ξ

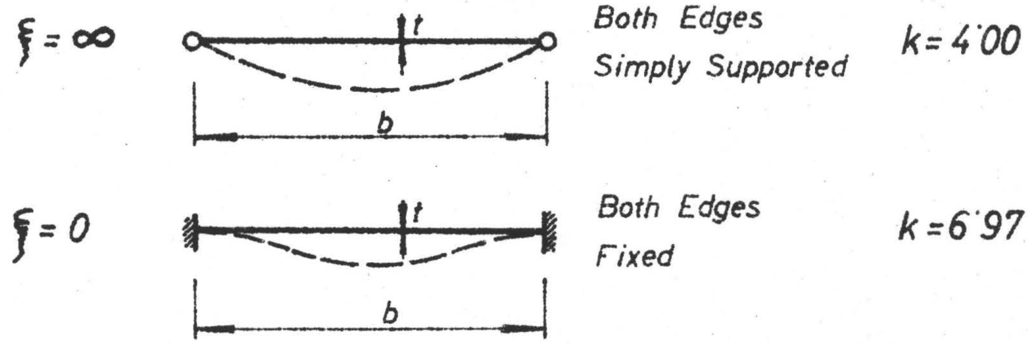

FIGURE 2·20 Extreme Cases of Restraint

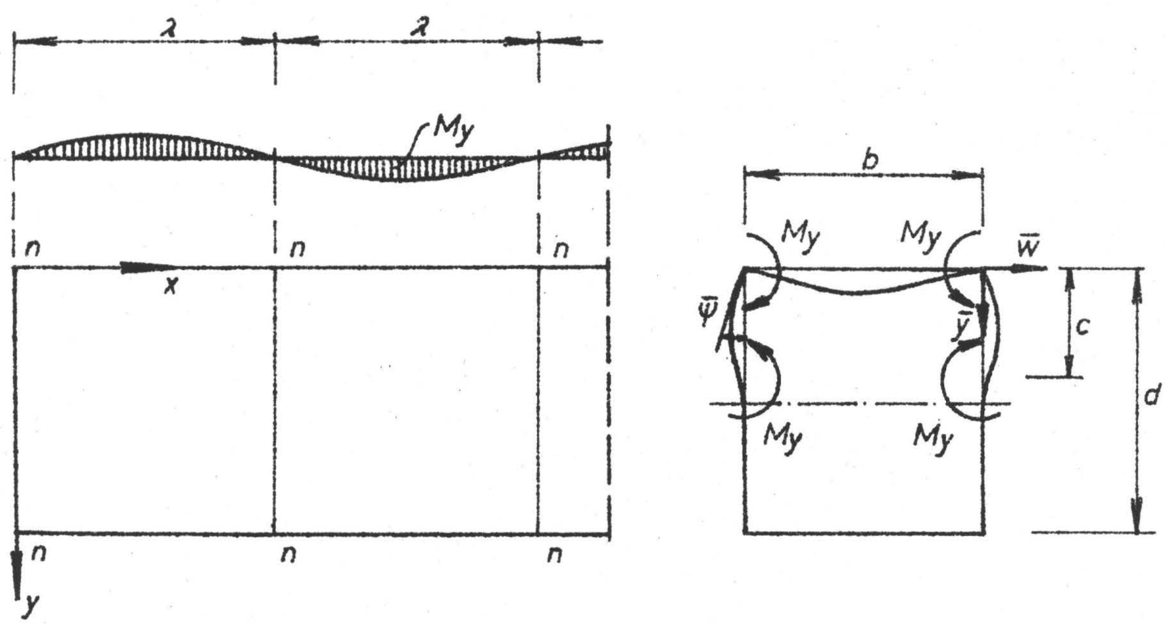

FIGURE 2·21 Assumed Shape of Buckling

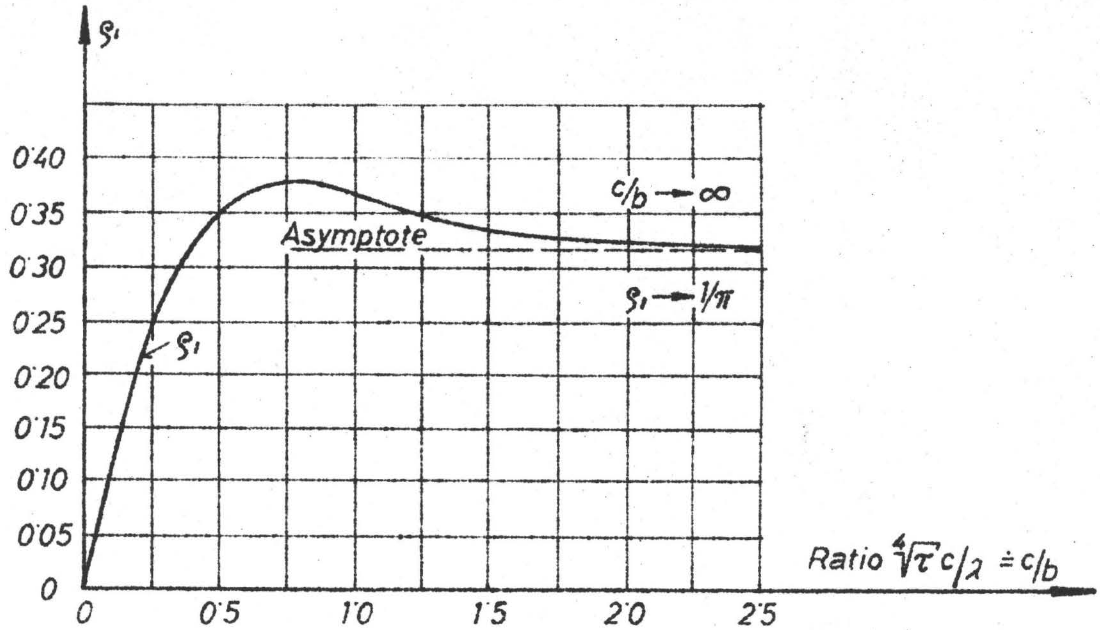

FIGURE 2·22 Relationship Between ρ_1 and c/b

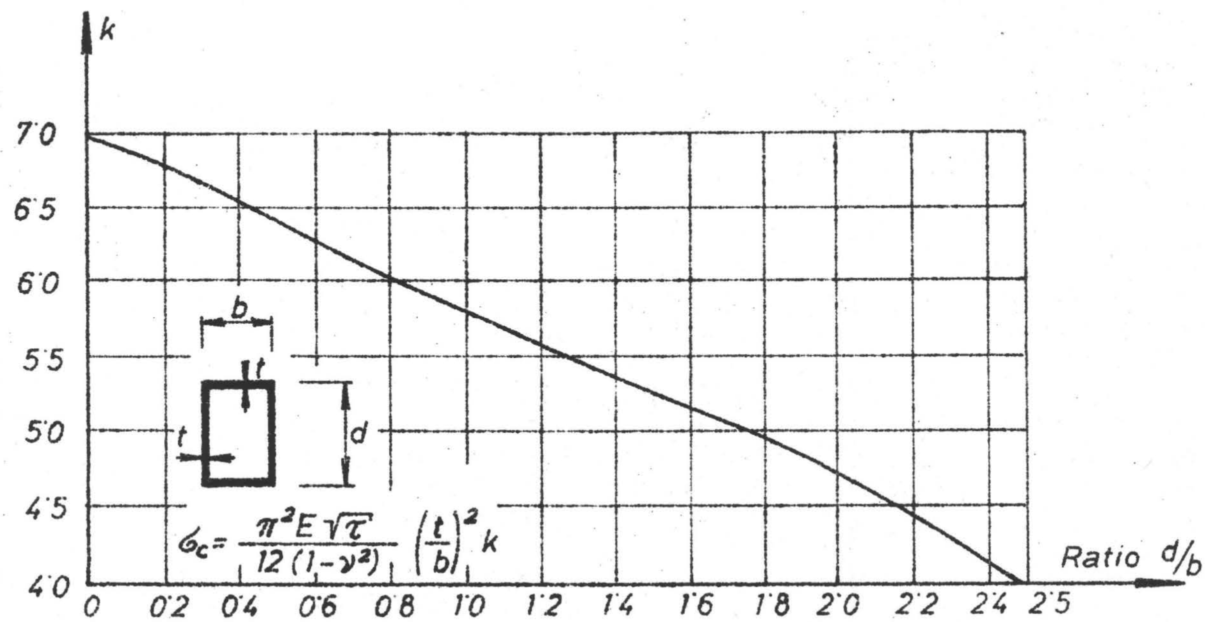

(a) Plate Coefficient k as Function of d/b

HSS — 2·0 × 4·0 × t	$b = 4{\cdot}0$	$k = 6{\cdot}41$
HSS — 4·0 × 4·0 × t	$b = 4{\cdot}0$	$k = 5{\cdot}79$
HSS — 4·0 × 2·0 × t	$b = 2{\cdot}0$	$k = 4{\cdot}71$

(b) Some Typical Examples

FIGURE 2·23 Plate Coefficient k for Critical Stress σ_c

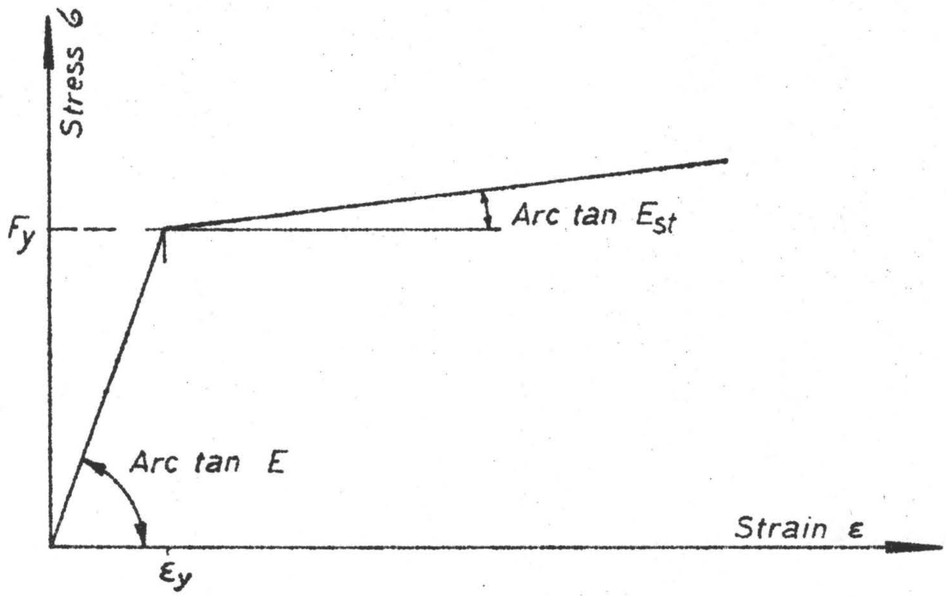

FIGURE 2.24 Simplified Stress – Strain Curve

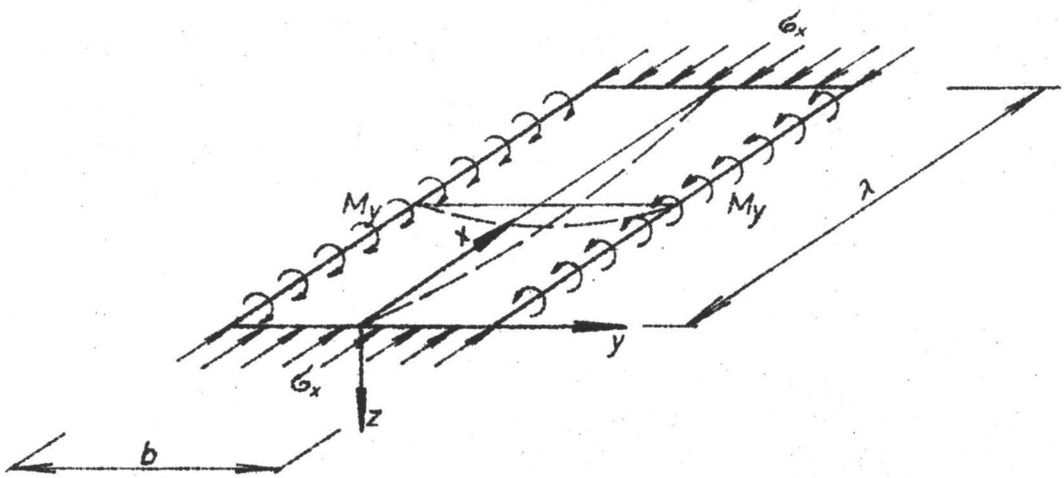

FIGURE 2.25 Plate Supported at All Four Edges

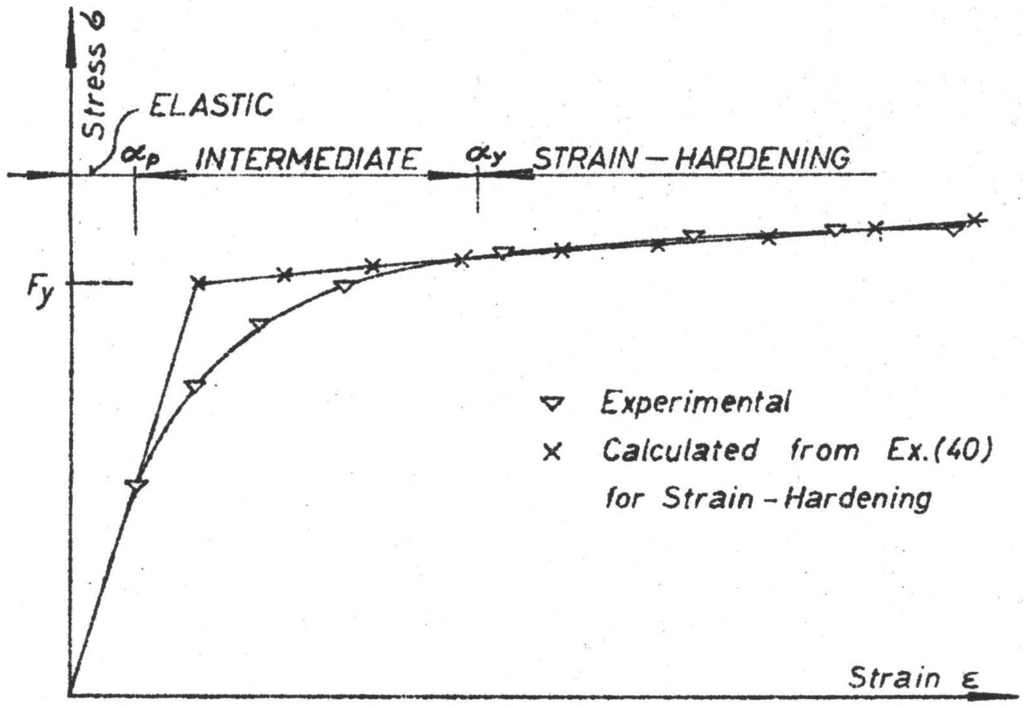

FIGURE 2·26 Typical Stress— Strain Curve

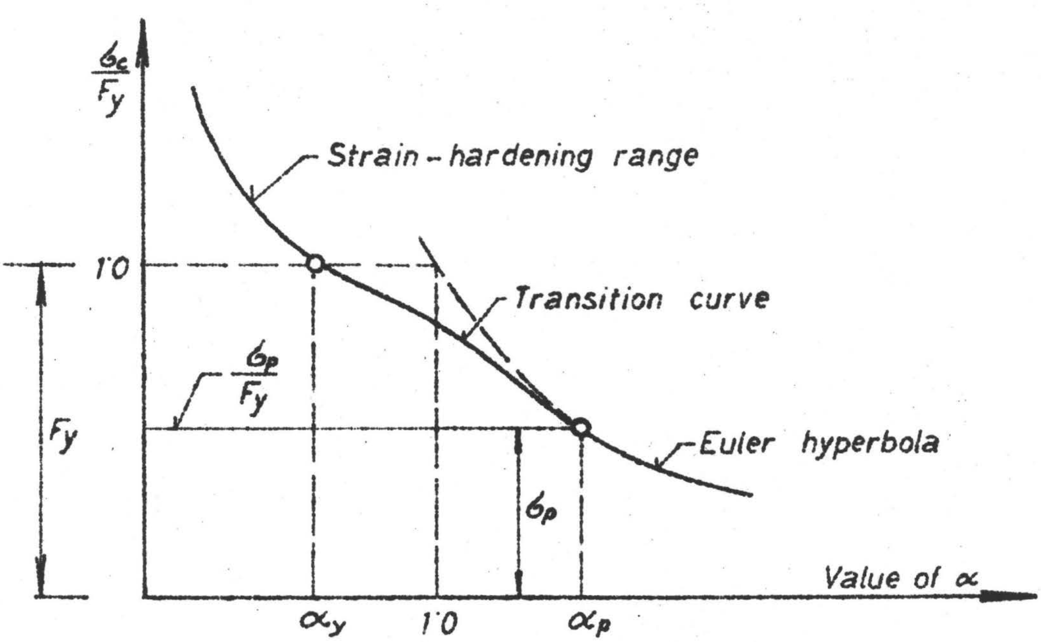

FIGURE 2·27 Buckling Strength of Plates

d/b	c/b	ς_1	A	ξ	p	q	k
	$=0{\cdot}4\,\frac{d}{b}$	FIG.2·22	eg.(27)	$=\varsigma_1 A$	FIG.2·19		
0	0	0	0	0	2·50	5·00	6·97
0·2	0·08	0·072	0·08	0·006	2·42	4·80	6·80
0·4	0·16	0·144	0·164	0·024	2·32	4·45	6·54
0·6	0·24	0·216	0·255	0·055	2·25	4·05	6·28
0·8	0·32	0·28	0·357	0·10	2·19	3·70	6·04
1·0	0·40	0·32	0·476	0·152	2·14	3·32	5·79
1·2	0·48	0·34	0·623	0·212	2·10	3·00	5·56
1·4	0·56	0·36	0·817	0·294	2·08	2·70	5·37
1·6	0·64	0·37	1·085	0·40	2·05	2·35	5·12
1·8	0·72	0·38	1·50	0·57	2·04	2·08	4·93
2·0	0·80	0·38	2·22	0·84	2·04	1·78	4·71
2·2	0·88	0·375	3·91	1·46	2·03	1·46	4·45
2·4	0·96	0·37	12·00	4·43	2·01	1·16	4·17
2·5	1·00	0·37	∞	∞	2·00	1·00	4·00

TABLE 2·1 The Plate Coefficient k

$\sigma_c \left[\frac{kp}{in^2}\right]$	τ	$\sqrt{\tau}$	$\frac{\sigma_c}{\sqrt{\tau}} \left[\frac{kp}{in^2}\right]$
48·0	1·00	1·00	48·0
49·0	0·875	0·935	52·5
50·0	0·745	0·862	58·0
51·0	0·607	0·780	65·4
52·0	0·464	0·680	76·5
53·0	0·315	0·561	94·5
54·0	0·160	0·400	135
54·8	0·0326	0·181	303

TABLE 2·2 Dependence of σ_c on the Ratio τ

CHAPTER III

EXPERIMENTAL PROGRAM

3.1 Testing Material

HSS are manufactured by two methods; sections up to 16" periphery are hot formed by the continuous weld process; larger sections are cold formed by the Electric Resistance Welding process.

Sections for the test series were selected to provide a range of flange slenderness ratios of b/t for compact and non-compact sections. The square, rectangular and round sections are indentified by examples such as those in Figure 3.1.

A summary of the geometric properties of the sections tested is given in Table 3.1.

3.2 Material Properties

The hot formed sections are manufactured from Columbium High Strength Steel with a low carbon content; the shapes of their stress-strain curves are similar to those for cold formed sections.

A typical stress-strain curve obtained from a tension test is shown in Figure 3.2. The yield stress F_y is the stress corresponding to a total strain of 0.5 percent, which is easily obtained in routine spot checks in the steel industry. This stress usually corresponds closely to the constant stress at yielding and is close to the stress obtained by the conventional 0.2% offset (0.002 in/in) or plastic strain method. The simplified stress-strain curve for an analysis by computer is given by the idealized yield stress, YS, the modulus of elasticity, E=29600 ksi, and the strain-hardening modulus E_{st} obtained by tension tests.

Table 3.2 summarizes the material properties obtained from tension tests performed on coupons cut from each of the sections. Figures 20a, 22a, 4a ... show the stress-strain curves for the flats, corners and weld coupons of the cross-sections. The locations from which the coupons were taken are shown in the inset of figures. In Table 3.2 is given for these coupons: area of their cross-section, the ultimate load P_{max}, the ultimate stress F_u and the yield stress F_y. For the cold-formed sections are calculated the average yield stresses F_{ya}. The last two columns prescribe the values of the simplified bilinear stress-strain relationship for an analysis by computer. Plastic strains are presumed to begin at stresses greater than YS in the simplified model shown by the dash-dot straight line in Figures 20a, 22a, ...

The tests were performed in a hydraulic testing machine using tensile specimens conforming to ASTM Specification A 370-65(14). For the first five tension tests the strain rate was reduced to zero for a short period before taking readings, so that the values were the "static" yield stress. In the above procedure it was observed that leaking of hydraulic fluid occurred and therefore there was a great influence on the drop of the tensile strength. Thus, the other tension tests were performed at a common constant "slow" strain rate of 100 micro-in/in/sec.

The value of E_{st} was obtained by graphically measuring the approximate slope of the strain-hardening branch of the recorded stress-strain curves.

In Figure 3.3 is shown a typical variation of yield stress of cold-formed sections from corners to flats. The average yield stress F_{ya} based on appropriate flange area weightings is given by

$$F_{ya} = \frac{2A_c F_{yc} + A_f F_{yf}}{2A_c + A_f}$$

where F_{yc} = the yield stress of corner (.5% total strain)

F_{yf} = the yield stress of a flat (.5% total strain)

A_c = area of corner

A_f = area of flat part

It is of interest that for the cold-formed HSS used in this test series the following average stress ratios were found

$$\frac{F_{yc}}{F_{yf}} = 1.135 \qquad \frac{F_{uf}}{F_{yf}} = 1.128 \qquad \frac{F_{uw}}{F_{uf}} = 1.175 \qquad F_{yc} = F_{yw}$$

where the second subscript is defined in Figure 22a.

The overall view of all test tensile coupons is shown in Figure 3.4. In the background can be seen the pieces of sections from which the coupons were cut.

3.3 Testing Arrangement

a) Simple Span

The test setup was designed to confirm computed shape factors of HSS to assess the problem of local buckling in a pure moment domain. Figure 3.5 shows the overall experimental setup. This experiment was designed to simulate 2-point loading on a simple span beam. Two equal vertical loads were applied with a hydraulic jack midway between load points onto a spreader beam. This load at midspan was measured by a load cell which was located between the jack and a ball and socket on the spreader beam. The central part of the beam between the two load points was therefore subject to uniform moment. Electric resistance strain gauges were placed at midspan, having been mounted on the top and bottom flanges of the test HSS; at the load points gauges were located only on the bottom. One of the strain gauges at midspan was placed at right angles to the direction of bending.

The moment-curvature relationship was determined by monitoring the loads with the load cell and the strains by strain gauges.

The vertical deflection at midspan was measured by means of a dial gauge. The accuracy of the dial gauge was ±0.001 inches. Because the displacements were very large (usually to 10 inches), measurement of deflection was sufficiently accurate by this method.

b) Three Span Beam

A similar loading condition applied symmetrically to a three span beam is shown in Figure 3.6. As shown in Figure 2.2b the magnitude of the moments at interior supports exceeds the positive moment in midspan. As the load is increased the negative moments $-M_p$ are initiated over the interior supports which must be maintained until $+M_p$ occurs in the positive moment region at which time a mechanism is formed.

At the interior supports, the electric strain gauges were mounted on the top flange of HSS. Two other load cells were placed at the ends of the beam to make the structure determinate (see Figure 3.6). This arrangement determined the negative moments over the interior supports by using the load cells at the ends.

The movement of the exterior supporting channels was checked by means of dial gauges. Very little change was recorded in the readings of dial gauges from the initial readings. Thus, this arrangement effectively restrained vertical movement of the exterior supports.

The details associated with loading of the circular sections are shown in Figure 3.7.

3.4 Preparations of Beam for Testing

For the experiments, the type of electric strain gauging used was:

EP-08-500BH-120 made by the Micro-Measurement Co. at Romulus, Michigan.

Specifications for the gauges are as follows

Resistance in ohms	:	120 ± 0.15%
Gage factor at $75^{O}R$	:	2.055 ± 0.5%
Strain limits	:	approximately 15%.

For the gauge installation M-BOND AE-10 adhesive was used. This is a 100% solids epoxy system which provides rapid room temperature cures, together with ease of handling and mixing. The surface preparation, the gauge preparation and installation were made as recommended in Instruction Bulletin B-137 provided by the manufacturer.

PREPARATION OF TEST APPARATUS

It was found that the hydraulic jack and the load cells provided accurate control over the loads when they are calibrated before each test. The load cells were calibrated in the 120 kip Tinius testing machine available in the laboratory. The calibration curves were very nearly linear. The load cells together with the electric strain gauges were connected to a balancing and switching box unit which was connected to a strain indicator.

3.5 Testing Procedure

In the elastic range of the test, the hydraulic pressure was increased in increments to give predetermined elastic behaviour of HSS. The load was maintained at each of these values until all readings had been taken.

After yielding had occurred, the midspan deflection was increased in increments to get sufficient values for plotting a moment-curvature relationship. The flow of hydraulic fluid to the ram was then closed off for a short stabilization period before readings were taken. The readings of the electric strain gauges and dial gauge at midspan for the deflection were recorded for each increment of the load.

The section was deformed well into the yield zone to ensure a rotation from 4 to 8 times the rotation at the elastic limit. For those tests in which flange buckling predominated, the visual observations and measurements of the progression yielding and local buckling were recorded into the unloading range using the above procedure.

The redistribution of moments for a three span beam was checked by the load cells at the ends of the beam. The same constant readings of these load cells indicated the maintenance of resisting negative plastic moments $-M_p$ at the interior supports until $+M_p$ occured in the middle span. When local buckling was observed at the interior supports, the readings of the end load cells decreased due to the reduced moment resistance at the section.

Figures 3.8 and 3.9 show overall views of the test setup. The general arrangement of the loading system for a round HSS can be seen in Figures 3.10, 3.11 and 3.12.

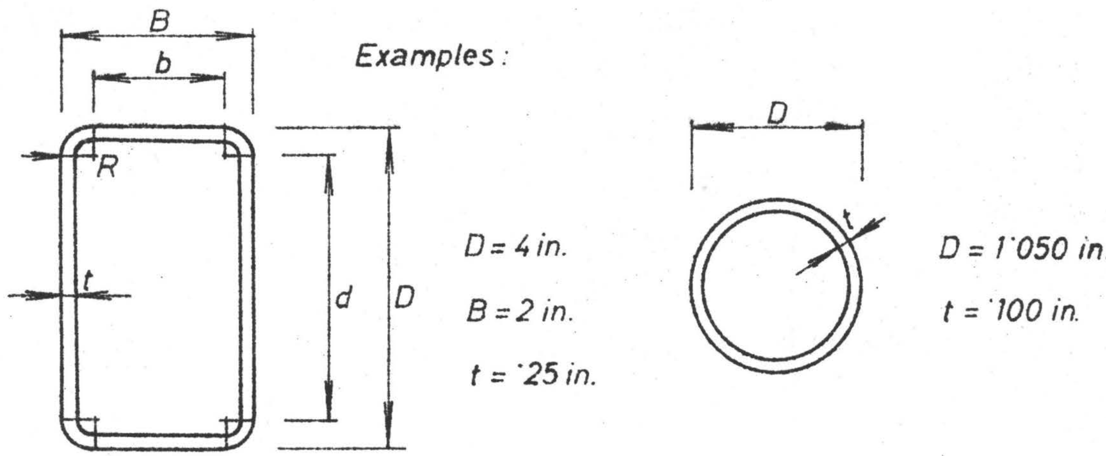

HSS – 4 × 2 × 0·250

HSS – 1·050 OD × 0·100

(a) RECTANGULAR

(b) ROUND

FIGURE 3·1 Hollow Structural Sections

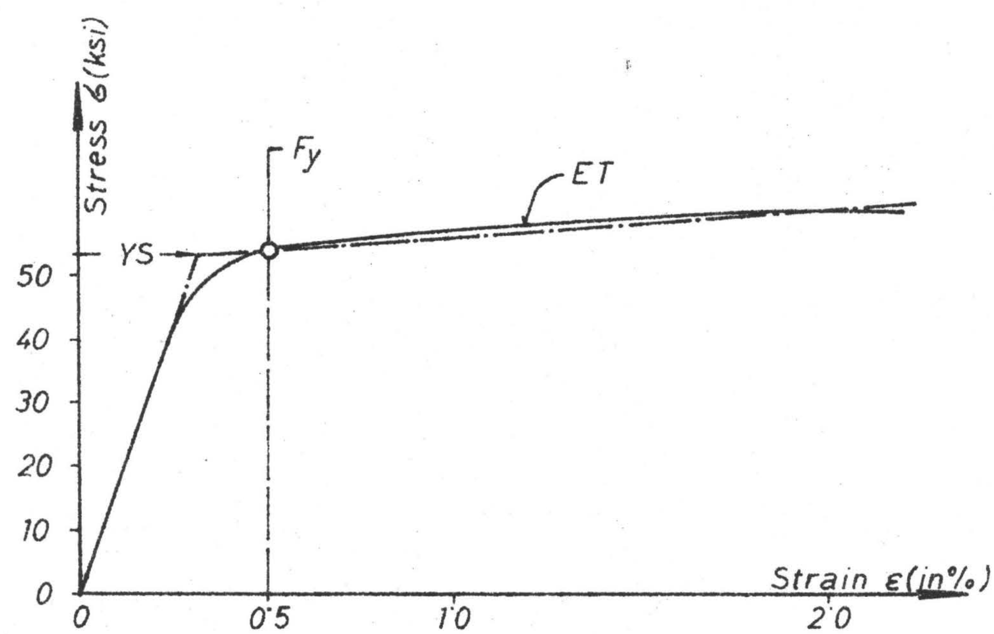

FIGURE 3·2 Typical Stress – Strain Curve

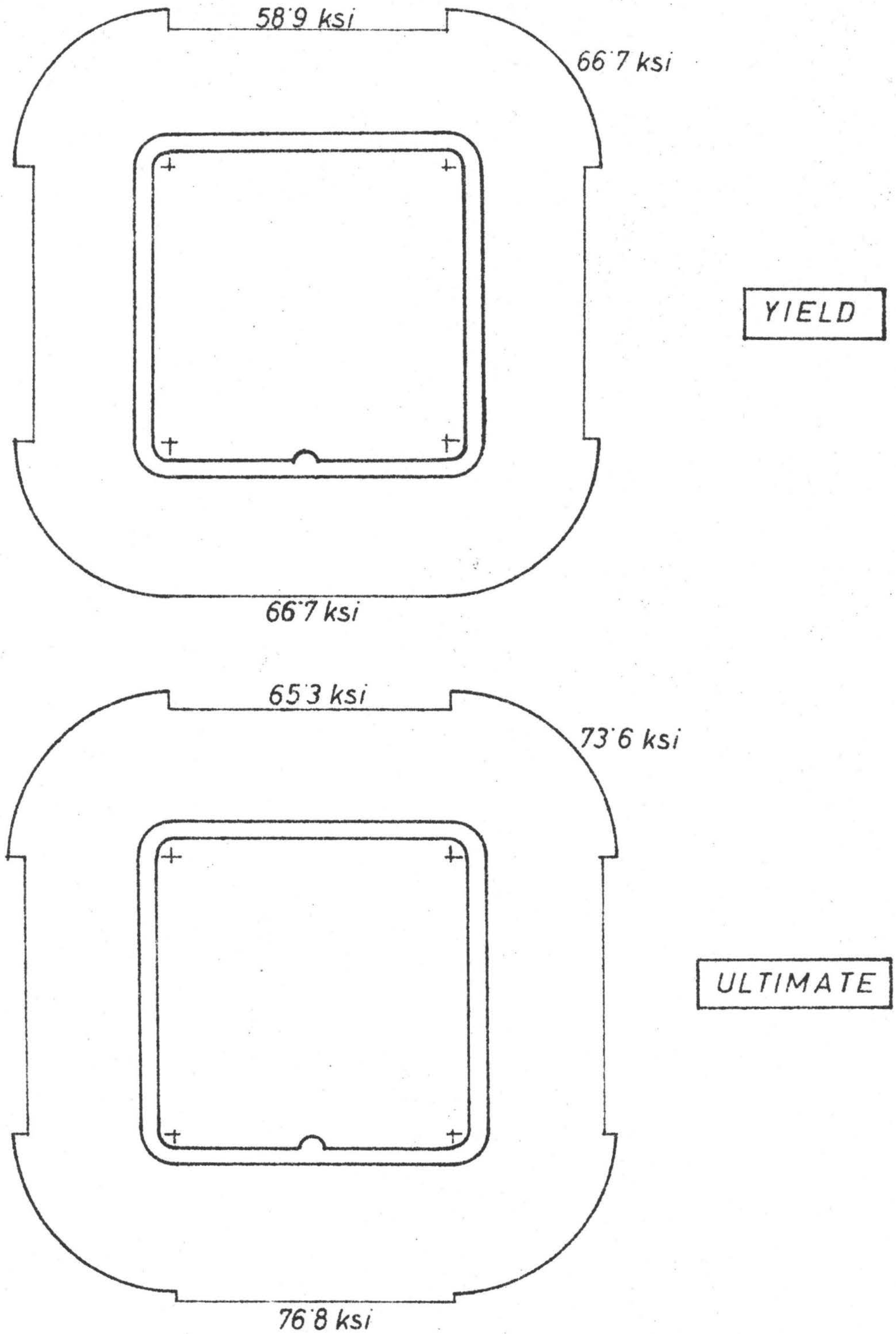

FIGURE 3·3 Variation of Yield and Ultimate Tensile Around Periphery of Typical Cold-Formed HSS

No.	H.S.S.	Spans	No.	H.S.S.	Spans
1	6·0 x 6·0 x ·437	3	17	5·0 x 5·0 x ·250	1
2	6·0 x 6·0 x ·188	3	18	8·0 x 8·0 x ·312	1
3	6·0 x 6·0 x ·188	1	19	6·0 x 6·0 x ·188	1
4	6·0 x 6·0 x ·437	1	20	10·0 x 10·0 x ·375	1
5	5·0 x 3·0 x ·230	3	21	3·5 O.D. x ·150	1
6	5·0 x 3·0 x ·230	1	22	10·0 x 6·0 x ·500	1
7	4·0 x 2·0 x ·235	3	23	10·0 x 10·0 x ·375	1
8	4·0 x 2·0 x ·235	1	24	10·75 O.D. x ·500	1
9	2·5 x 2·5 x ·210	1	25	7·0 x 7·0 x ·188	1
10	2·5 x 2·5 x ·210	3	26	7·0 x 7·0 x ·250	1
11	6·0 x 4·0 x ·437	1	27	6·0 x 6·0 x ·250	1
12	6·0 x 4·0 x ·437	3	28	4·0 x 4·0 x ·188	1
13	4·0 x 4·0 x ·250	1	29	3·5 O.D. x ·150	1
14	4·5 O.D. x ·250	3	30	4·0 O.D. x ·188	1
15	4·5 O.D. x ·250	1	31	4·5 O.D. x ·188	1
16	7·0 x 7·0 x ·312	1			

TABLE 3·1 Test Sections

Material Properties										
No.	H.S.S.	R (in.)	Loc.*	Area ($in.^2$)	P_{max} (kp)	F_u (ksi)	F_y (ksi)	F_{ya} (ksi)	YS (ksi)	ET (ksi)
20a	10·0 x 10·0 x ·375	·750	f	·220	14·5	66·0	56·5	58·2	57·0	350·
			w	·491	37·8	77·0	66·5			
			c	·433	32·5	75·0	66·5			
22a	10·0 x 6·0 x ·500	1·00	f	·650	39·6	60·9	56·3	58·8	58·0	273·
			w	·655	46·8	71·4	62·0			
			c	·805	55·4	68·8	62·0			
4a	6·0 x 6·0 x ·437	·875	f	·643	40·8	63·5	56·3	58·8	58·0	320·
			w	·435	32·0	73·6	64·0			
			c	·365	26·3	72·0	64·0			
11a	6·0 x 4·0 x ·437	·875	f	·688	49·3	71·7	66·5	69·5	68·5	307·
			c	·311	24·8	79·8	72·8			
13a	4·0 x 4·0 x ·250	·375	f	·348	26·3	75·4	55·5	55·5	53·5	687·
			c	·311	23·4	75·1	55·5			
8a	4·0 x 2·0 x ·235	·352	f	·339	25·2	74·4	59·5	59·5	58·0	528·
			c	·296	22·1	74·7	59·5			
6a	5·0 x 3·0 x ·230	·345	f	·356	25·4	71·4	52·0	52·0	50·0	683·
			c	·295	20·9	70·9	52·0			
9a	2·5 x 2·5 x ·210	·315	f	·143	10·3	71·8	61·3	61·3	60·5	333·
			c	·197	14·1	71·6	61·3			
24a	10·75 O.D. x ·500	—	r	·738	40·0	54·2	43·0	43·0	41·5	366·
			w	·729	40·8	56·0	50·2			
15a	4·5 O. D. x ·250	—		·275	19·8	71·8	58·0	58·0	56·0	674·
21a	3·5 O. D. x ·150	—		·098	7·5	76·4	57·0	57·0	55·0	656·

* See Fig. 22a and 24a for location

TABLE 3·2 Tensile Test Data

Material Properties										
No.	H.S.S.	R (in.)	Loc.*	Area (in^2)	P_{max} (kp)	F_u (ksi)	F_y (ksi)	F_{ya} (ksi)	YS (ksi)	ET (ksi)
19a	6·0 × 6·0 × ·188	·376	f	·239	17·1	71·5	56·0	57·2	56·0	357·
16a	7·0 × 7·0 × ·312	·624	f	·405	28·4	69·3	60·0	61·6	60·5	305·
18a	8·0 × 8·0 × ·312	·624	f	·402	28·8	71·6	63·0	64·5	63·7	250·
17a	5·0 × 5·0 × ·250	·500	f	·334	21·8	65·2	58·0	59·8	59·0	250·
25a	7·0 × 7·0 × ·188	·376	f	·231	17·1	74·0	57·0	58·0	57·0	350·
26a	7·0 × 7·0 × ·250	·500	f	·330	21·8	66·1	57·0	58·3	58·0	194·
27a	6·0 × 6·0 × ·250	·500	f	·340	22·4	65·8	59·5	61·0	60·5	167·
28a	4·0 × 4·0 × ·188	·282	f	·257	18·2	70·8	53·0	53·0	51·0	660·
29a	3·5 O.D. × ·150	–	r	·173	12·2	70·6	52·0	52·0	50·0	650·
30a	4·0 O.D. × ·188	–	r	·196	14·1	71·8	53·5	53·5	51·0	735·
31a	4·5 O.D. × ·188	–	r	·229	15·8	69·0	52·5	52·5	50·5	650·

TABLE 3·2 (cont'd)

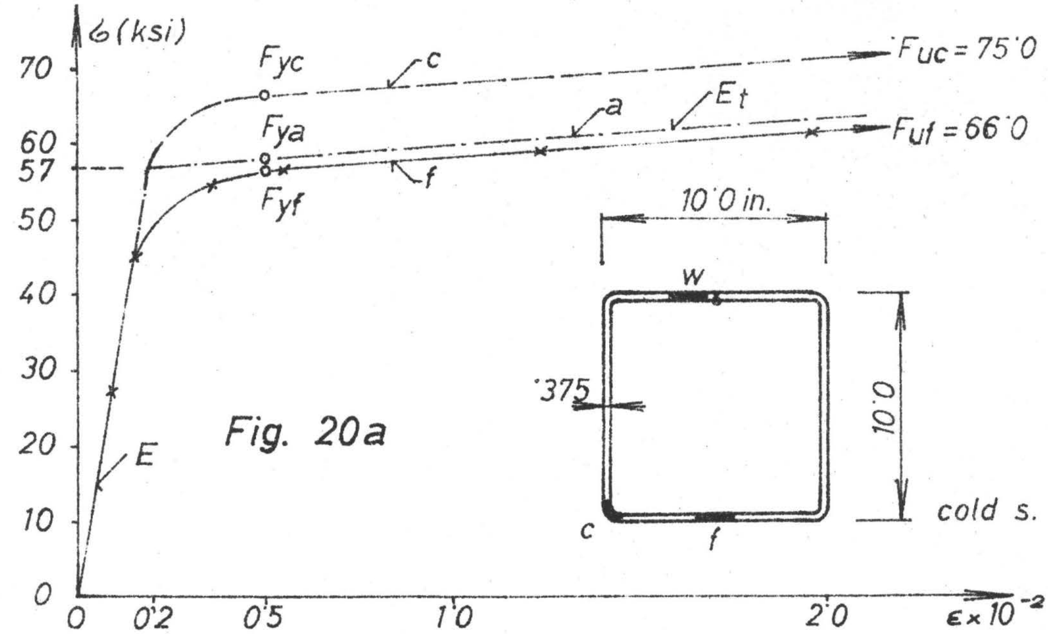

Fig. 20a

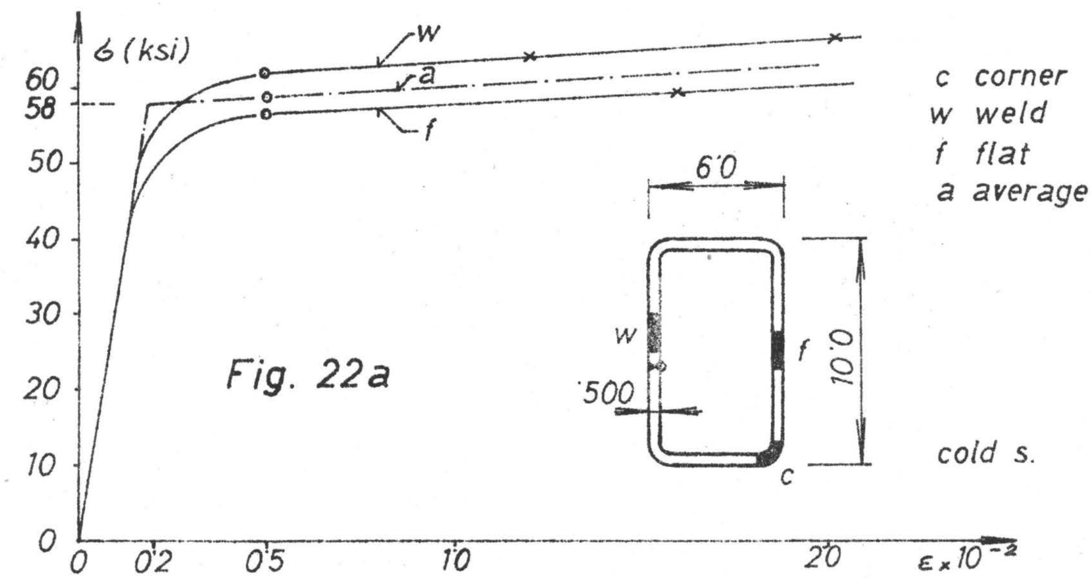

Fig. 22a

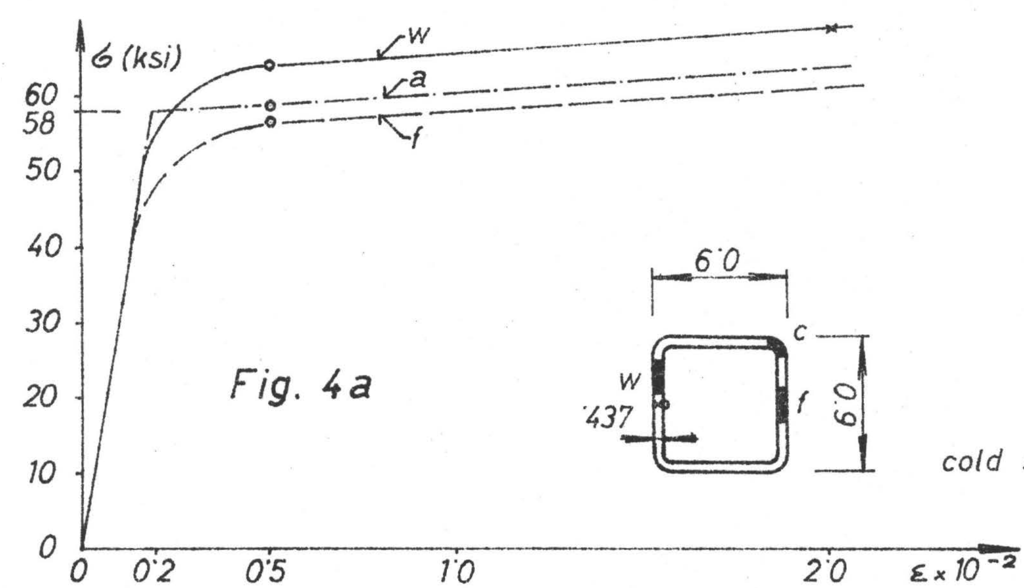

Fig. 4a

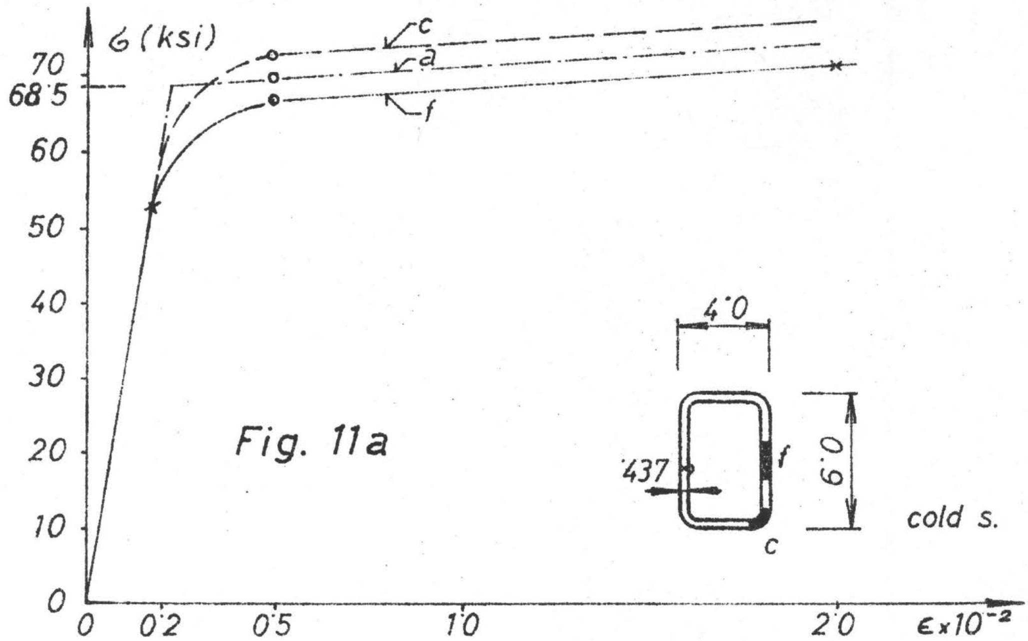

Fig. 11a

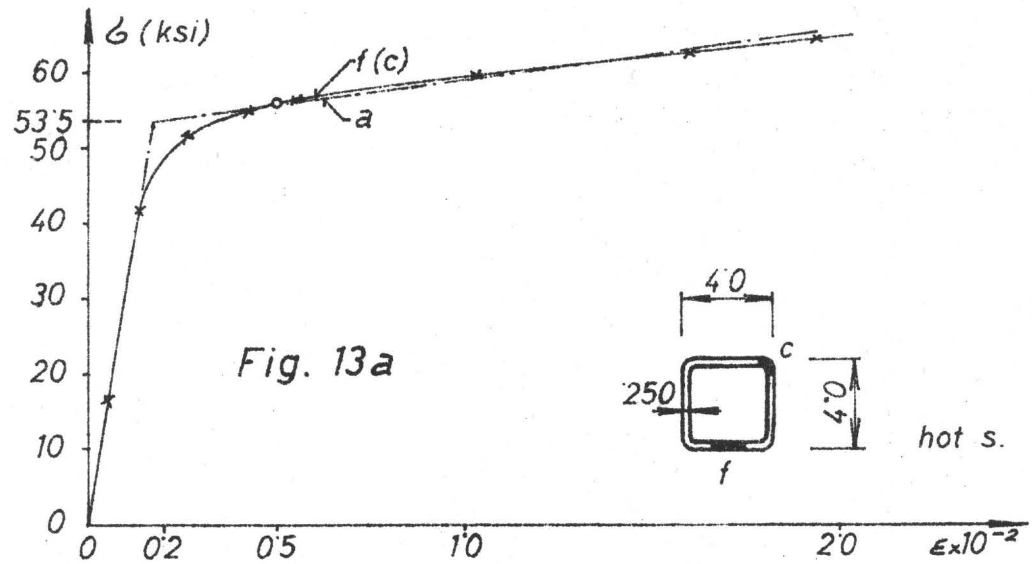

Fig. 13a

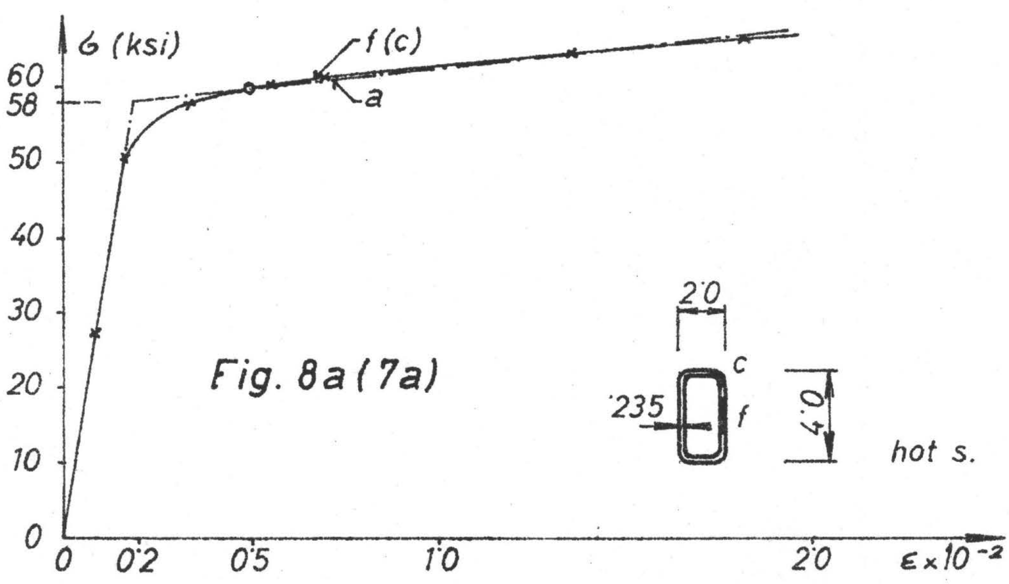

Fig. 8a (7a)

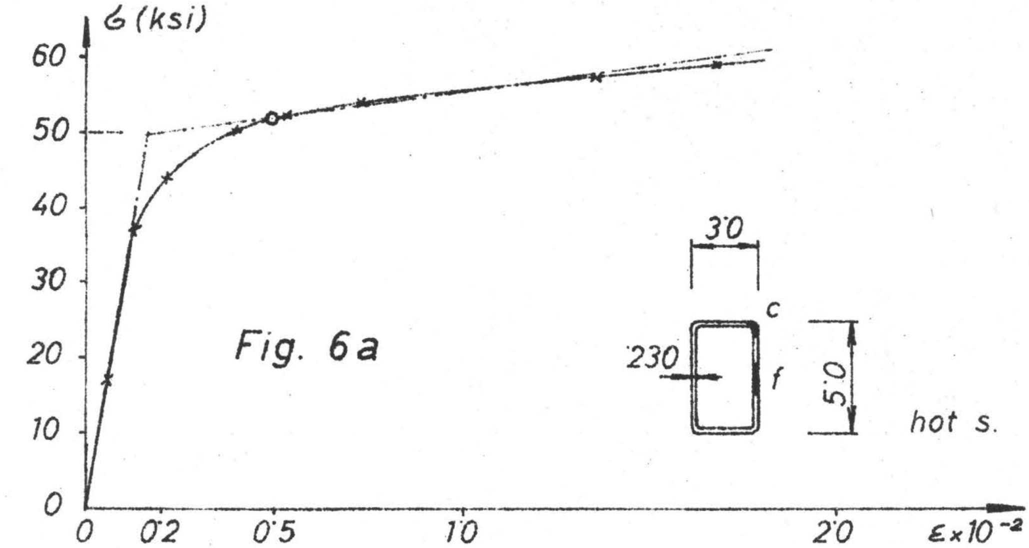

Fig. 6a

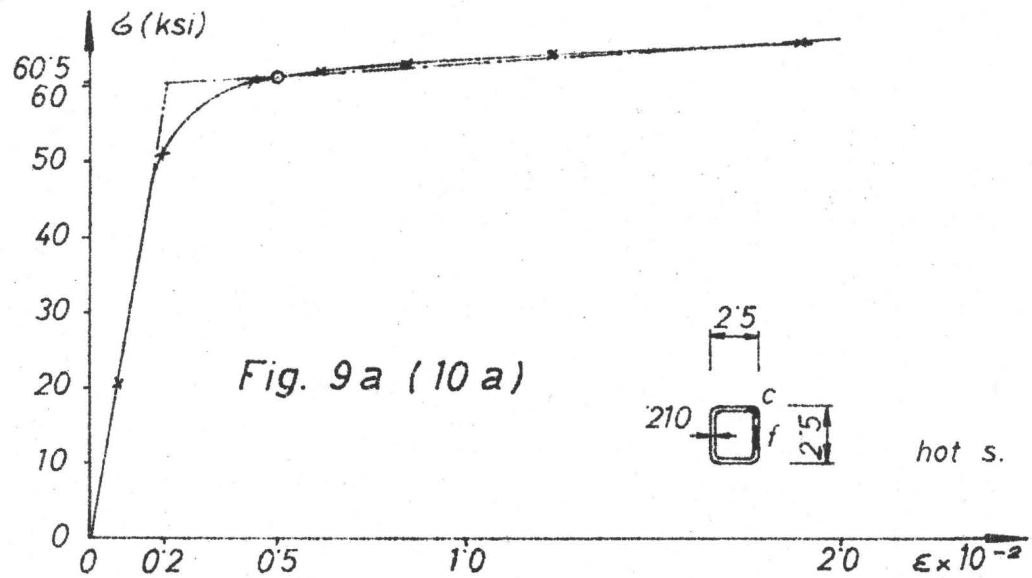

Fig. 9a (10a)

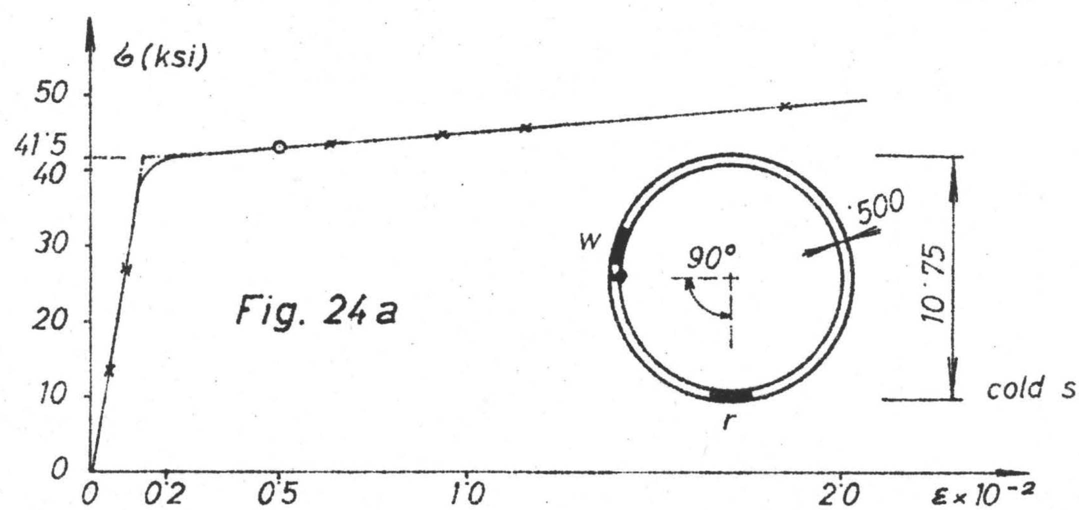

Fig. 24a

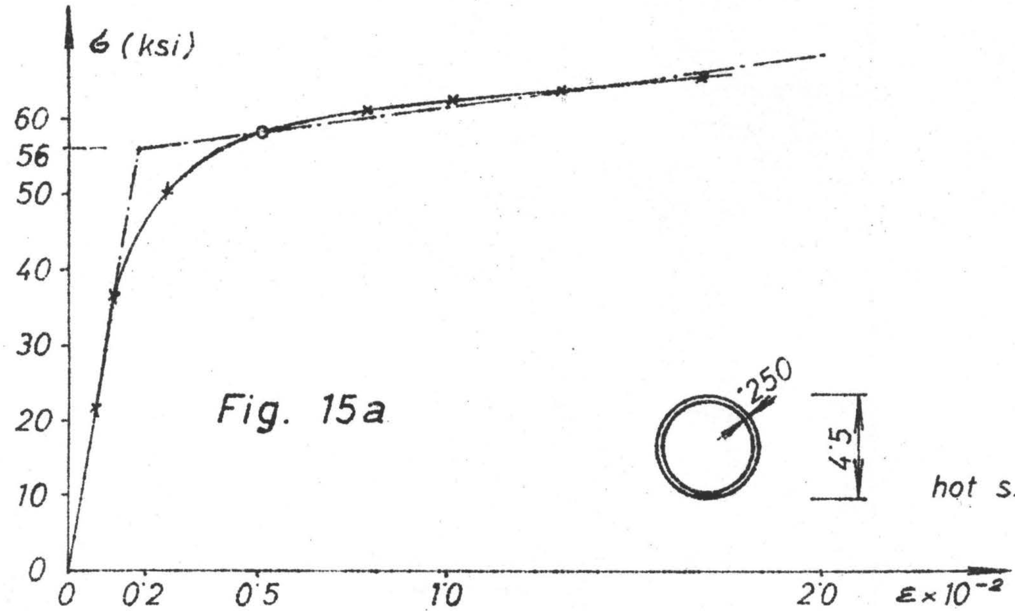

Fig. 15a

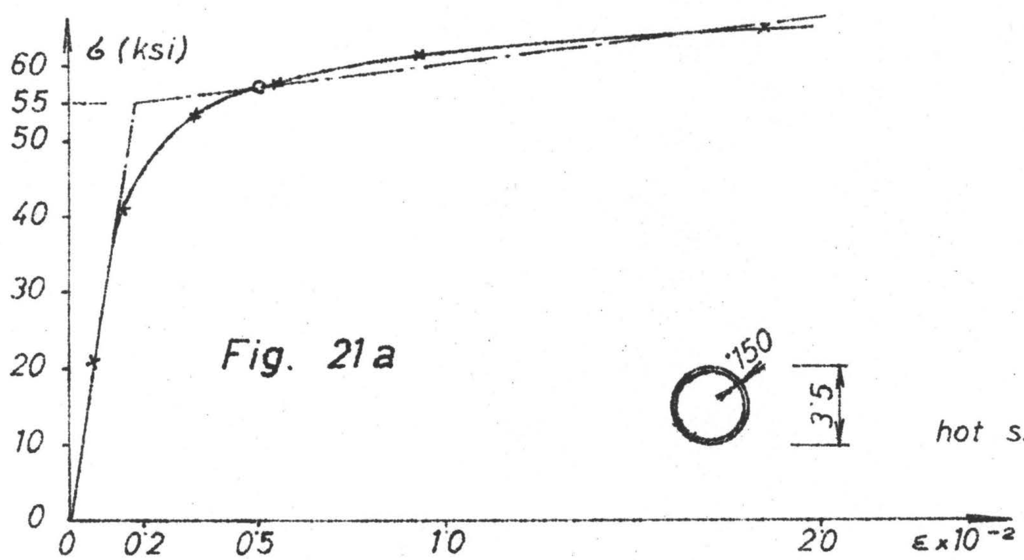

Fig. 21a

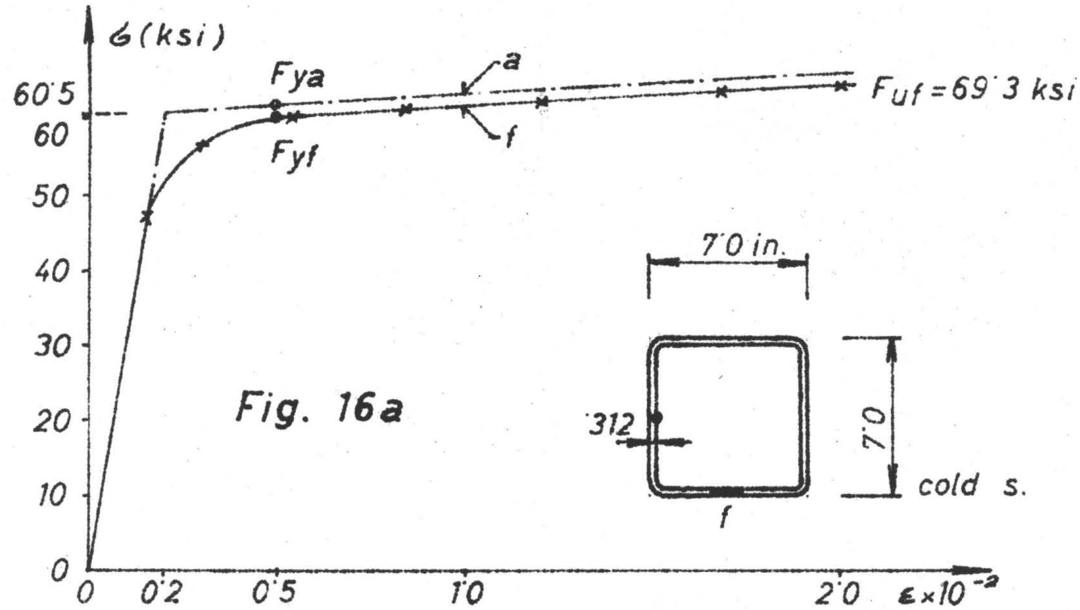

Fig. 16a

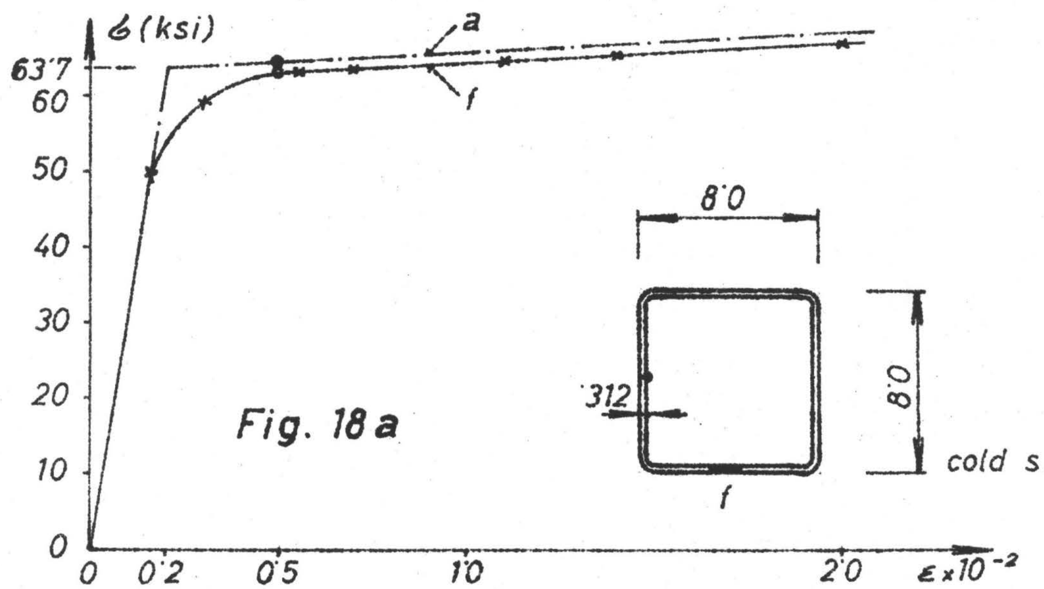

Fig. 18a

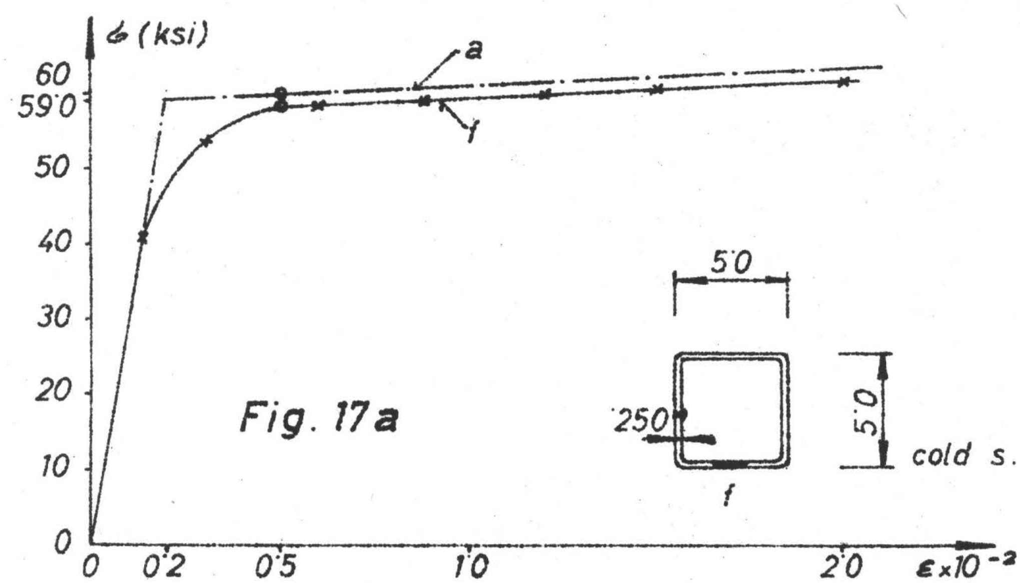

Fig. 17a

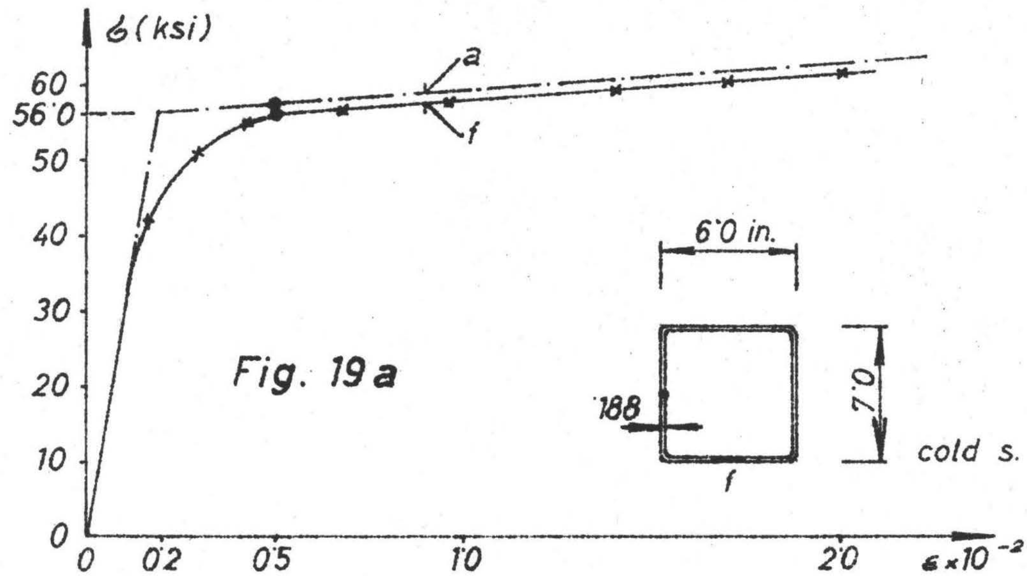

Fig. 19 a

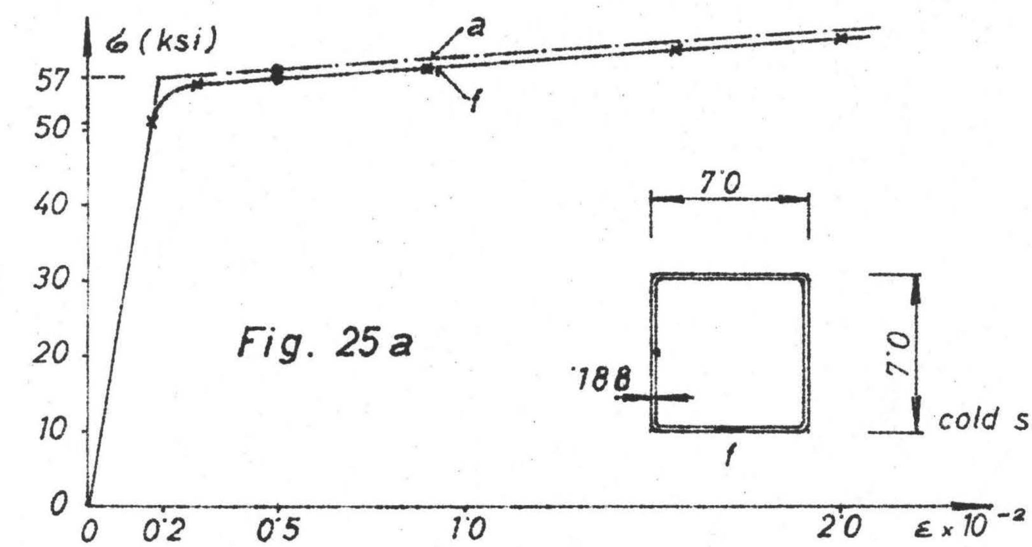

Fig. 25 a

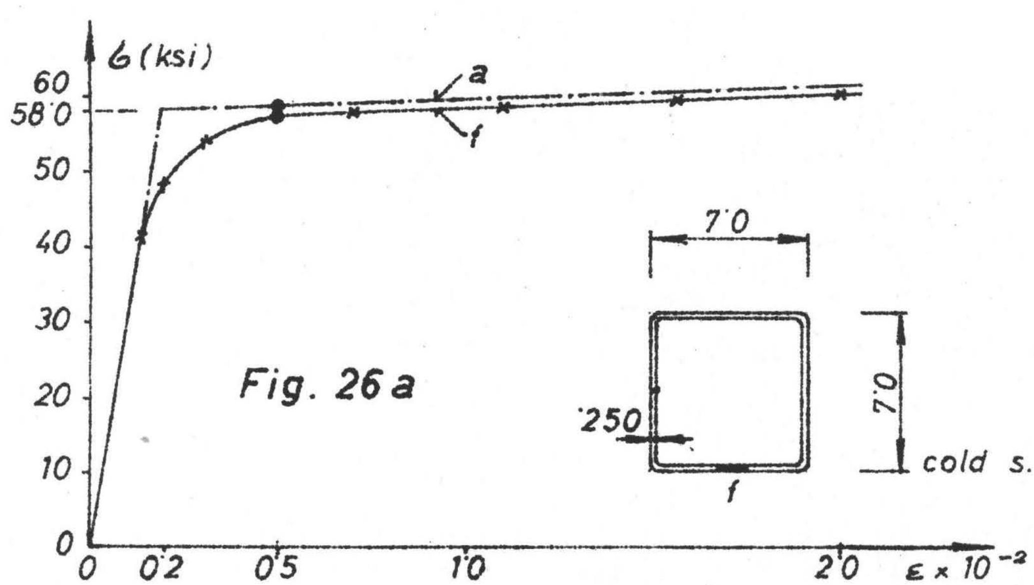

Fig. 26 a

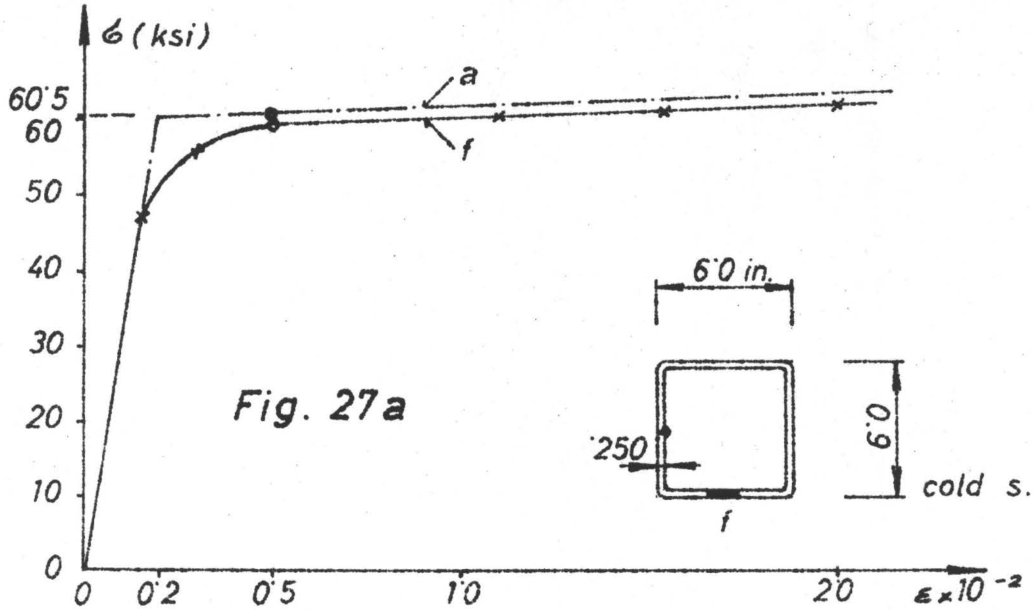

Fig. 27a

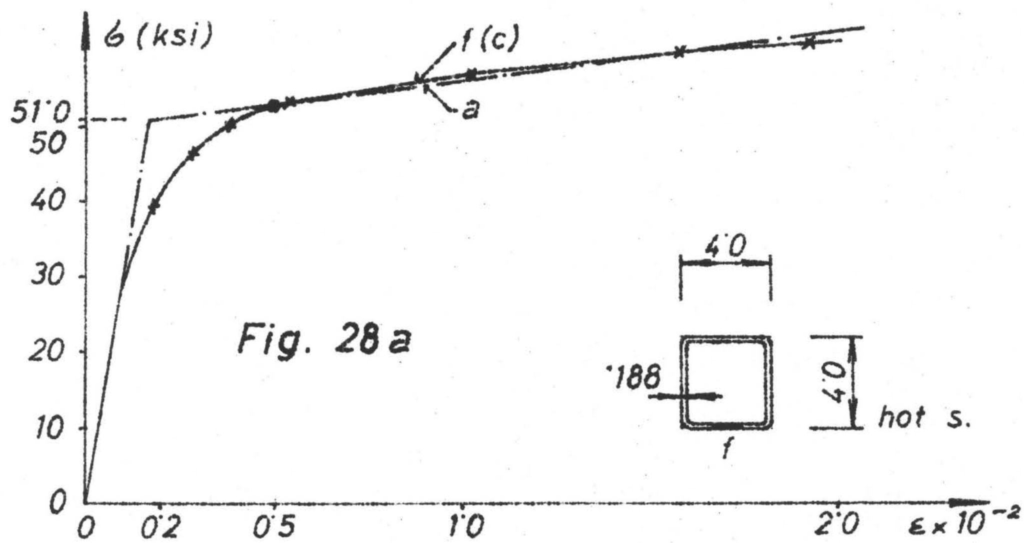

Fig. 28a

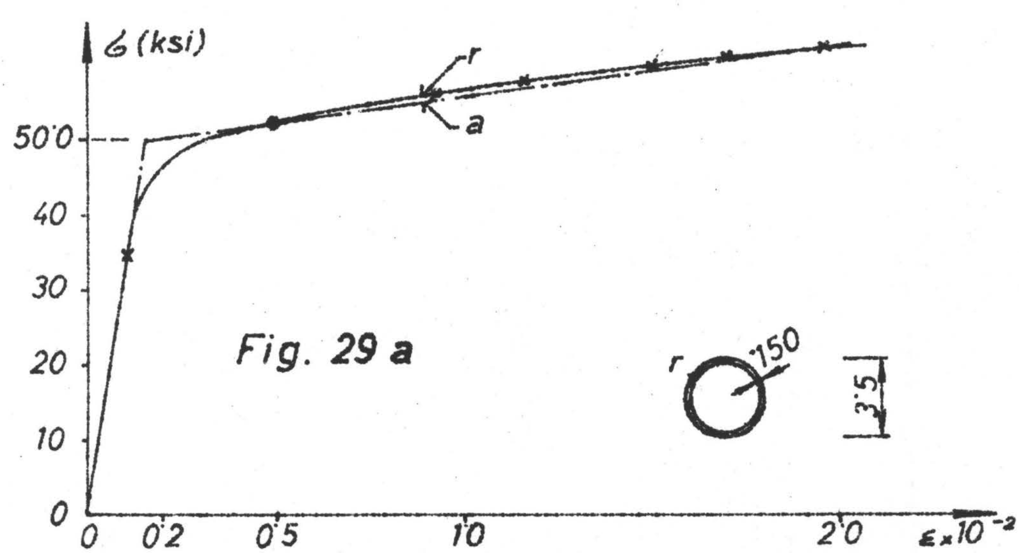

Fig. 29a

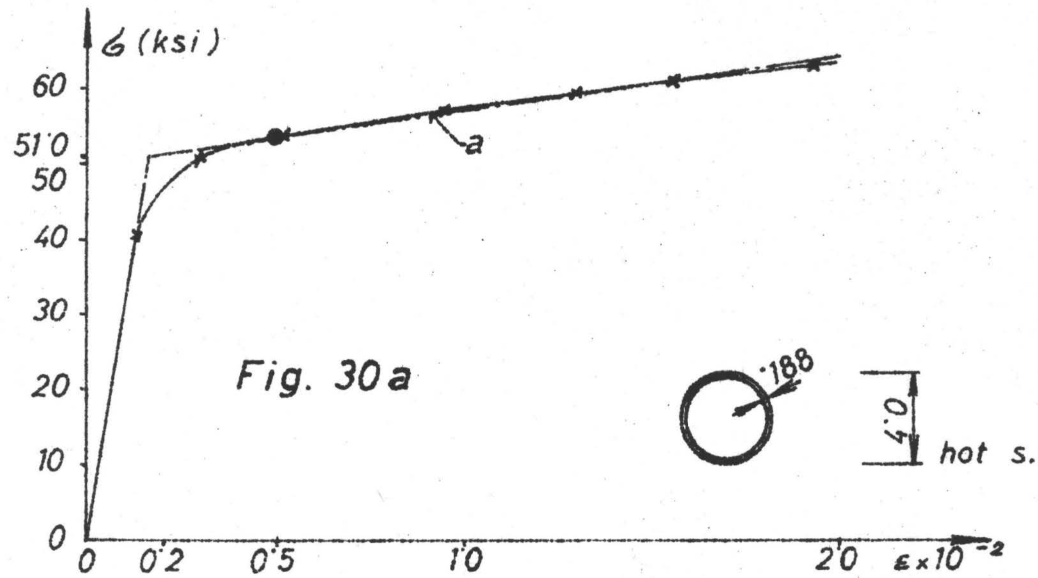

Fig. 30a

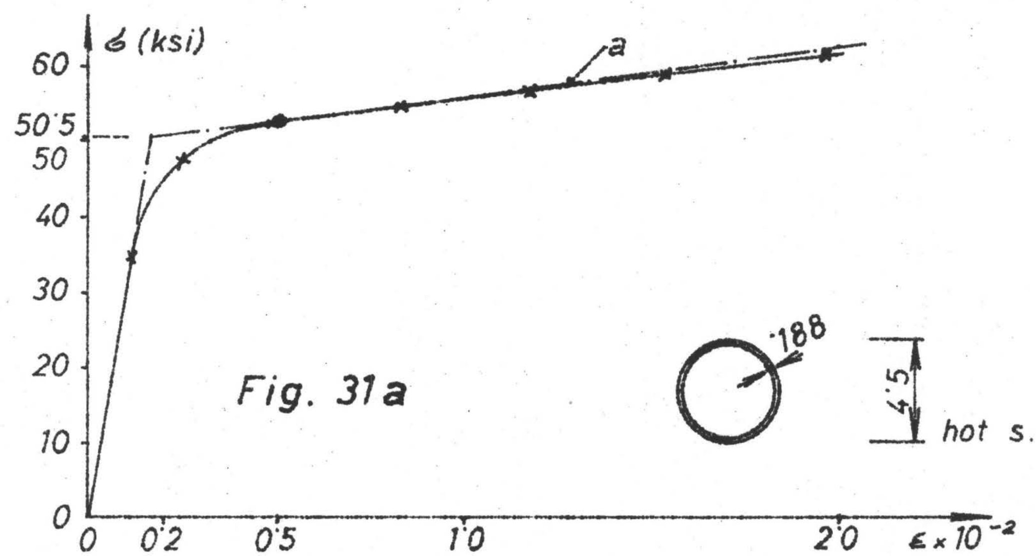

Fig. 31a

FIGURE 3.4 Tensile Test Specimens

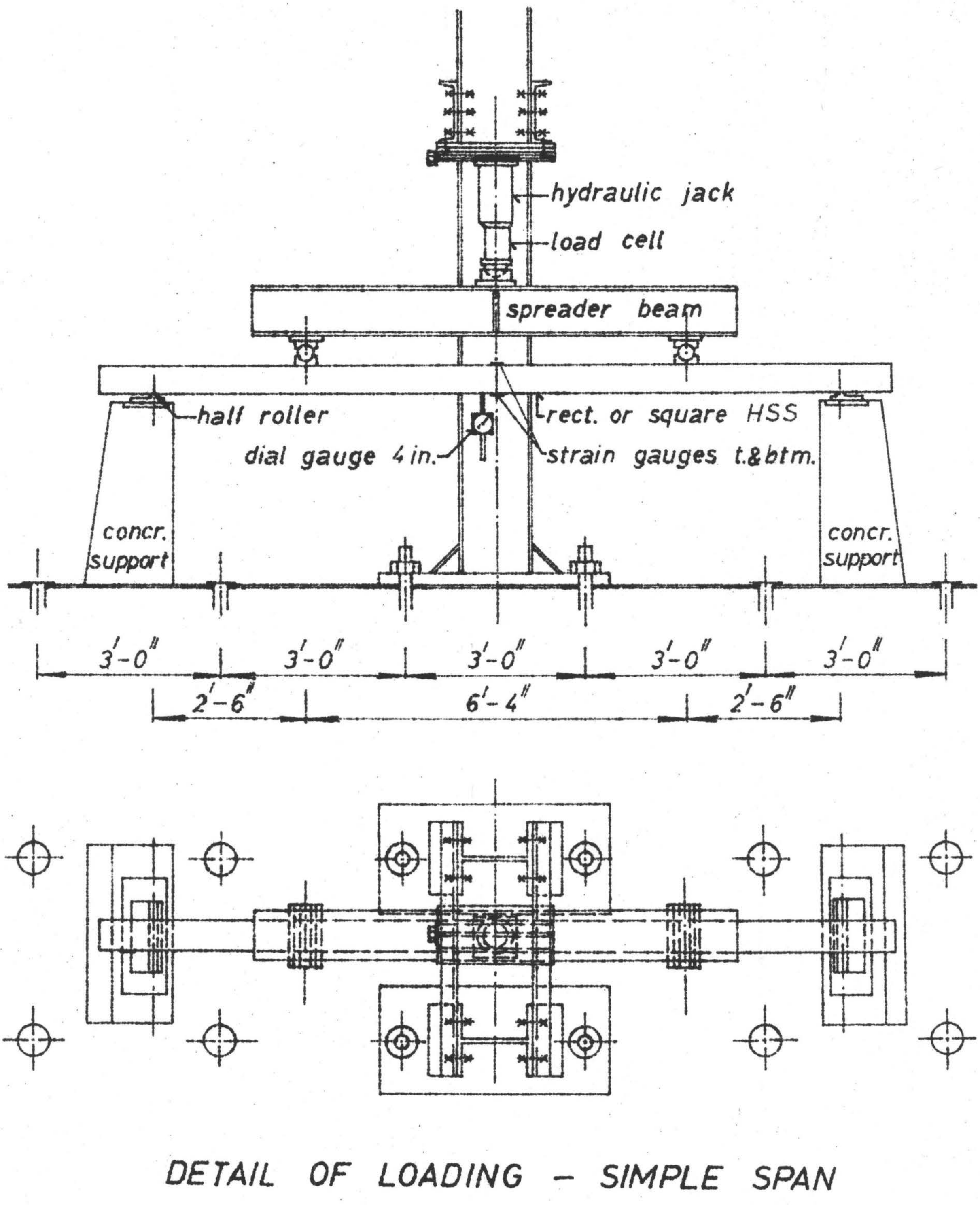

DETAIL OF LOADING – SIMPLE SPAN

FIGURE 3·5

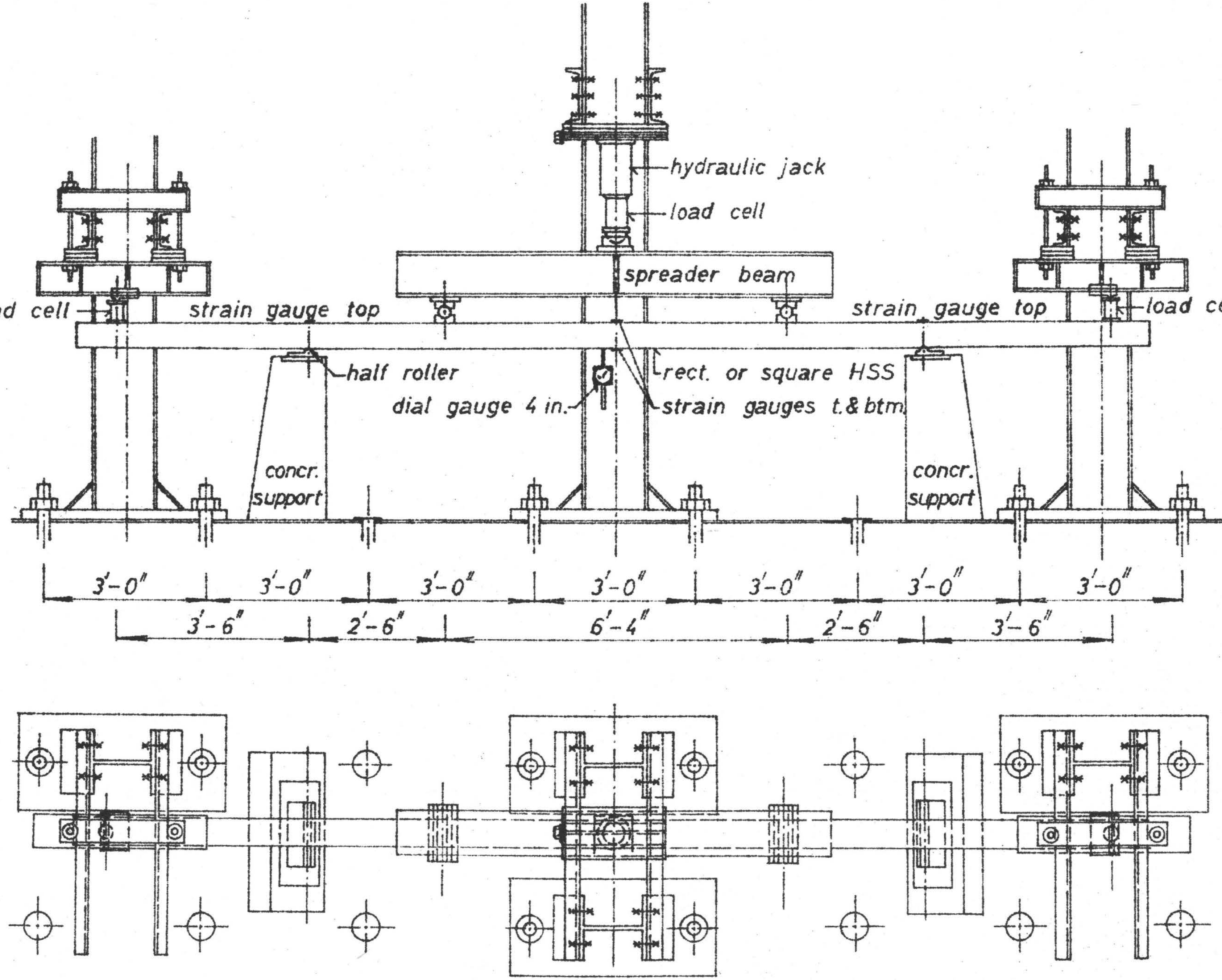

FIGURE 3.6 DETAIL OF LOADING - THREE SPAN BEAM

DETAILS OF CIRCULAR SECTIONS

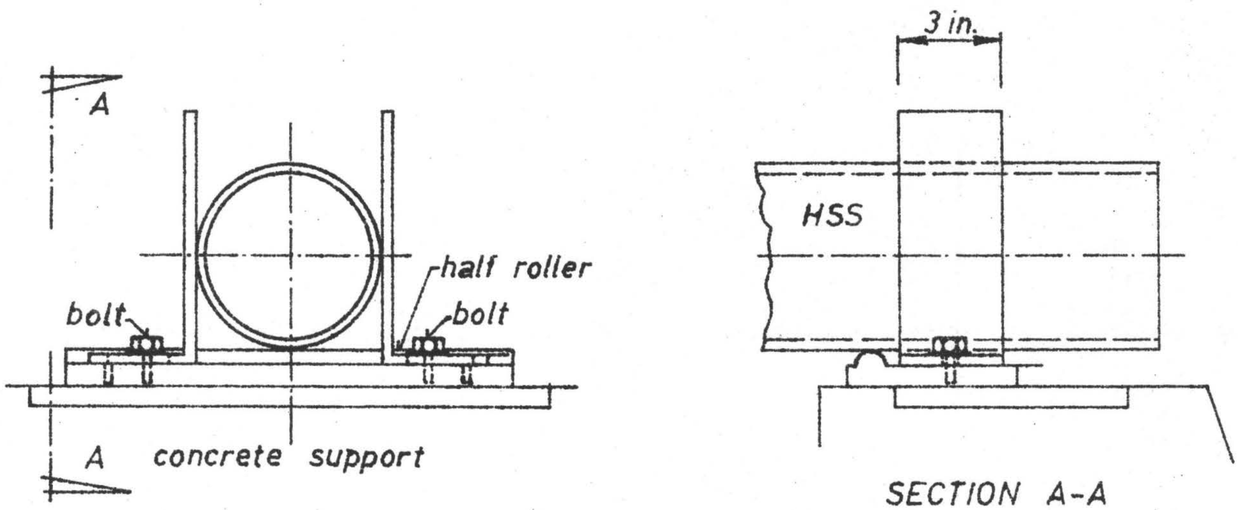

END DETAIL

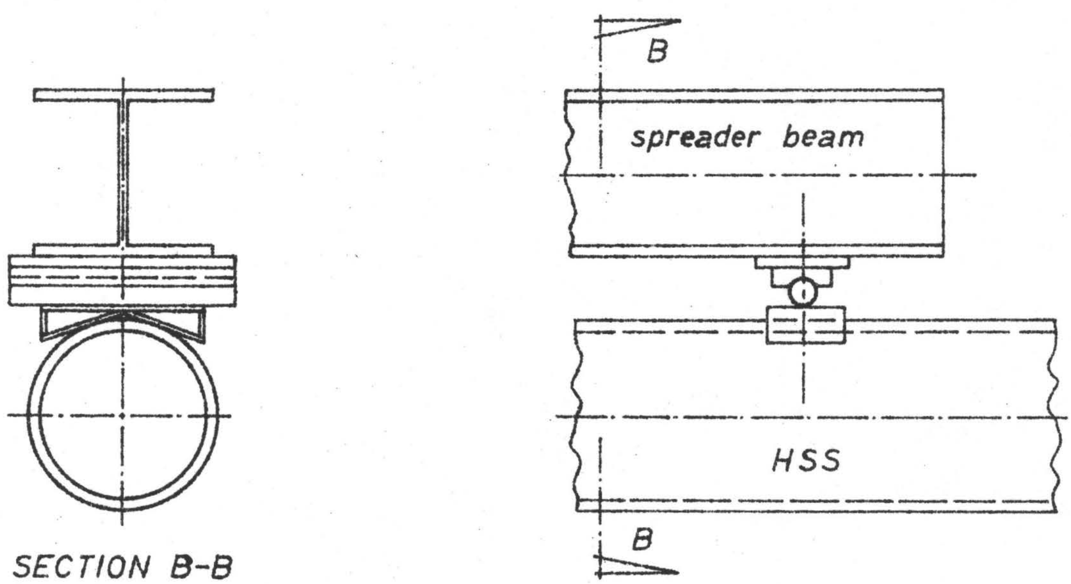

SPREADER BEAM ON CIRCULAR SECTION

FIGURE 3.7

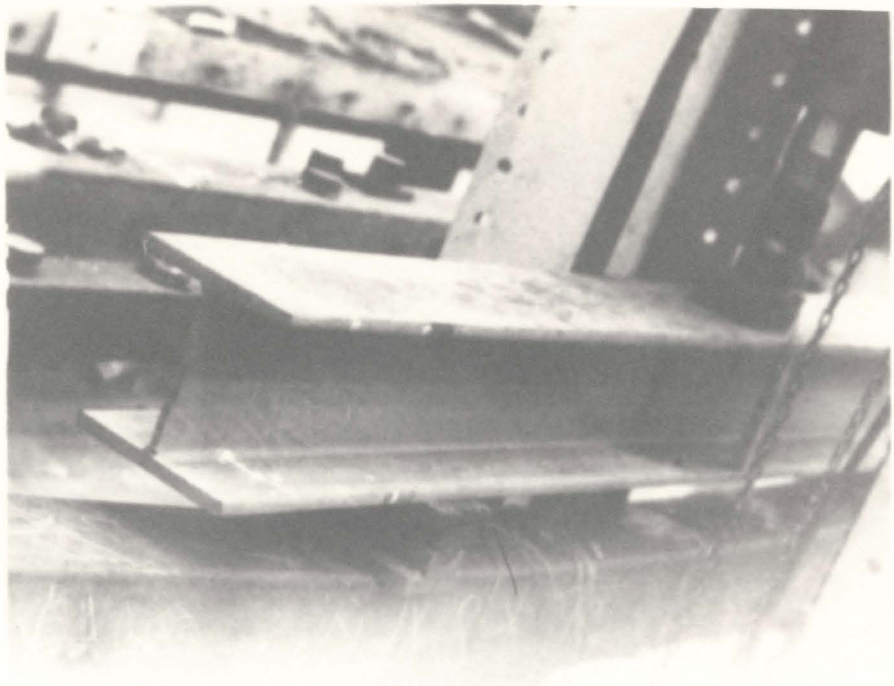

(a)

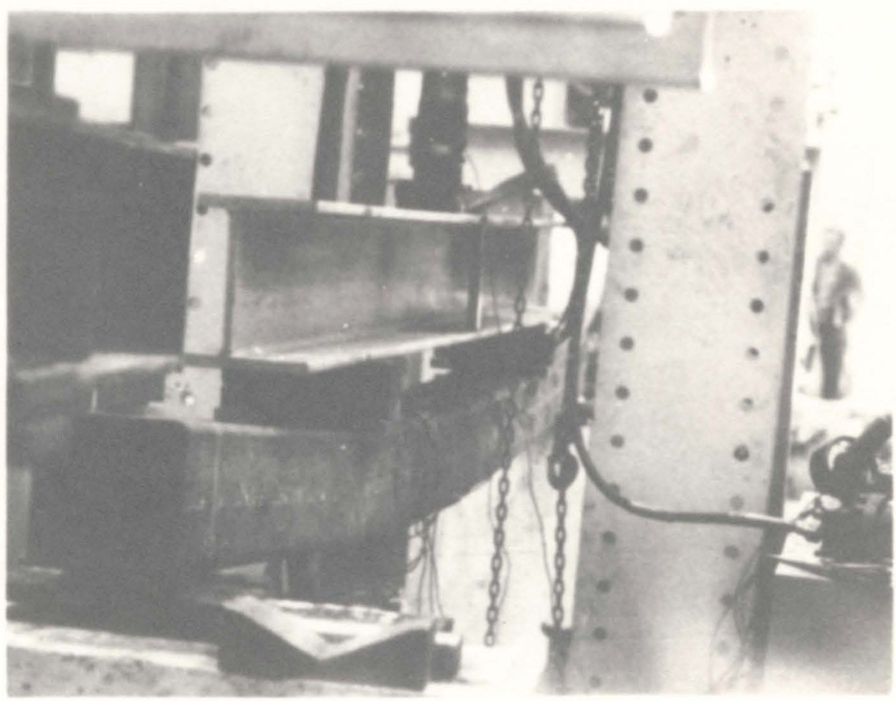

(b)

FIGURE 3.8 HSS-8"x8"x.312 During Testing

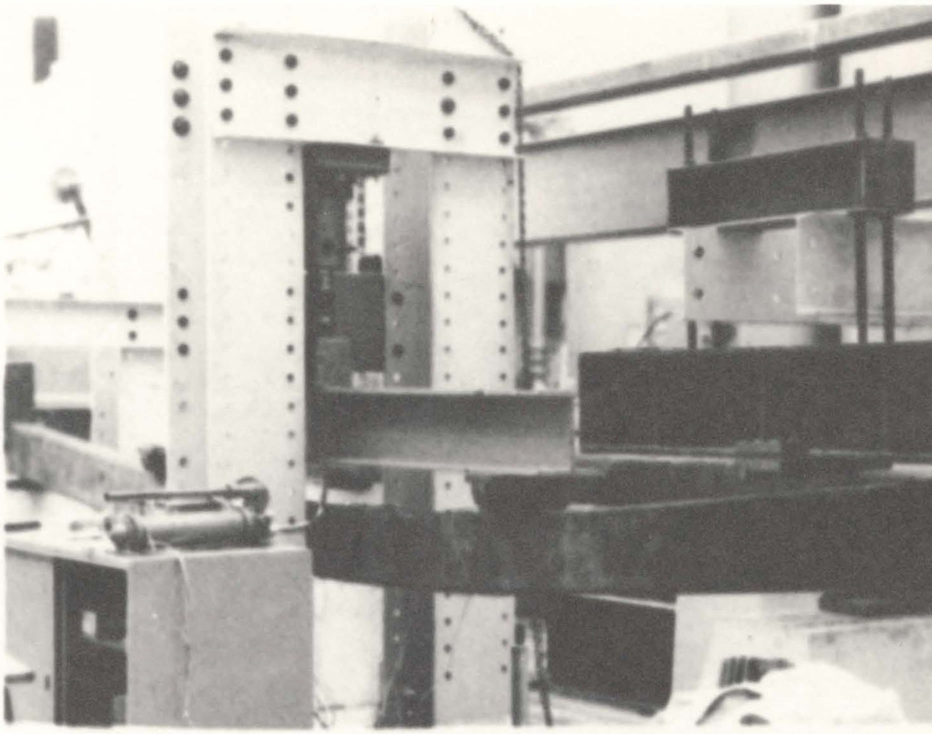

FIGURE 3.9 Overall Test Setup

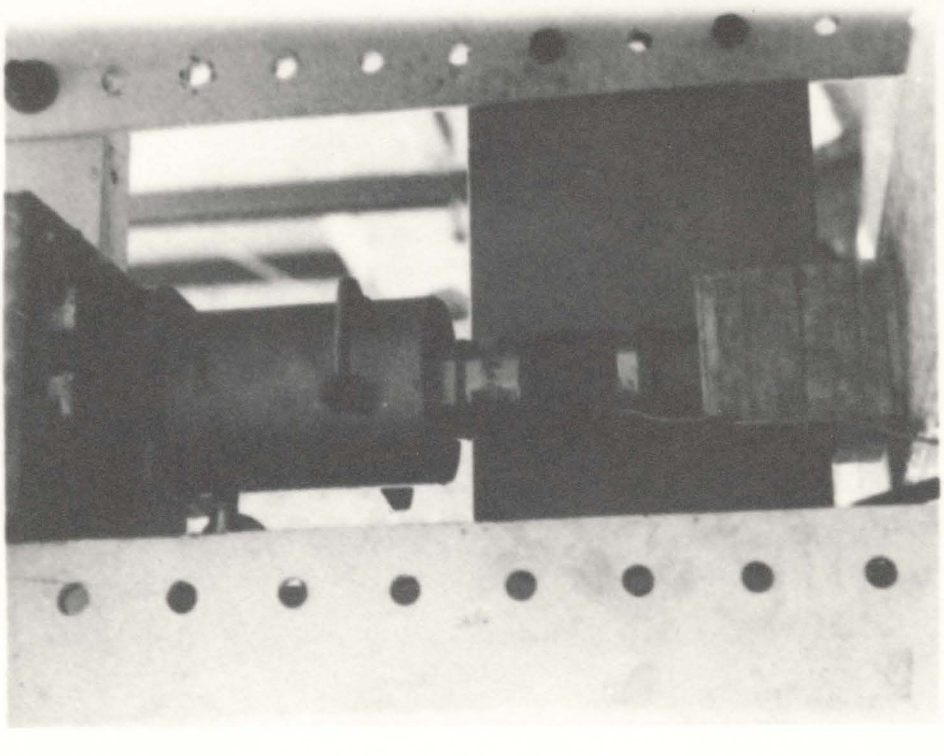

FIGURE 3.10 Loading Jack

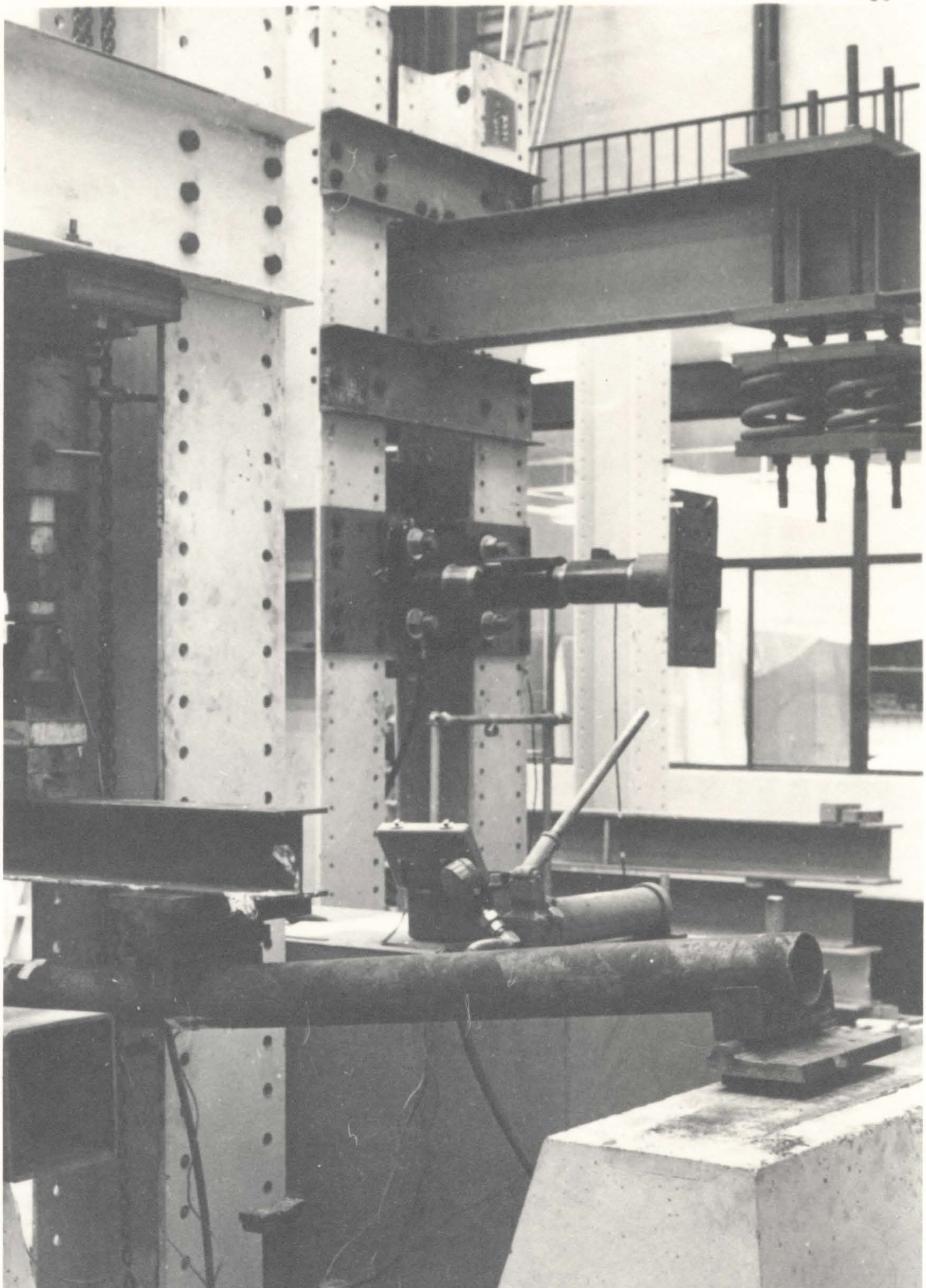

FIGURE 3.11 Test Setup - Front View

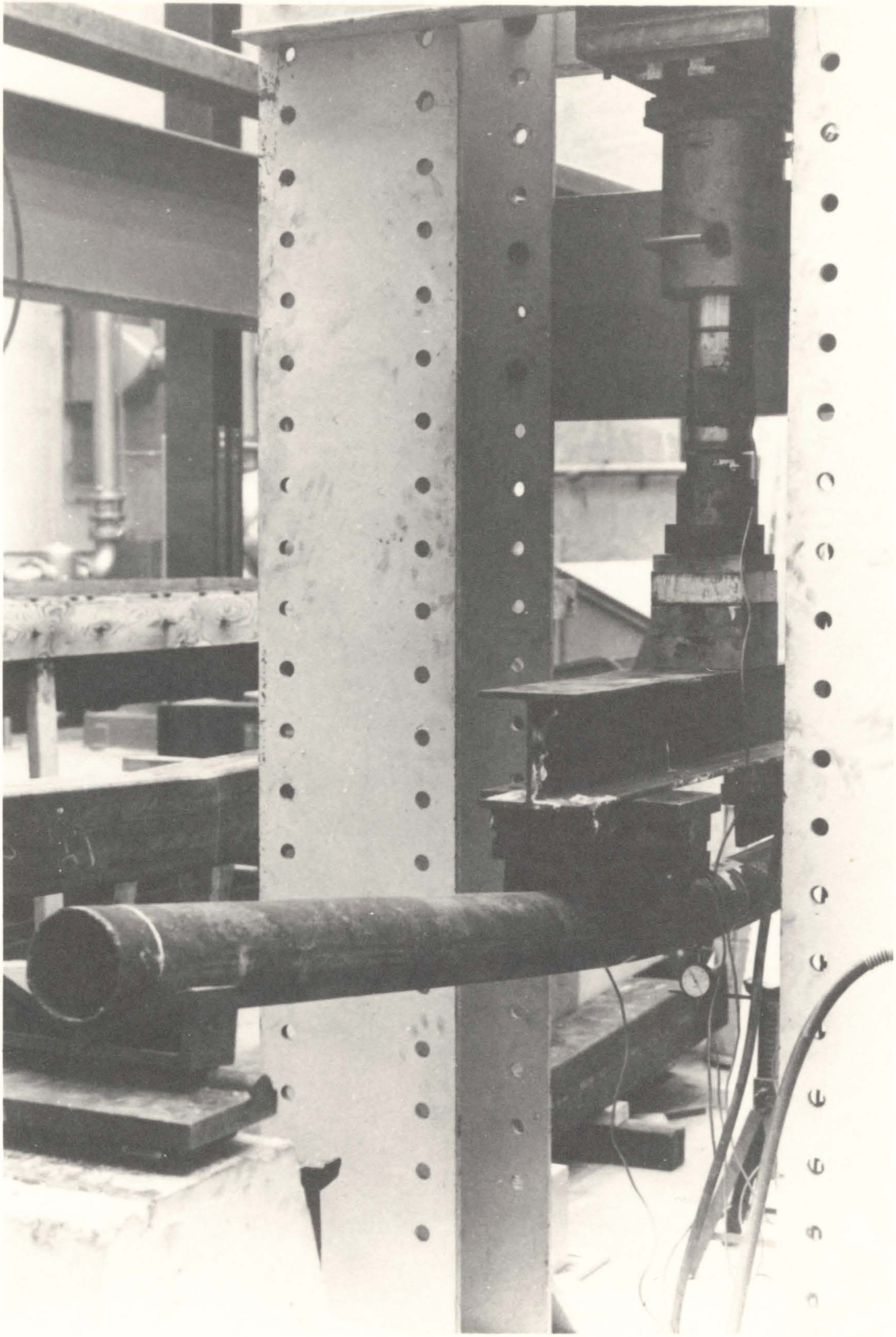

FIGURE 3.12 Test Setup - Top Front View

CHAPTER IV

TEST RESULTS

4.1 Comparison on the Basis of Actual YS of HSS

4.11 Description of Computer Analysis

This comparison was carried out on the basis of actual yield stress of HSS. For each beam the bilinear behaviour simplification of the stress-strain relation as defined in Figures 3(20a, 22a, etc.) was used to relate analytical predictions to experimental results. The values of elastic modulus E, tangent modulus E_{st}, yield stress YS and the cross sectional dimensions were considered for each beam in the analysis to obtain the M-K relation.

The following designations for the calculation of M-K relation are used in the computer program:

W = K curvature

WY = K_y curvature at yield stress

WR = K/K_y nondimensional curvature

ST = ε strain

STY = ε_y yield strain

M moment

MY yield moment

MR = M/M_y nondimensional moment

ER $= E_{st}/E = \tau$ ratio strain-hardening to elastic modulus

S elastic section modulus

F shape factor

The nondimensional M-K relation relating the reduced moment M/MY to this reduced curvature W/WY is calculated by the following equations for:

i) a straight elastic part

$$MR = WR \ ,$$

ii) the case when the flanges are partly plastic

$$MR = WR(1 - \frac{B.D^2}{6.S}) + \frac{B.D^2}{4.S}(1 - \frac{1}{3.WR^2}) \ ,$$

iii) the case when the webs are partly plastic

$$MR = (F - \frac{T.D^2}{6.S.WR^2}) \frac{ER-1}{ER} + \frac{WR}{ER} \ .$$

The maximum elastic strain STY = YS/E and the corresponding curvature and moment are

$$WY = \frac{2.STY}{D}$$

$$MY = YS.S$$

and

$$W = WR.WY$$

$$M = MR.MY \ .$$

For the calculation of the load-deflection curve at midspan for a simple span beam, the designations in the computer program are

$$\begin{aligned} SE &= a \\ SM &= b \end{aligned} \qquad \text{see Figure 2.3(b)}$$

$$PL = \text{load}$$

$$DL = \text{deflection} \; .$$

The loads and the corresponding deflections are computed from equations which are derived in Subsection 2.12(B) to be

$$PL = MR \; . \; \frac{2.MY}{SE}$$

$$DL = WR \; . \; \left(\frac{SE^2}{3} + SE.SM + \frac{SM^2}{2}\right) \; . \; WY \; .$$

The theoretical solution by computer is considered for the compact section (no local buckling considered) without taking account the residual stresses of the given cross-section. The reader is referred to Appendix 1 for further details.

4.12 Comparison with Experimental Results

The results of the analysis are given in Figures 4(1) to 4(31) with the experimental results added for comparison. The tests are numbered according to chronological order of testing. The behaviour predicted by the analysis is shown as the full line with black triangles while the actual experimental behaviour is given by the full line joining the white triangles and squares. Each white triangle and associated white square (where applicable) represents a stage during the test at which data was recorded.

For three span beams it should be noted that for a given stage of loading the curvature associated with a support position, will exceed that at midspan. Figure 4(1) for example shows that the last recorded data for M-K correspond to a load of P=132 kp in which the moments over the support and at midspan are 950 in-kips and 1000 in-kips respectively but with considerably different curvatures.

There is good correlation between test results and analytical predictions for those sections in which local buckling did not occur until well into the plastic range. Separate subsections follow describing well behaved sections and those undergoing local buckling.

4.13 Results of Sections Without Local Buckling in Tests

Results for sections without local buckling are shown in Figures 4(4,6,8,9,11,13,15,16,17,21,22,24,29,30 and 31) for the simple span of rectangular, square and round sections. The three span experimental results free of local buckling are shown in Figures 4(7,10,12). These former two sections were hot rolled while the latter was cold rolled. All exceeded the predicted moment capacity somewhat at large curvature K. Thus, these sections would be classified as compact in plastic design.

The following observations are pointed out from these test results:

(1) There is considerable influence from residual stresses of cold formed sections in the neighbourhood of the first yielding -- see for example Figures 4(4,16,17,18,19 etc.).

The proportional limit stress can be taken as approximately half of the yield stress.

(2) The repeated loading in the plastic region appears to have an influence on the increase of the moment capacity at large curvature K. This can be seen in Figures 4(4,8,11 and 12) which represent a few cycles of repeated loading.

In the tests a jack with only 3 inches of travel was used which was not enough to obtain the required rotation capacity. For that reason, unloading of the beam was undertaken followed by the inserting of steel plates between the jack and the beam. Loading was then continued. It was possible by this means to obtain the required plastic deformation of the beam.

(3) The load-deflection curves show the maintenance of the predicted loads at the region of large curvature. Only in the cases of repeated loading were the loads significantly greater than the predicted values.

(4) The bearing surface of HSS is a very important condition for design. Figure 4(5) of rectangular HSS and Figure 4(14) of a round show the experimental M-K relations for three span beams. These sections can be classified as compact in spite of negative moments over the interior

supports being maintained at a value less than the moment capacity M_p. For these cases of point bearing, local buckling was observed on the bearing surface of HSS.

A four inch wide plate was inserted under the loading and bearing points of the beams for subsequent tests. In the case of square and rectangular HSS plates were used following test No. 5 while for circular HSS they were used after No. 14.

It is clear from the tests that the behaviour of cold rolled HSS is sensitive to the bearing stresses imposed on loading. Further study is deemed necessary to couple the width to thickness ratio of a compression flange with the bearing stress intensity imposed on that flange.

4.14 Results of Sections With Local Buckling

The experimental moment-curvature relationships for all 8 beams tested with local buckling occurred are summarized in Figure 4.32. The flange slenderness ratios b/t have been adjusted by the factor $\sqrt{YS/50}$ to bring the results for sections having different yield stress levels to a common base.

The "rotation capacity" of the beam has been defined as $\Theta = K/K_p - 1$, in which K is the curvature at which the moment begins to decrease relative to the predicted M-K relation for the section without local buckling. The point at which the drop was observed is indicated on each curve by a vertical arrow. K_p is the curvature which would correspond to a moment

M_p if the beam were to remain completely elastic to that capacity. The vertical dash-dot above the idealized transition to plastic response indicates K_p in Figure 4.32. The last column of the table in this figure is the ratio of the maximum buckling moment to the calculated yield moment. These ratios for compact sections in working stress design are higher or equal to their associated shape factors F which are written in brackets.

Figure 4.33 is a plot of the rotation capacity, Θ, versus an equivalent flange slenderness ratio which takes into account the buckling moment and shape factor from Figure 4.32. The highest flange slenderness ratio, when the ratio of the buckling moment to the yield moment is equal to the shape factor, is the limiting b/t value for compact sections in working stress design. This limiting b/t ratio for YS of 50 ksi is approximately 29.5 and for the different yield stresses it can be rewritten as $b/t \leq 210/\sqrt{YS}$.

For non-compact sections, the buckling moment has to reach the value of yield moment without the presence of local buckling. From this assumption the limiting b/t value for YS of 50 ksi is approximately 34.5. The corresponding limiting ratio for different yield stresses assuming the same form as above is $\frac{b}{t} \leq \frac{245}{\sqrt{YS}}$.

For a more exact limiting b/t value in working stress design more tests are necessary in the range of flange slenderness between 28 and 36 for a yield stress of 50 ksi.

4.2 Comparison on the Basis of a Guaranteed Minimum YS for HSS

In this comparison it was assumed that the sections will buckle for a yield stress of 55 and 50 ksi with the same moment-curvature relationships as are given by the experimental curves. That is, if a moment-curvature plot is known for YS=55 ksi, it is assumed that this curve can be translated downwards by the appropriate ratio 50/55 for a postulated YS=50 ksi. This assumption is based on tests 20 and 23 in Figure 4.34 which pertain to a 10x10x.375 HSS each giving rise to a different YS value. The full line with the white triangles is the experimental M-K relation and will be related to the yield stress of the flat part of the compressive flange (YS^f = 55.3 ksi for test No. 20). The yield stresses therefore were 55.3 and 61.8 ksi respectively. The similarity in the response curves is shown in Figure 4.34 which give rise to identical rotation capacities when related to the same flange yield stress (55 ksi). Figures 4.34 and 4.36 are similar in that they indicate the influence of flange slenderness ratio on the plastic rotation capacity.

Figure 4.36 includes both 50 ksi and 55 ksi "contours" to relate yield stress to rotation capacities for the numbered sections. The dot-and-dashed line is for 55 ksi and the dashed line is for 50 ksi. By simple plastic theory the levels can be determined for plastic moments with yield stresses of 55, 50 and 42 ksi. The rotations K for the yield stresses of 55 and 50 ksi can be found when these curves drop below the determined levels of M_p^{55}, M_p^{50} and M_p^{42}.

A section with a guaranteed yield stress of 55 ksi and a b/t > 22.7 will generate "contours" for 50 and 42 ksi which can be used for prescribing a rotation capacity. The 55 ksi curve will just touch the constant moment M_p^{55} line and therefore does not provide a rotation capacity. See for example test No. 20 in Figure 4.36. Similarly a section with YS=50 ksi and a b/t > 22.7 will generate only a contour of 42 ksi which can be used in plastic design.

It should be noted that for b/t < 22.7 the guaranteed minimum yield stress may be used in simple plastic design for the same stress level. For the required plastic rotation capacity Θ of 4, this limiting b/t ratio will be between 20 and 22.7 which is given by tests No. 27 and 20 in Figure 4.36.

4.21 Limiting b/t Values for Working Stress Design

The results of rotation capacities are summarized in the table on the right of Figure 4.34. The flange slenderness ratio is given for a yield stress of 55 ksi by comparisons with this level of yield stress. Only for No. 28 was an adjustment by the factor $\sqrt{50/55}$ needed. The last column is the ratio of buckling moment of compression flange to plastic moment. Assuming this ratio is close to the value of 1.0, it can be proposed <u>in working stress design</u>, that a section qualifies as <u>compact</u>, if the projecting elements of the compression flange have a width-to-thickness ratio not exceeding $210/\sqrt{YS}$.

The limiting b/t value for non-compact sections is given by the condition of an equality of $M_b{}^f$ and M_y and it cannot exceed the value of $245/\sqrt{YS}$. These limiting b/t values in working stress design are shown in Figure 4.35.

The corresponding value of the inelastic rotation capacity approximately equal to 2.0 will be quite satisfactory for compact sections of HSS in working stress design.

4.22 Limiting b/t Values for Plastic Design

The limiting b/t values for plastic design of HSS for minimum quaranteed yield stress of 55 and 50 ksi are shown in Figure 4.37. The rotation capacities from Figure 4.36 are plotted against the flange slenderness ratios for different yield stresses in Plastic Design.

The criterion used is that a minimum plastic rotation of 4 times, that corresponding to M_p, is needed before the moment capacity of the section drops below M_p. The requirement of reaching the plastic moment is satisfied by this plastic rotation and can be seen from the ratios of $M_b{}^f/M_y$ in Figure 4.37.

The analysis of the three-span continuous beams shown in Figures 2.2, 2.7 and 2.8 can be used to estimate a practical maximum for the required rotation capacity of plastically designed continuous beams. The largest required plastic hinge rotation for a three-span beam such as that shown in Figure 2.8 is 0.425 M_pL/EI. The corresponding plastic rotation capacity to this value is approximately 4. In more complex structures the theoretical hinge angle required to form a mechanism may be rather large. However, for such structures, a load close to the ultimate can be attained with much smaller hinge rotations (see Figure 2.13). It was concluded in Subsection 2.12(D) that a rotation capacity requirement of 4 is considered satisfactory for design purposes for a majority of structural types.

Thus, from this requirement it is found that the ratios of b/t for different yield stresses in plastic design can be given in the form shown in Figure 4.37.

The limiting b/t value <u>for plastic design in the same level of yield stress</u> from this figure can be recommended as

$$\frac{b}{t}\sqrt{\frac{YS}{55}} \leqq 20 \qquad \text{(Figure 4.37a)}$$

$$\frac{b}{t} \leqq \frac{150}{\sqrt{YS}} .$$

$$\frac{b}{t}\sqrt{\frac{YS}{50}} \leqq 21 \qquad \text{(Figure 4.37b)}$$

Figure 4.38 shows the bent square and round hollow structural sections after testing. The square section buckled into the shape as shown in this photograph. The series of sections after testing appear in Figure 4.39.

FIGURE 4·1 to 4·31 Results of Test and Theory

No.	H.S.S.	R (in.)	S (in.³)	Z (in.³)	YS (ksi)	ET (ksi)	b/t
1	6·0 x 6·0 x ·437	·875	15·42	18·90	52·0	320·	9·8

Numbers for test data correspond to given loading

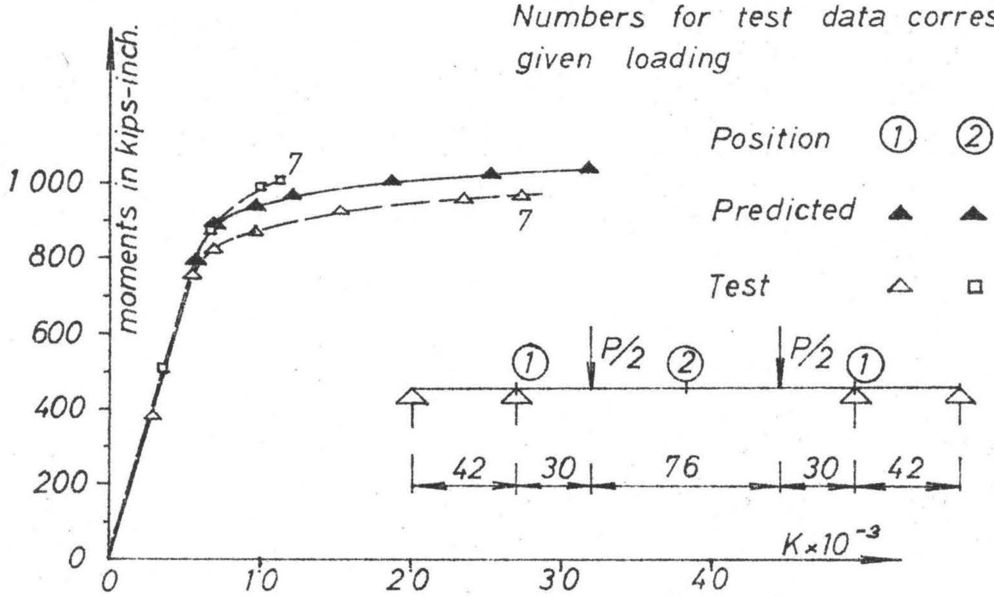

(4·1)

No.	H.S.S.	R (in.)	S (in.³)	Z (in.³)	YS (ksi)	ET (ksi)	b/t
2	6·0 x 6·0 x ·188	·376	7·94	9·26	56·0	357·	27·9

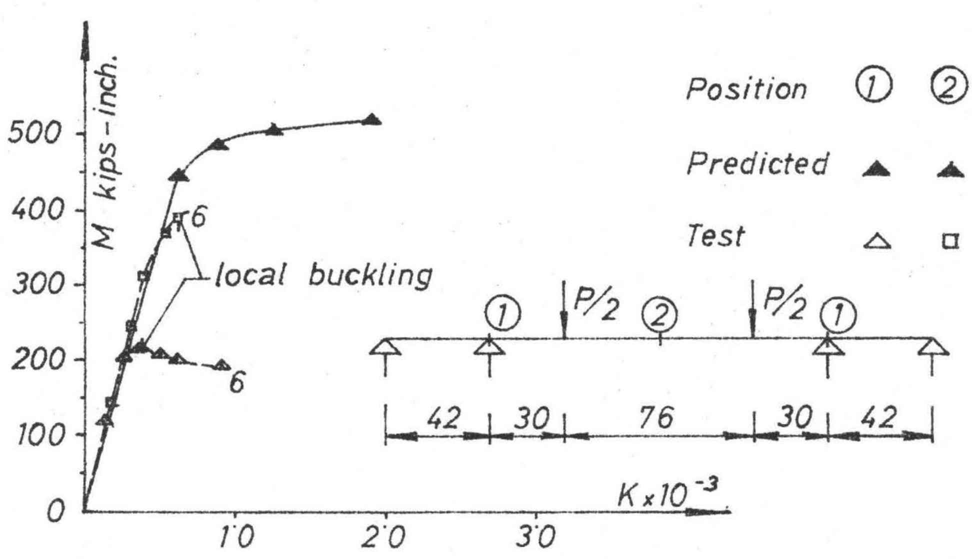

(4·2)

No.	H.S.S.	R (in.)	S ($in.^3$)	Z ($in.^3$)	YS (ksi)	ET (ksi)	b/t
③	6.0 × 6.0 × .188	.376	7.94	9.26	56.0	357.	27.9

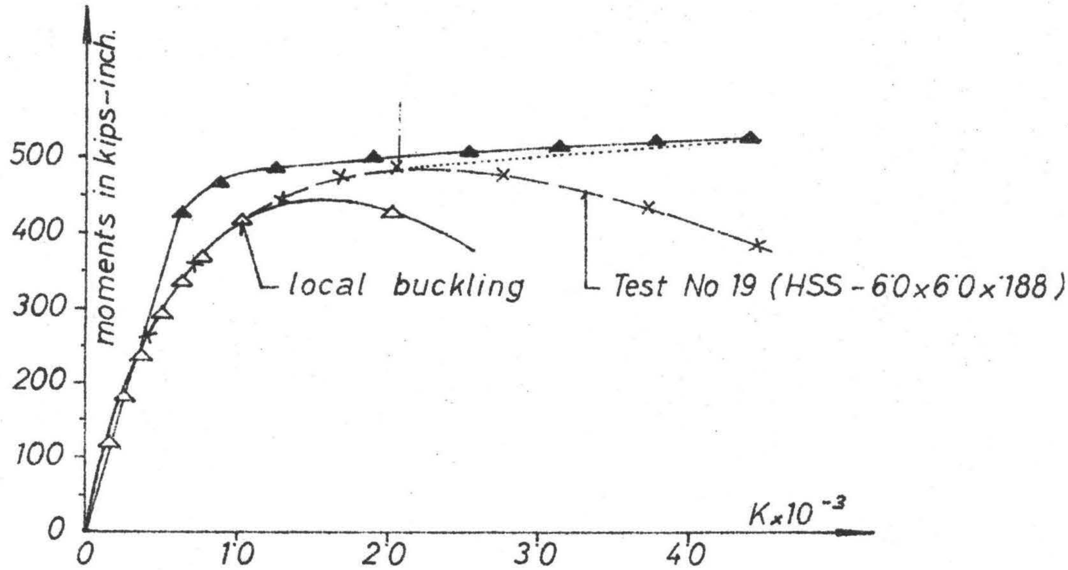

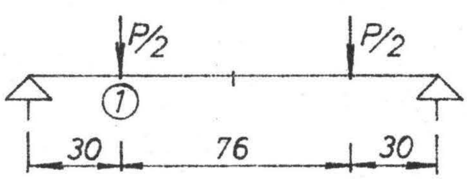

Predicted ▲

Test △

Bearing on H.S.S.

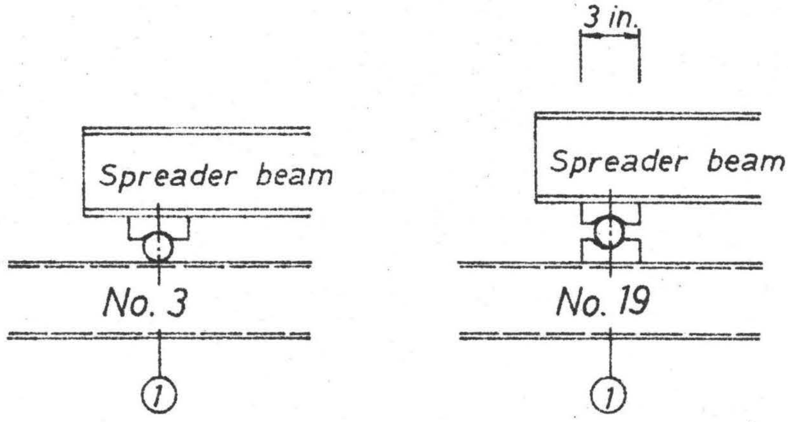

(4.3)

No.	H.S.S.	R (in.)	S (in.³)	Z (in.³)	YS (ksi)	ET (ksi)	b/t
4	6·0 × 6·0 × ·437	·875	15·42	18·90	58·0	320·	9·8

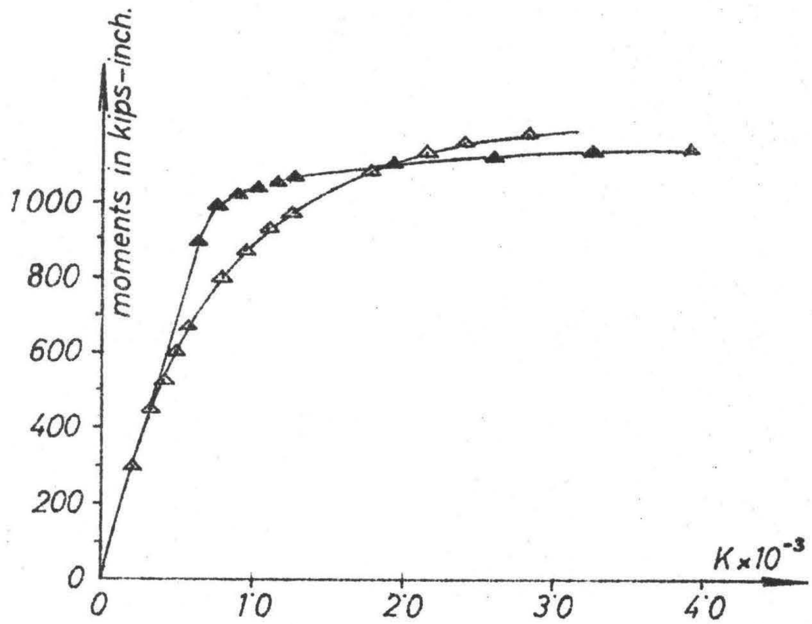

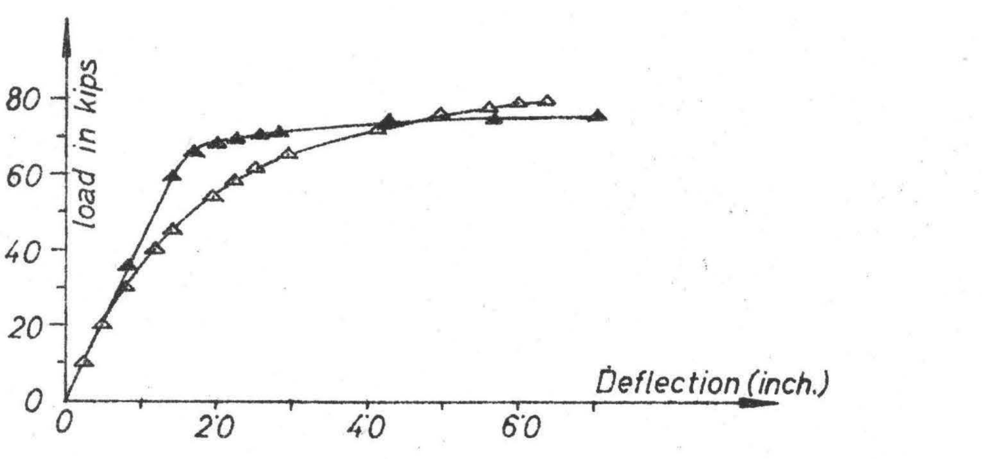

No. Local Buckling

R.S.

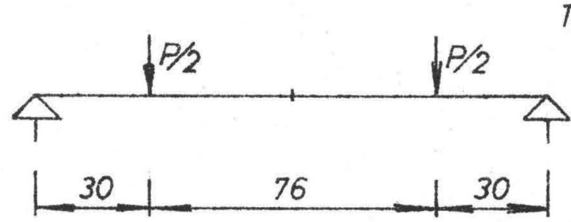

(4·4)

No.	H.S.S.	R (in.)	S (in^3)	Z (in^3)	YS (ksi)	ET (ksi)	b/t
(5)	5·0 × 3·0 × ·230	·345	4·33	5·42	50·0	683·	10·0

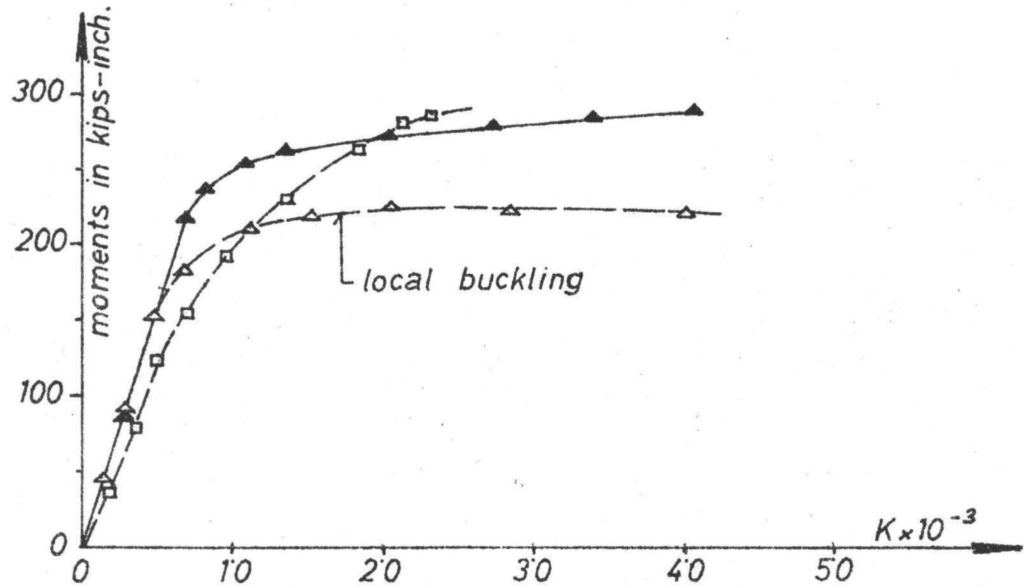

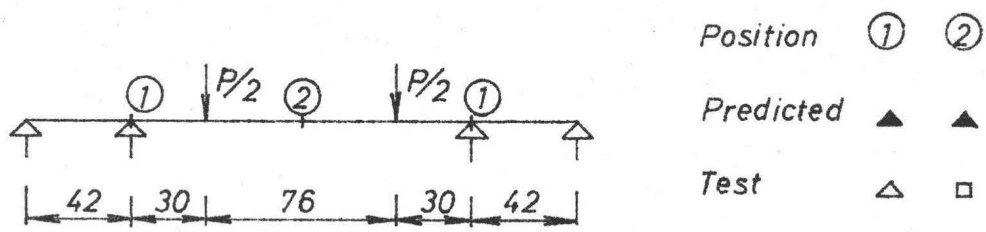

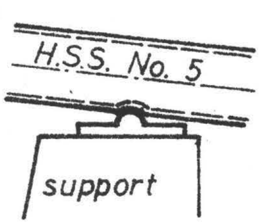

Compact Section

– local buckling at support

Bearing at support

No.	H.S.S.	R (in.)	S (in.³)	Z (in.³)	YS (ksi)	ET (ksi)	b/t
6	5·0 × 3·0 × ·230	·345	4·33	5·42	50·0	683·	10·0

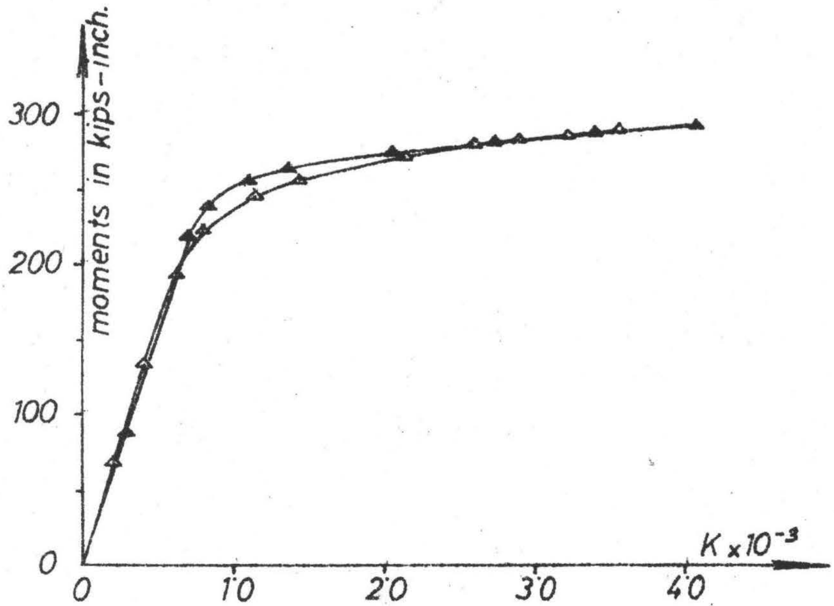

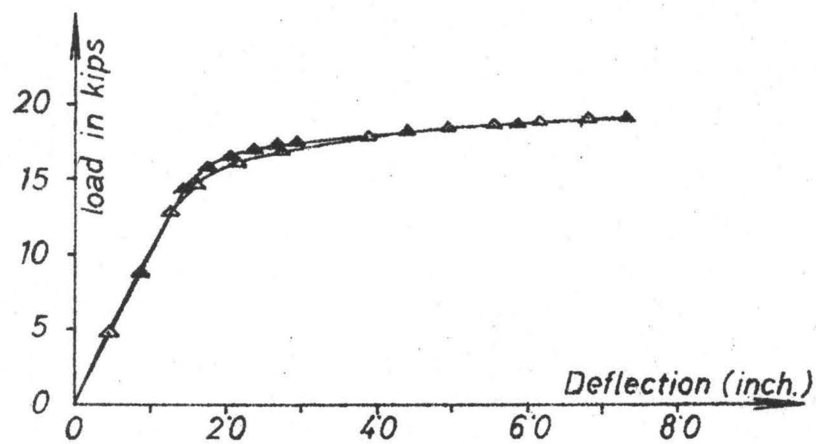

No L.B.

Predicted ▲

Test △

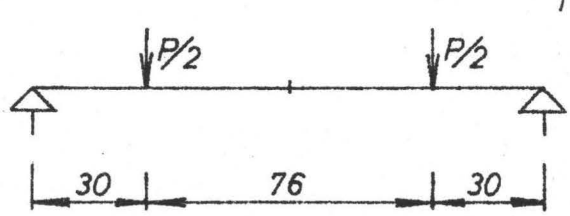

(4·6)

No.	H.S.S.	R (in.)	S (in^3)	Z (in^3)	YS (ksi)	ET (ksi)	b/t
7	4·0 × 2·0 × ·235	·352	2·32	3·03	58·0	528·	5·5

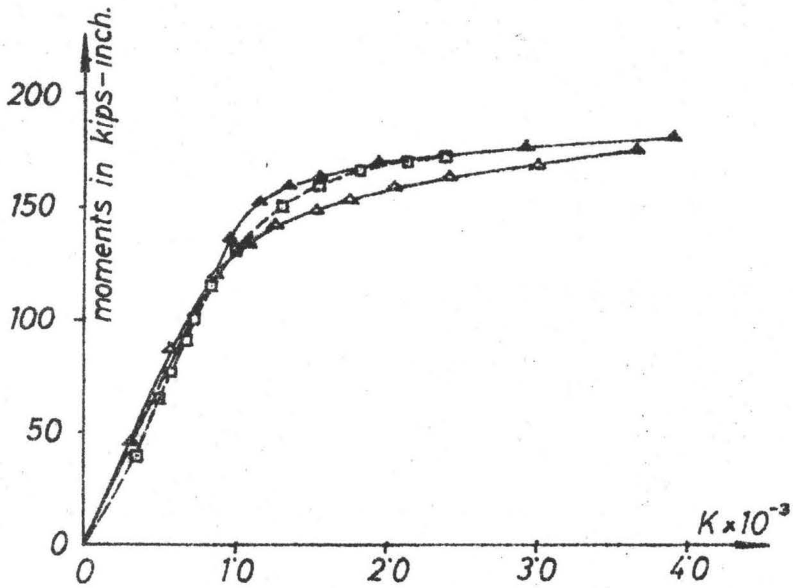

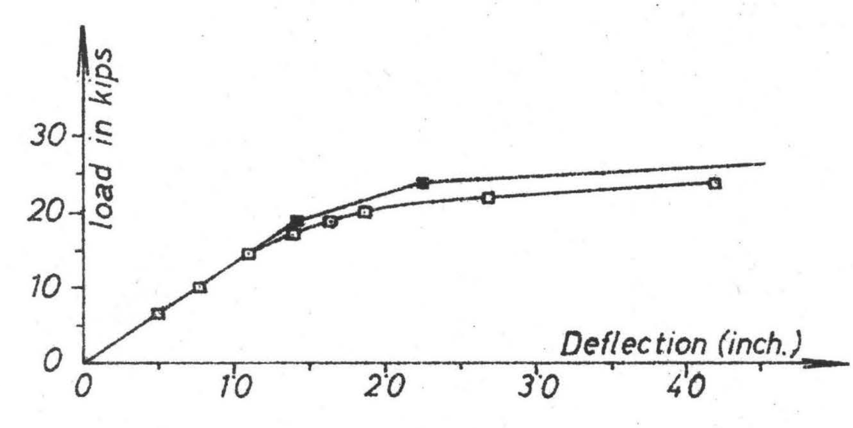

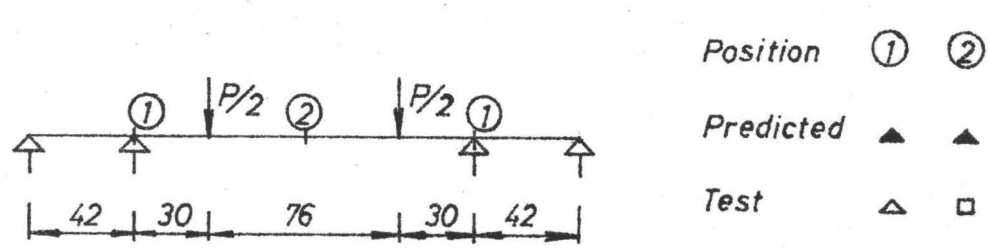

(4·7)

No.	H.S.S.	R (in.)	S (in^3)	Z (in^3)	YS (ksi)	ET (ksi)	b/t
8	4.0 × 2.0 × .235	.352	2.32	3.03	58.0	528.	5.5

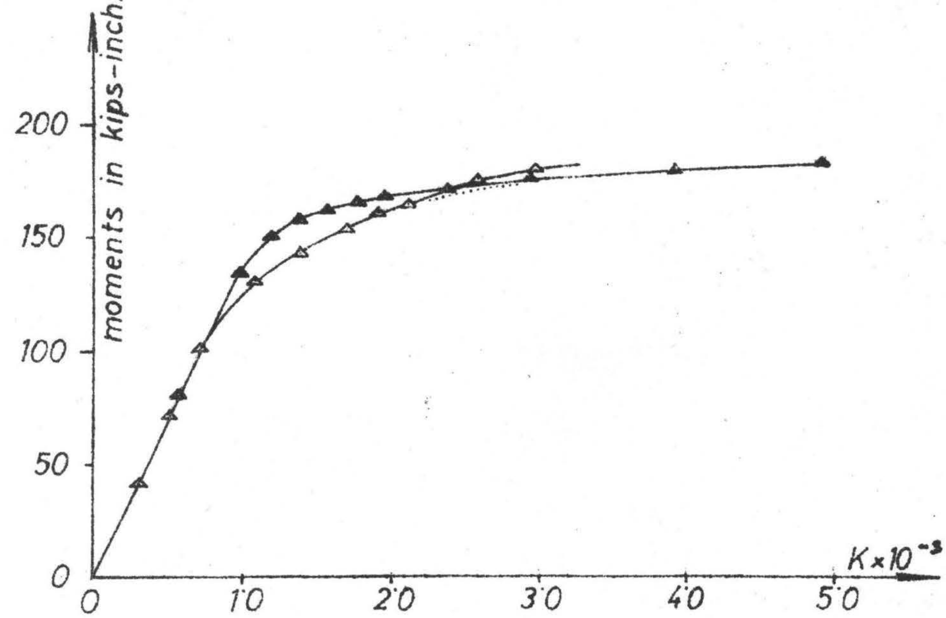

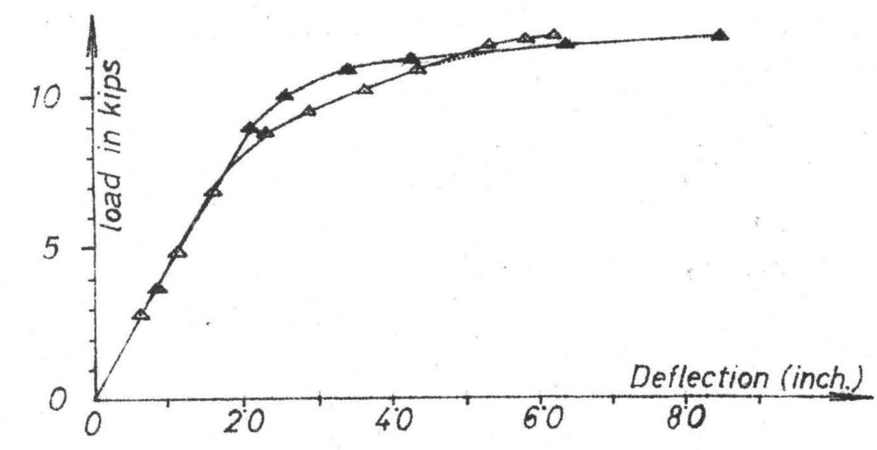

No L.B.

Predicted ▲

Test △

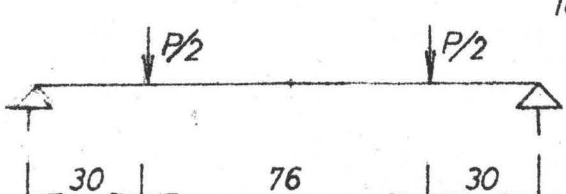

(4.8)

No.	H.S.S.	R (in.)	S (in^3)	Z (in^3)	YS (ksi)	ET (ksi)	b/t
9	2.5 × 2.5 × .210	.315	1.25	1.55	60.5	333.	8.9

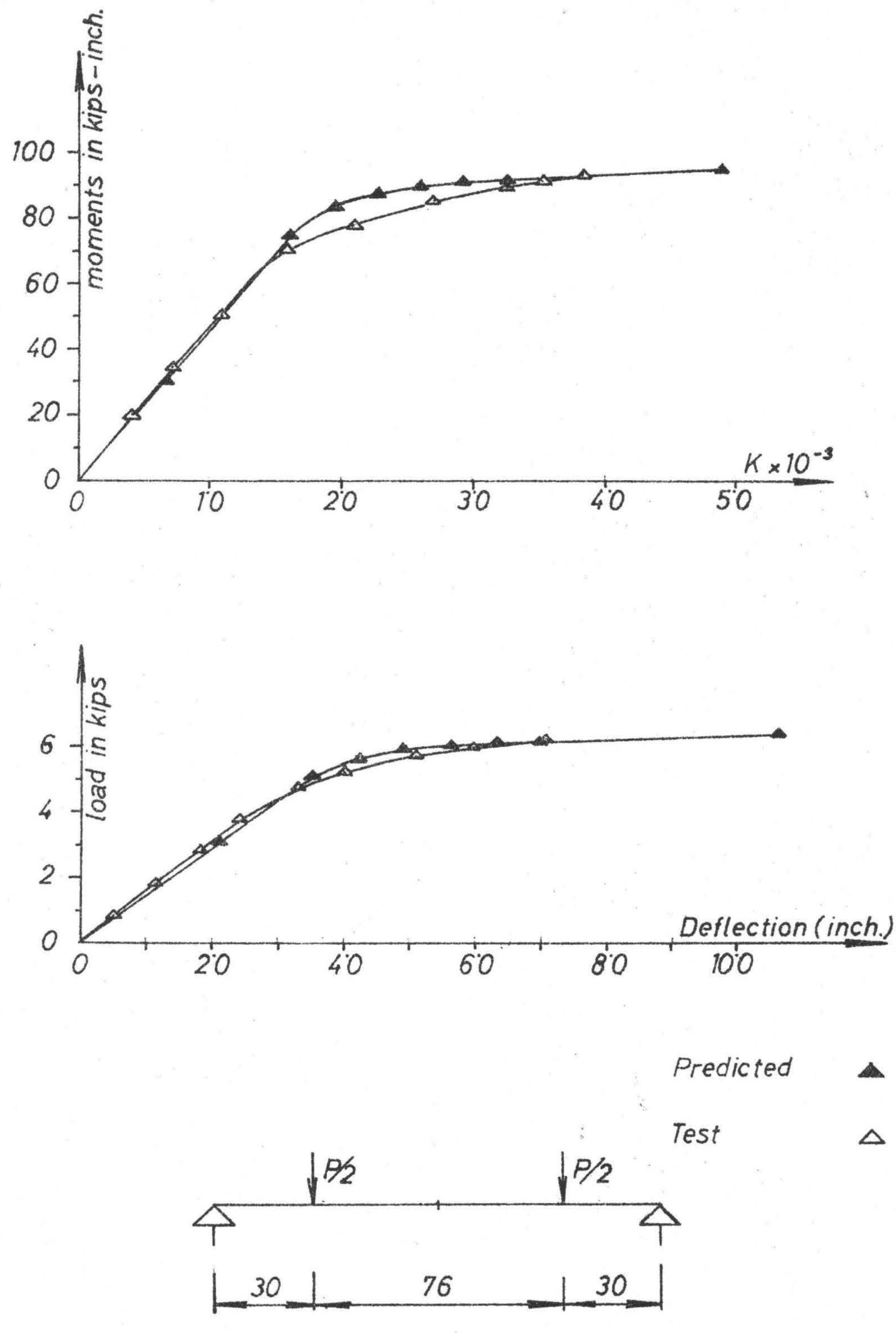

No L.B.

(4.9)

No.	H.S.S.	R (in.)	S (in.^{3})	Z (in.^{3})	YS (ksi)	ET (ksi)	b/t
10	2·5 x 2·5 x ·210	·315	1·25	1·55	60·5	333·	8·9

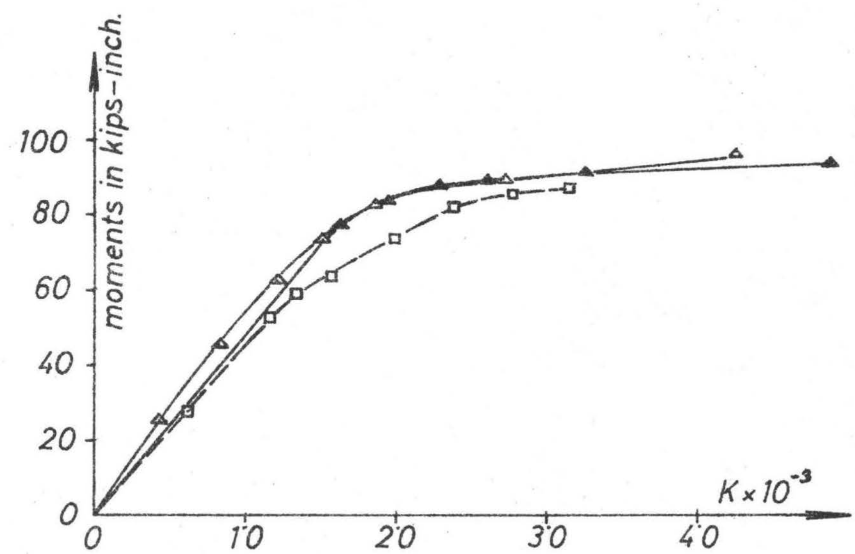

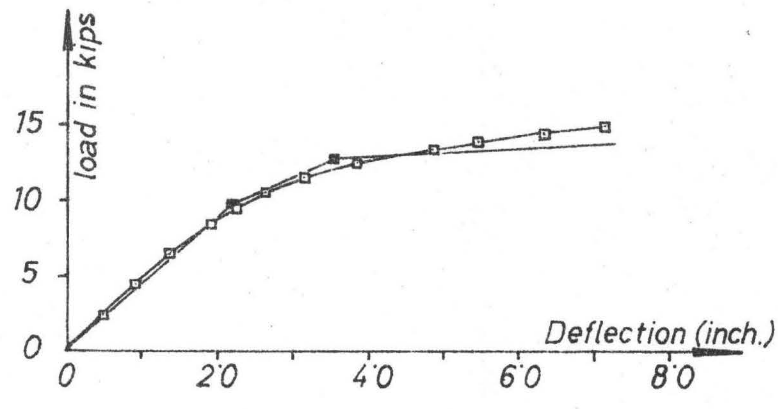

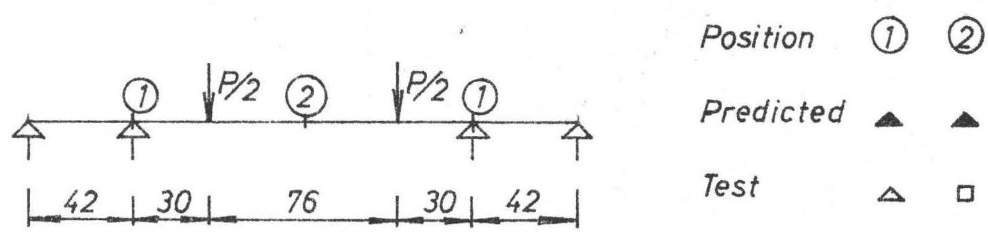

(4·10)

No.	H.S.S.	R (in.)	S (in.³)	Z (in.³)	YS (ksi)	ET (ksi)	b/t
11	6.0 × 4.0 × .437	.875	10.90	14.03	68.5	307	5.2

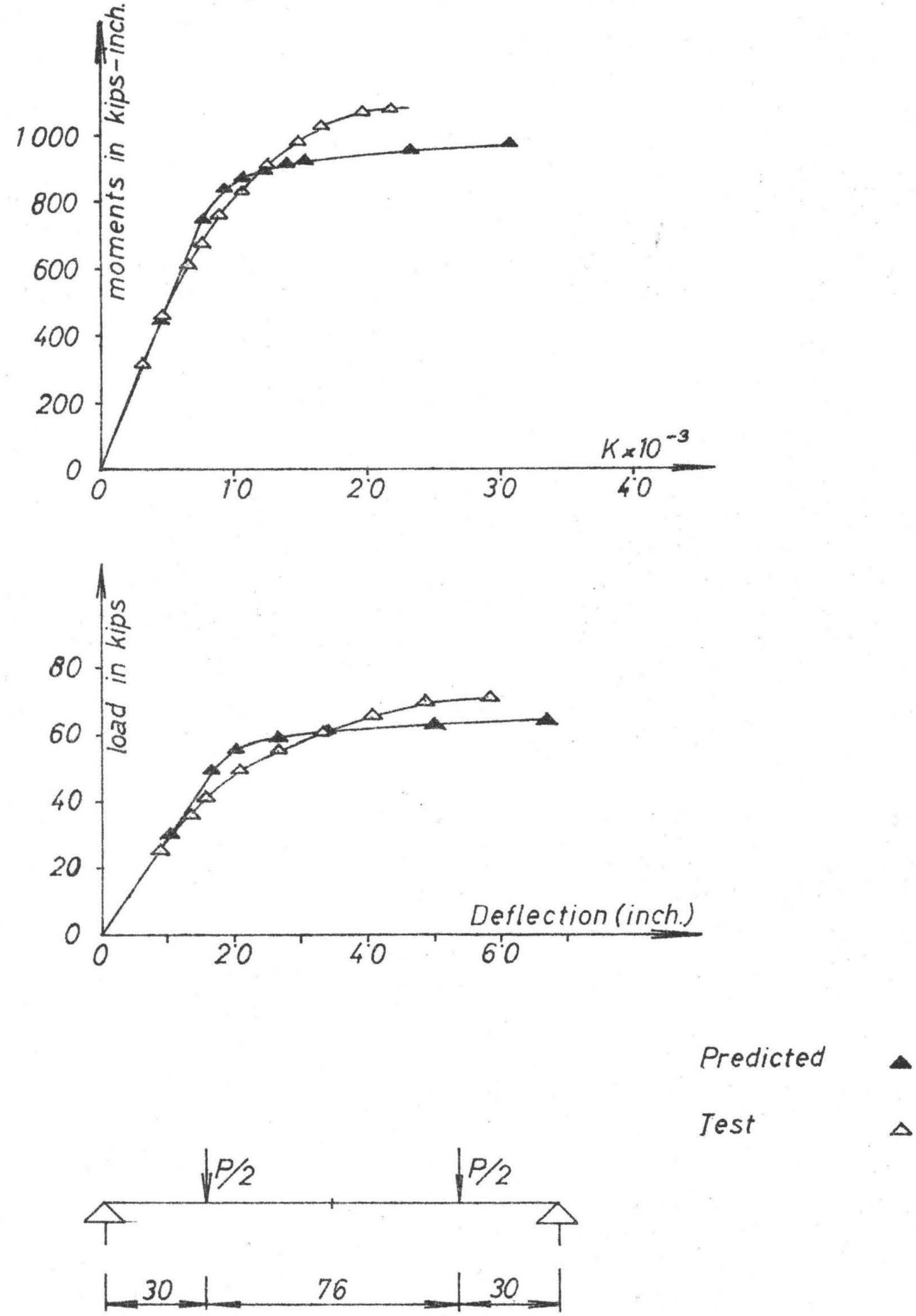

No L.B.

(4.11)

No.	H.S.S.	R (in.)	S (in^3)	Z (in^3)	YS (ksi)	ET (ksi)	b/t
12	6.0 × 4.0 × .437	.875	10.90	14.03	64.5	307.	5.2

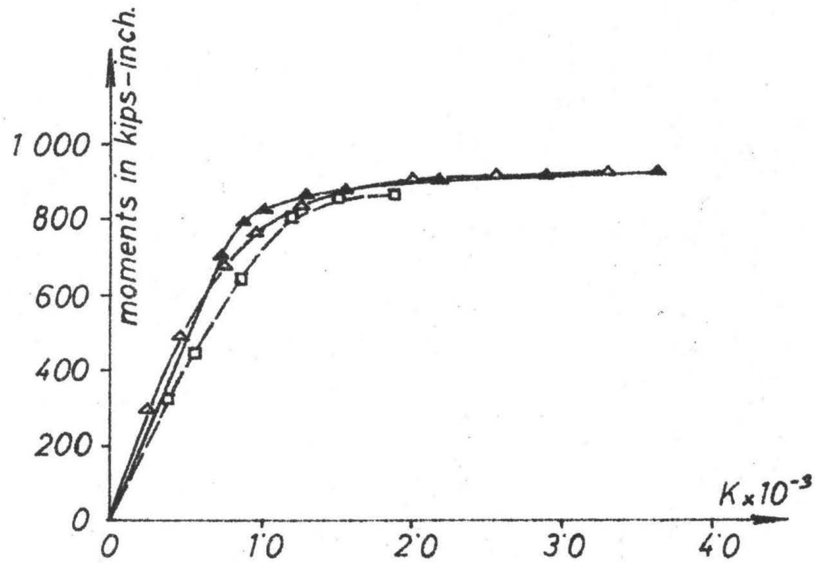

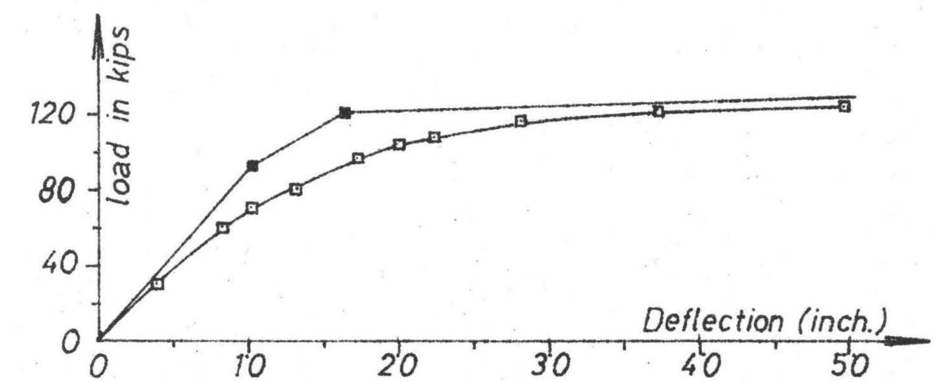

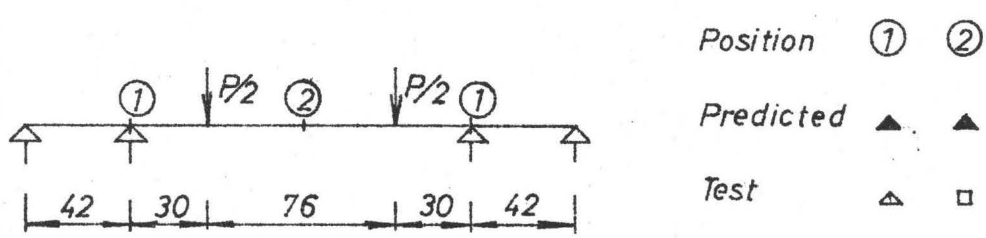

(4.12)

No.	H.S.S.	R (in.)	S (in³)	Z (in³)	YS (ksi)	ET (ksi)	b/t
13	4.0 x 4.0 x .250	.375	4.18	5.05	53.5	687.	13.0

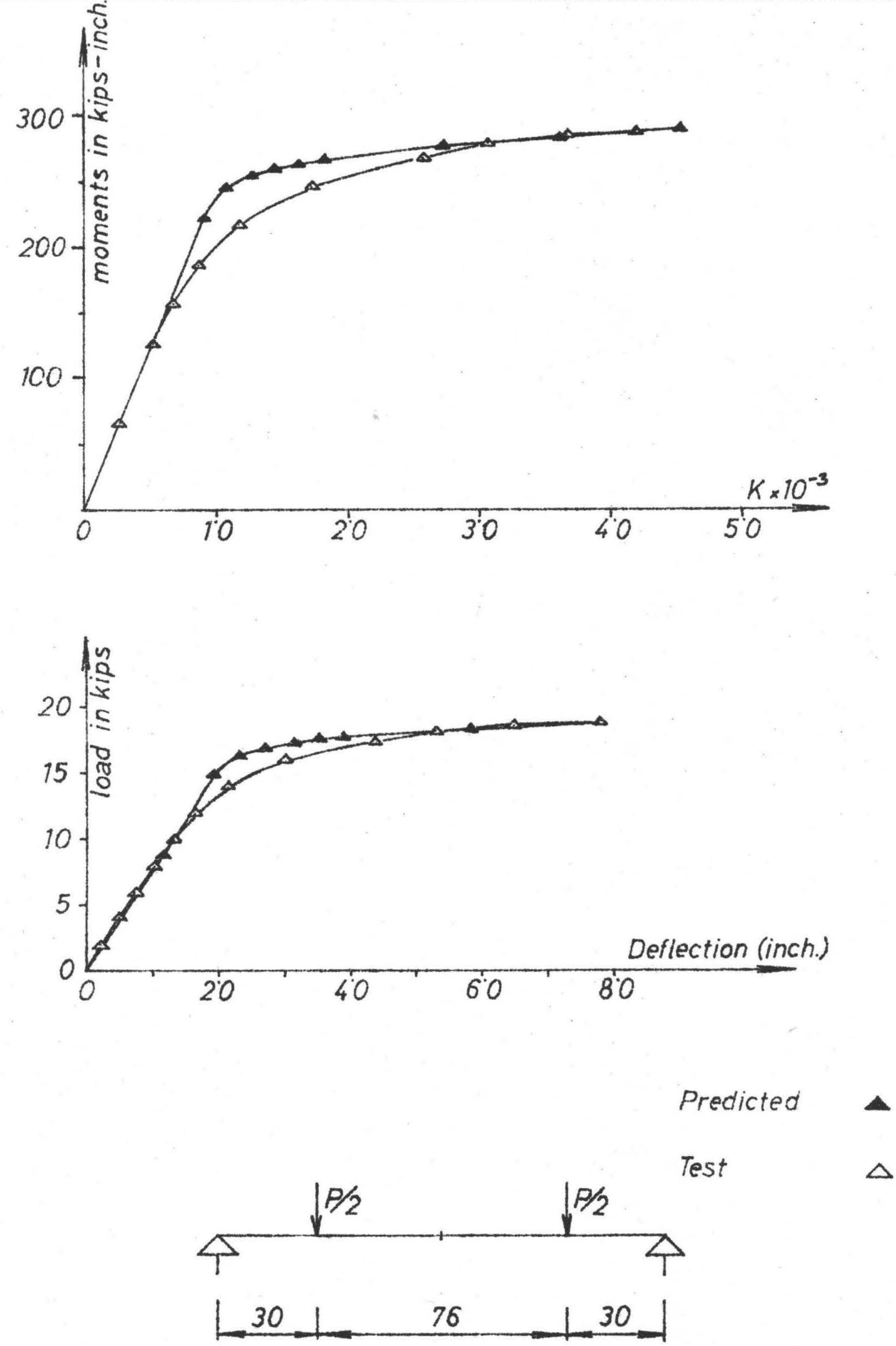

No L.B.

(4.13)

No.	H.S.S.	R (in.)	S (in^3)	Z (in^3)	YS (ksi)	ET (ksi)	b/t
(14)	4·5 O.D. x ·250	—	3·36	4·52	56·0	674	17·0

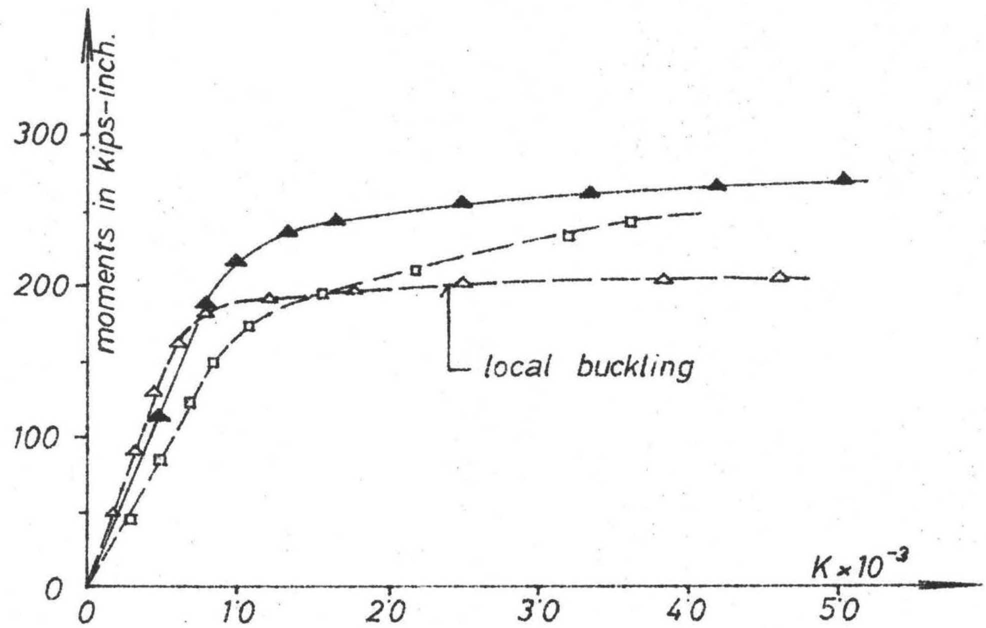

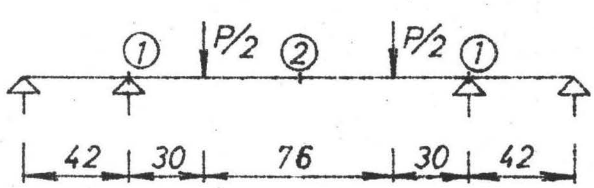

	(1)	(2)
Position	(1)	(2)
Predicted	▲	▲
Test	△	□

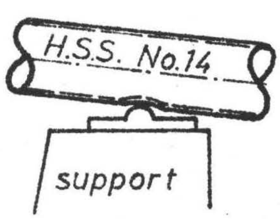

Compact Section

– local buckling at support

Bearing at support

No.	H.S.S.	R (in.)	S (in.^{3})	Z (in.^{3})	YS (ksi)	ET (ksi)	b/t
(15)	4·5 O.D. x ·250	—	3·36	4·52	56·0	674·	17·0

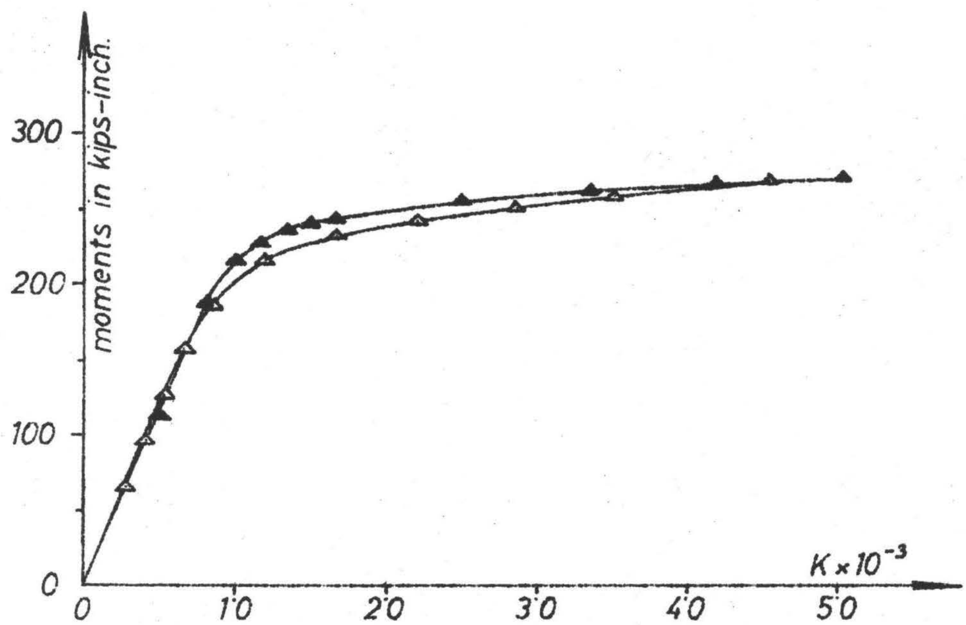

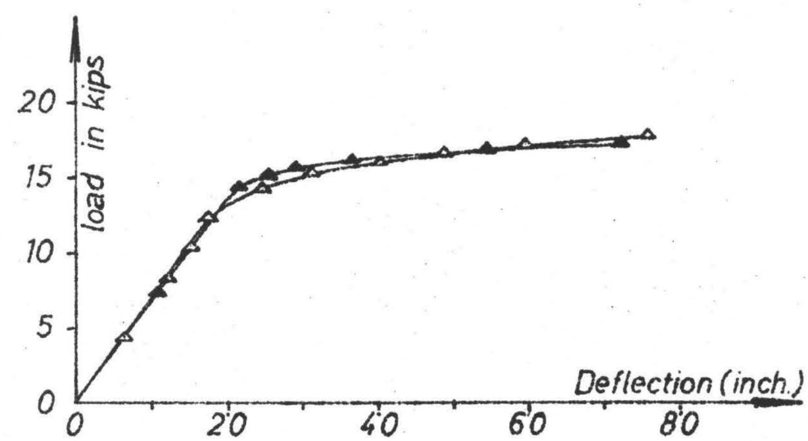

No L.B.

Predicted ▲

Test △

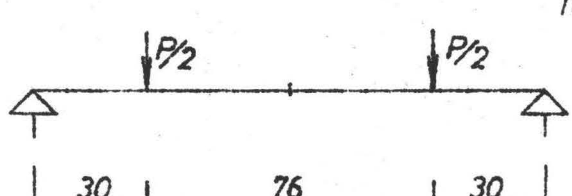

(4·15)

No.	H.S.S.	R (in.)	S (in.)	Z (in.)	YS (ksi)	ET (ksi)	b/t
16	7.0 × 7.0 × .312	.624	16.97	20.09	60.5	305.	20.5

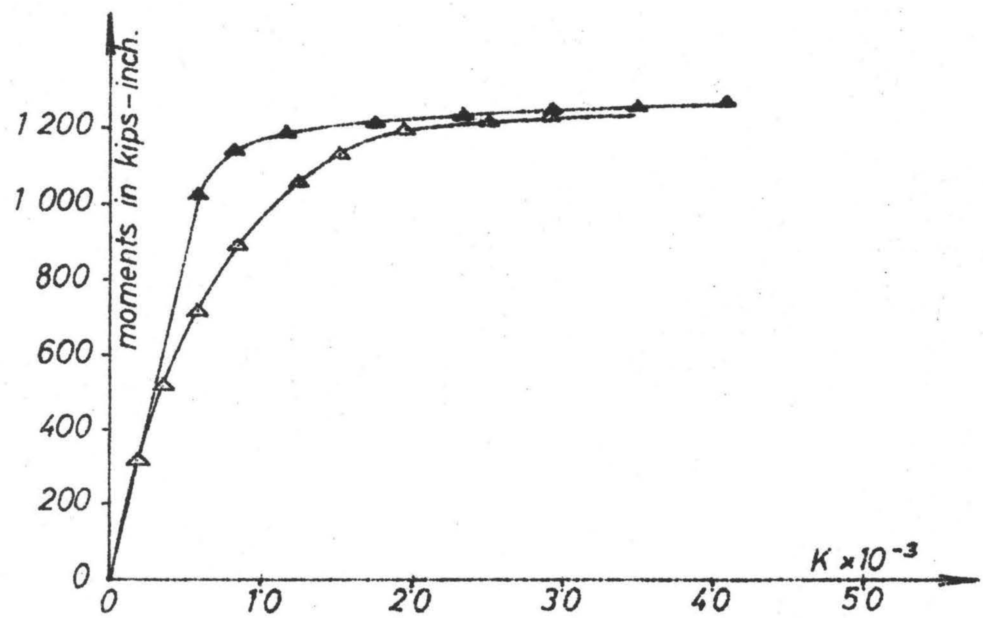

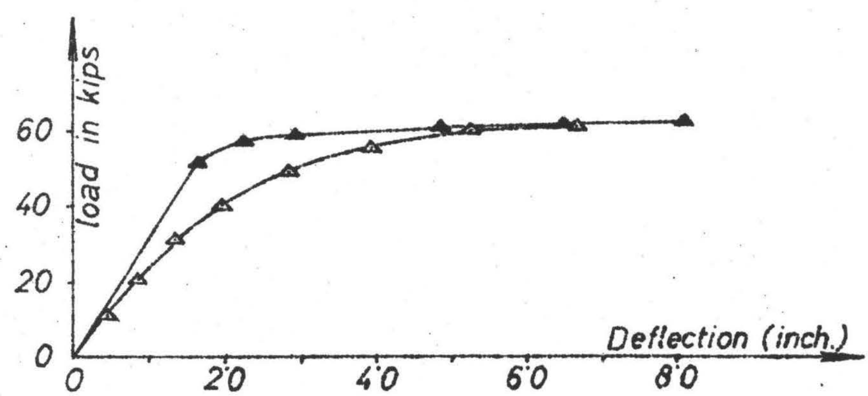

No L.B.

R.S.

Predicted ▲

Test △

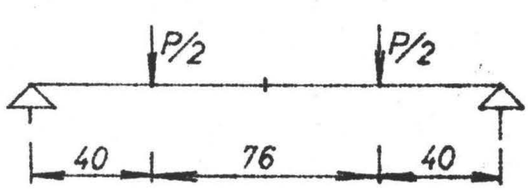

No.	H.S.S.	R (in.)	S (in.)	Z (in.)	YS (ksi)	ET (ksi)	b/t
17	5.0 × 5.0 × .250	.500	6.78	8.07	59.0	250.	16.0

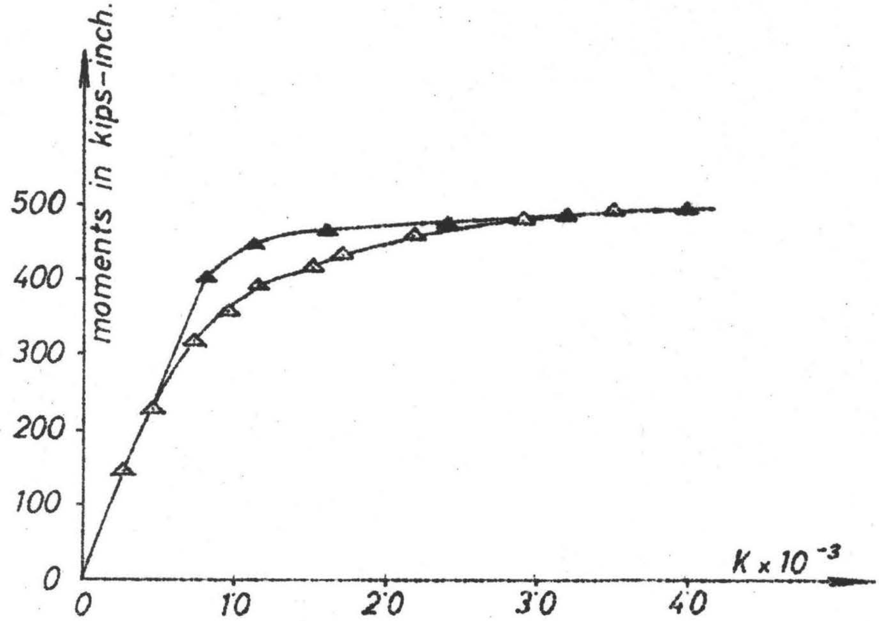

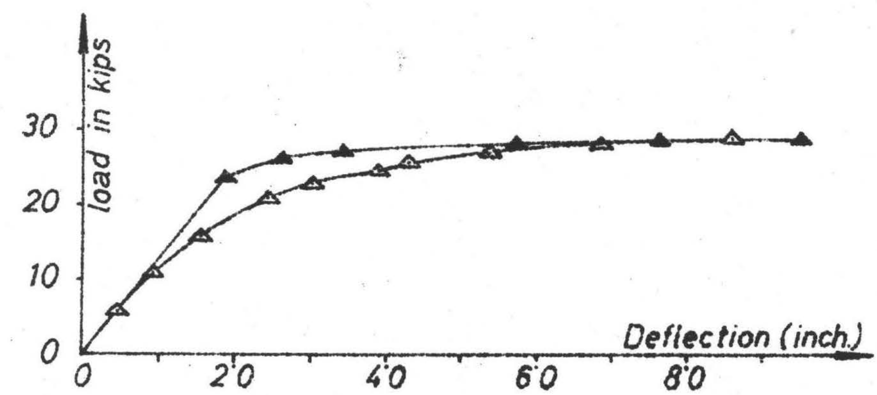

No L.B.
R.S.

Predicted ▲

Test △

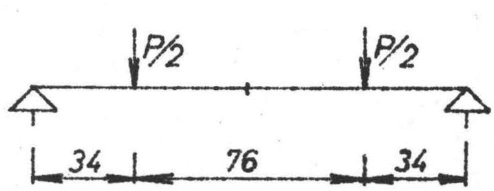

(4.17)

No.	H.S.S.	R (in.)	S (in.)	Z (in.)	YS (ksi)	ET (ksi)	b/t
18	8.0 × 8.0 × .312	.624	22.69	26.69	63.7	250	23.7

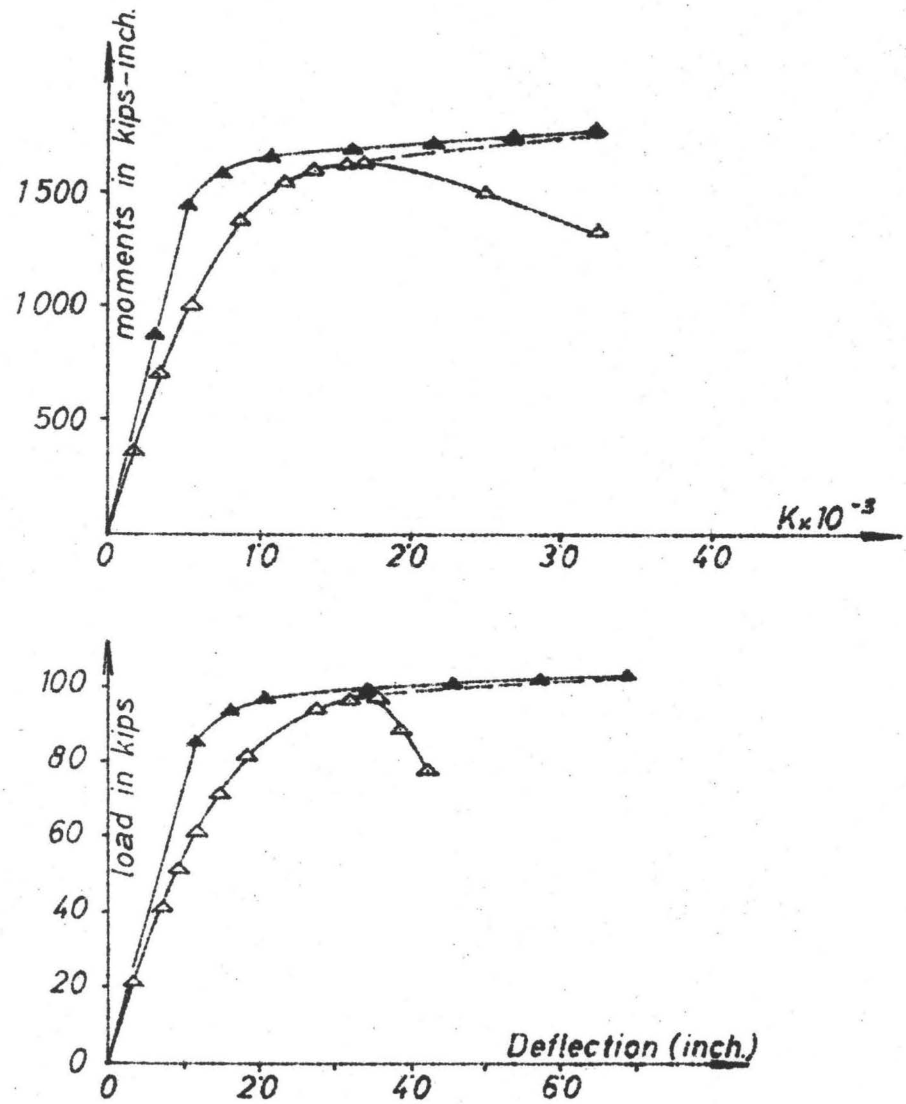

Predicted ▲

Test △

R.S.

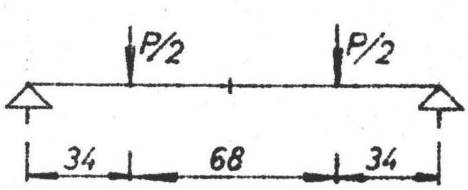

(4.18)

No.	H.S.S.	R (in.)	S (in^3)	Z (in^3)	YS (ksi)	ET (ksi)	b/t
19	6.0 × 6.0 × .188	.376	7.94	9.26	56.0	357.	27.9

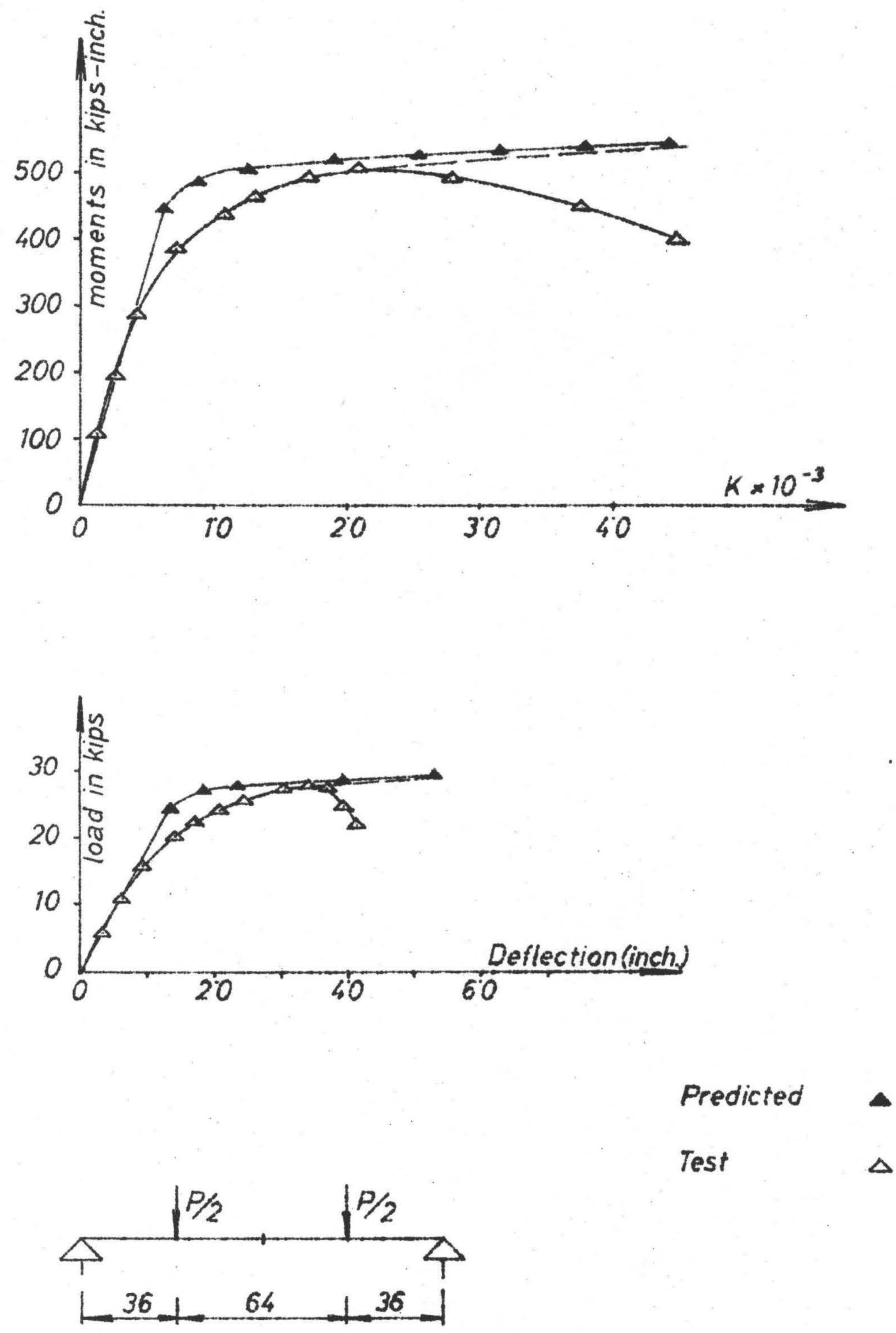

R.S.

(4.19)

No.	H.S.S.	R (in.)	S (in³)	Z (in³)	YS (ksi)	ET (ksi)	b/t
20	10·0×10·0×·375	·750	42·89	50·35	57·0	350·	22·7

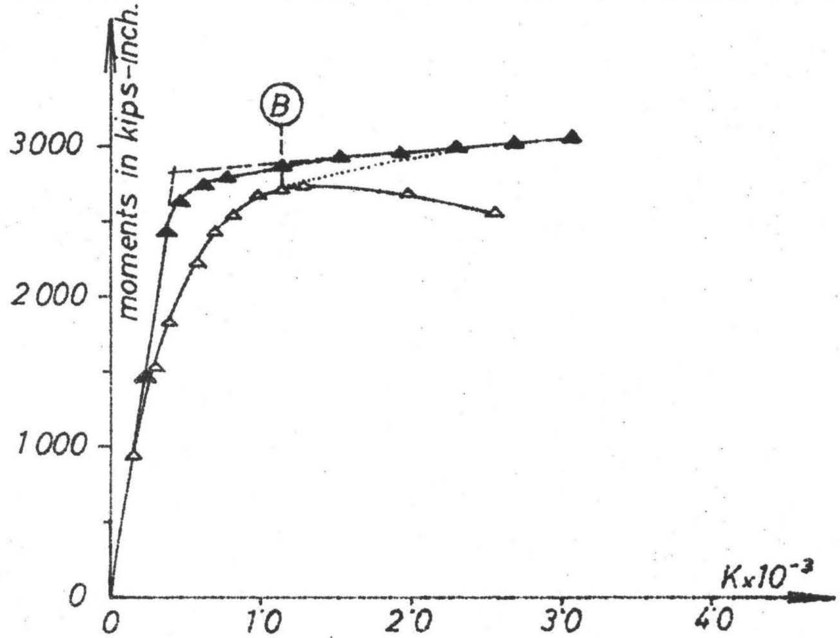

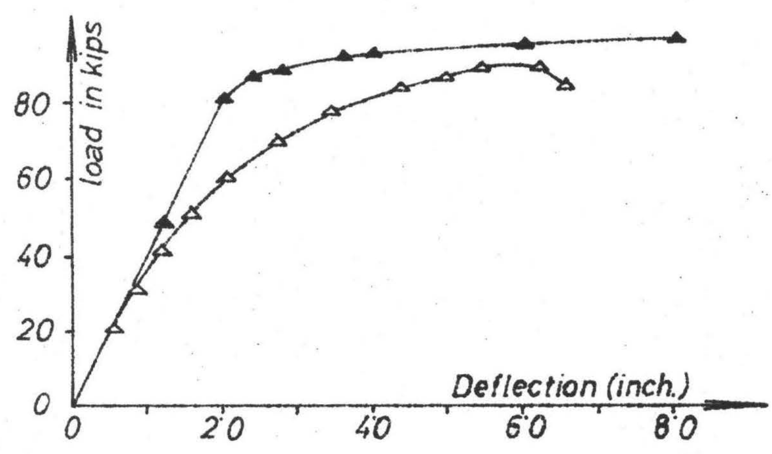

Predicted ▲

Test △

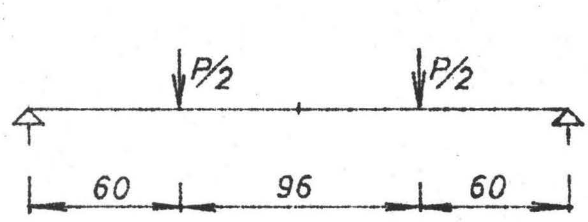

(4·20)

No.	H.S.S.	R (in.)	S (in.^{3})	Z (in.^{3})	YS (ksi)	ET (ksi)	b/t
21	3·50 O.D. × ·150	—	1·27	1·68	55·0	656·	22·3

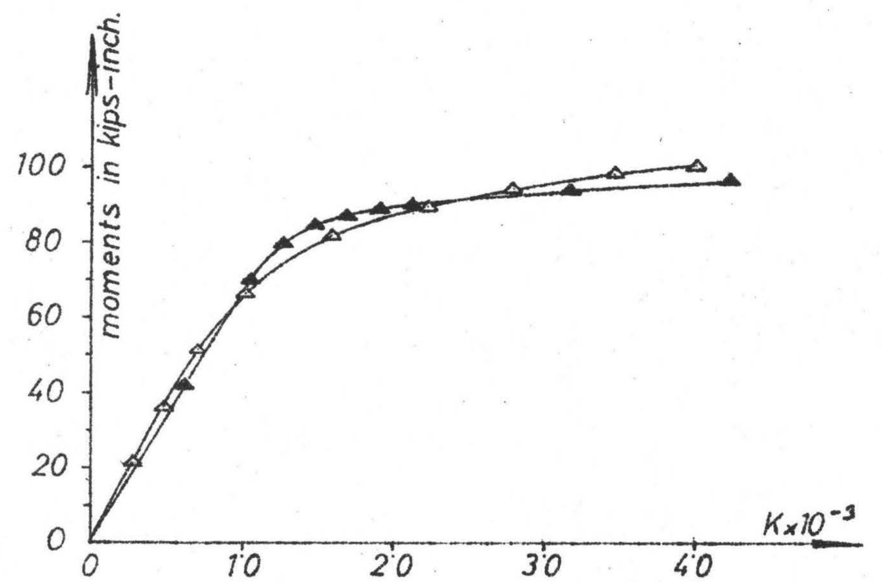

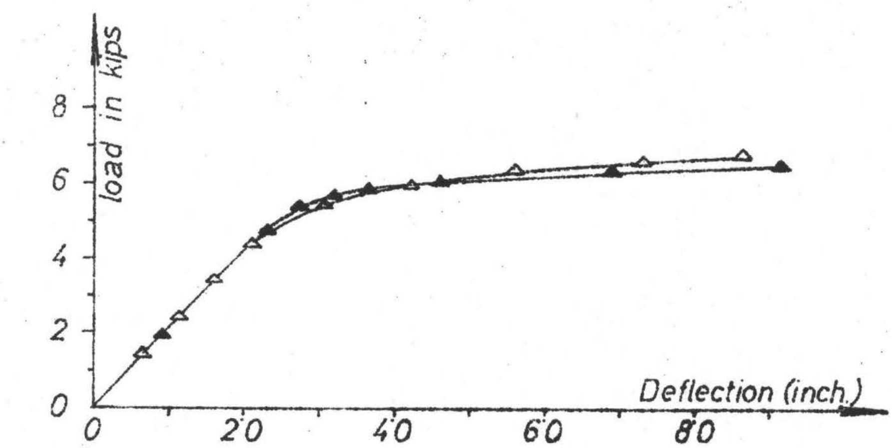

No L.8.

Predicted ▲

Test △

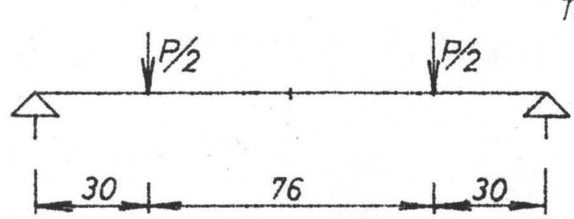

No.	H.S.S.	R (in.)	S (in³)	Z (in³)	YS (ksi)	ET (ksi)	b/t
22	10·0 × 6·0 × ·500	1·000	36·15	45·60	58·0	273·	8·0

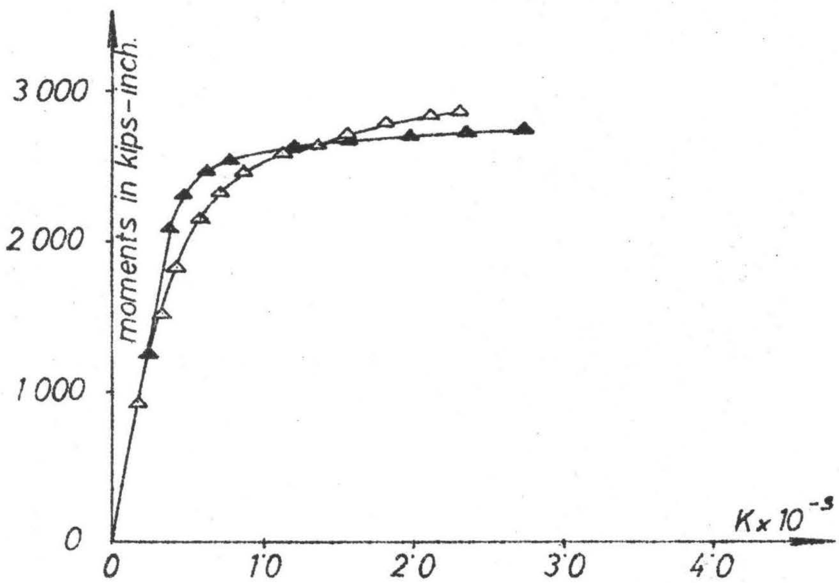

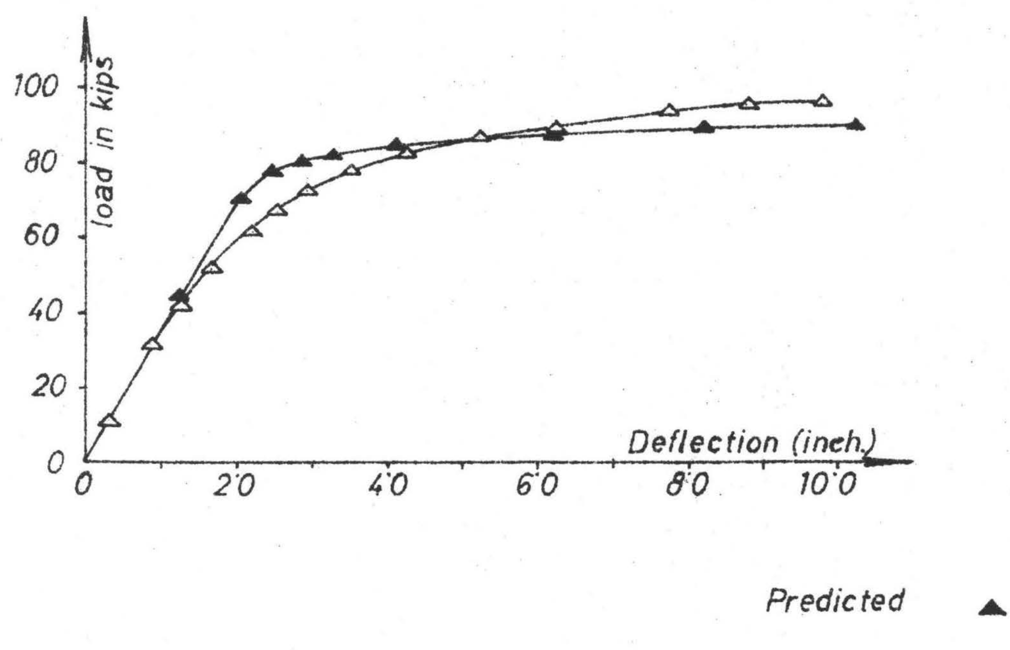

No L.B.

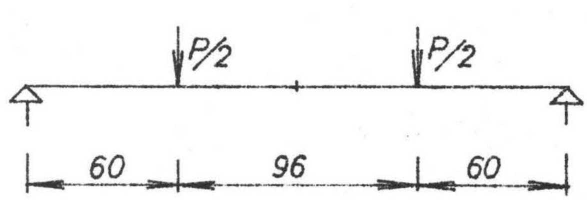

(4·22)

No.	H.S.S.	R (in.)	S ($in.^3$)	Z ($in.^3$)	YS (ksi)	ET (ksi)	b/t
23	10·0 × 10·0 × ·375	·750	42·89	50·35	63·5	350·	22·7

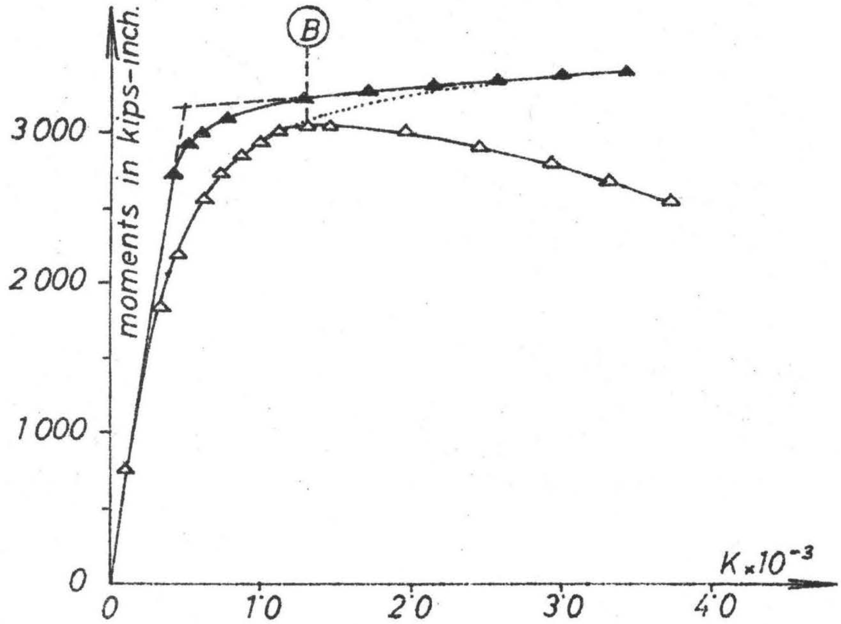

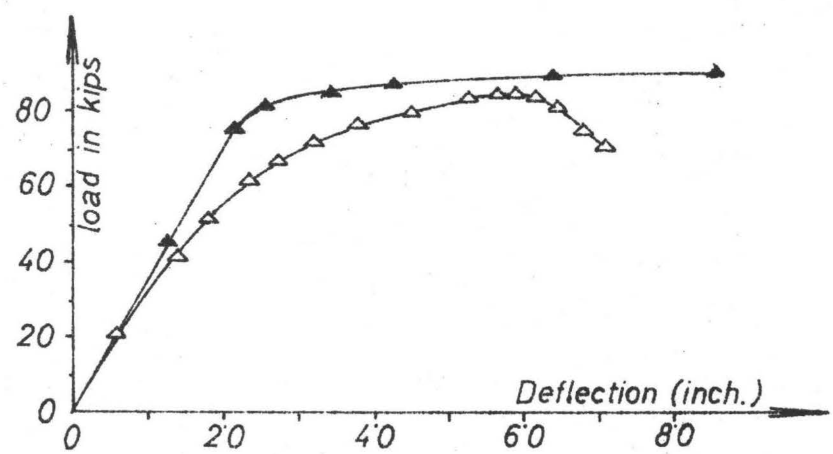

Predicted ▲

Test △

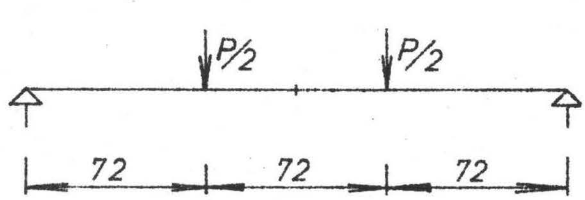

(4·23)

No.	H.S.S.	R (in.)	S (in^3)	Z (in^3)	YS (ksi)	ET (ksi)	b/t
(24)	10·75 O.D. × ·500	—	39·41	52·54	41·5	366·	20·5

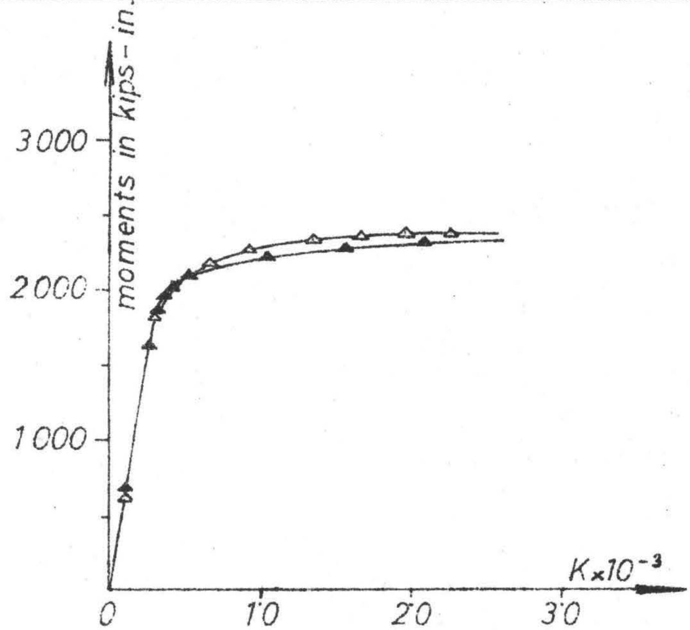

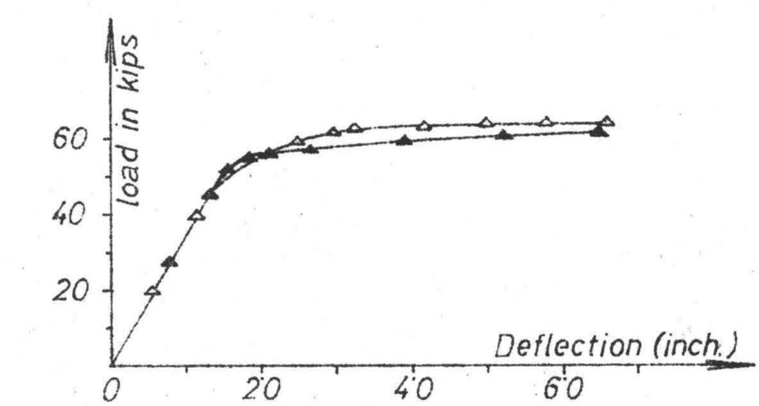

No L.B.

Predicted ▲

Test △

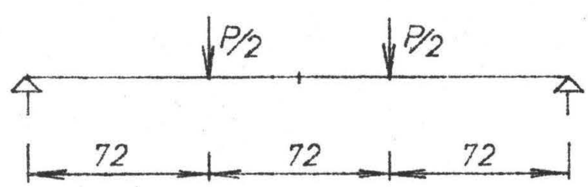

No.	H.S.S.	R (in.)	S (in.)	Z (in.)	YS (ksi)	ET (ksi)	b/t
25	7.0 × 7.0 × .188	.376	11.02	12.77	57.0	350.	33.3

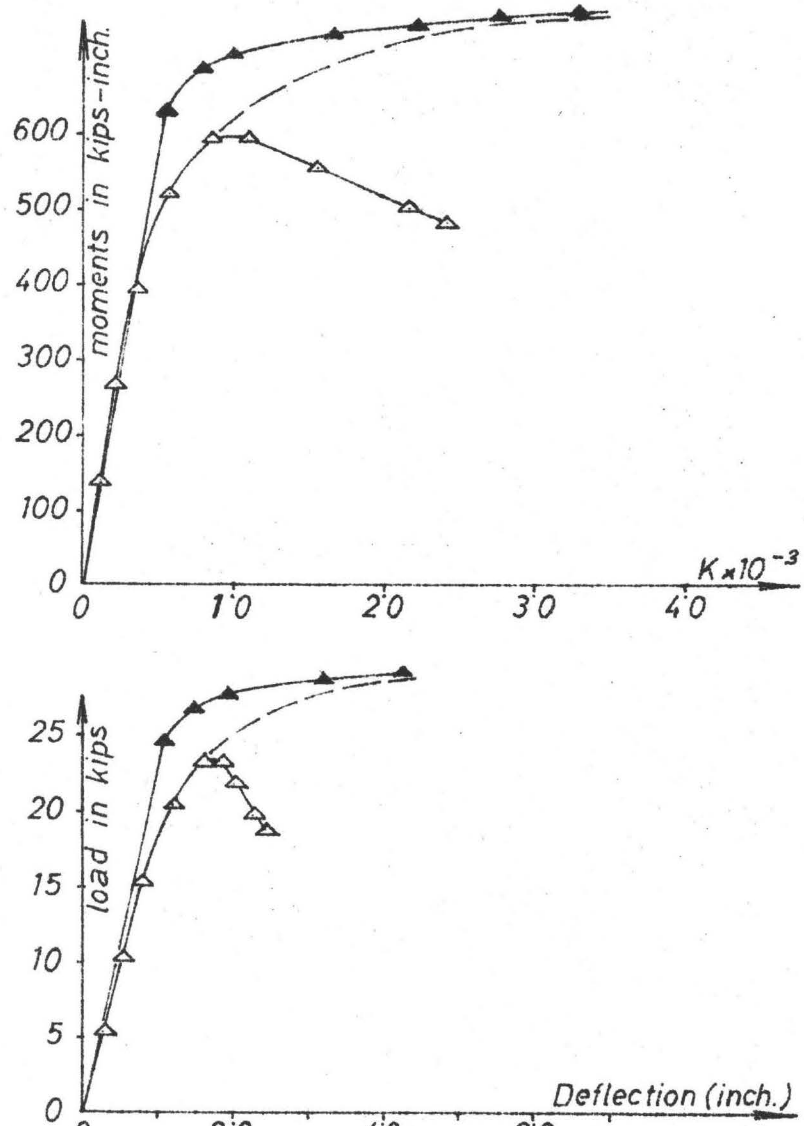

Predicted ▲

Test △

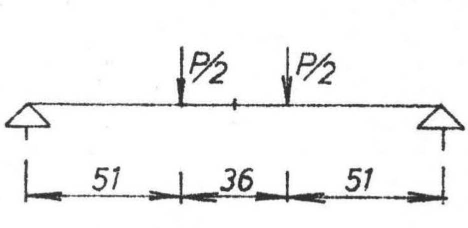

No.	H.S.S.	R (in.)	S (in.)	Z (in.)	YS (ksi)	ET (ksi)	b/t
26	7.0 × 7.0 × .250	.500	14.12	16.54	58.0	194.0	24.0

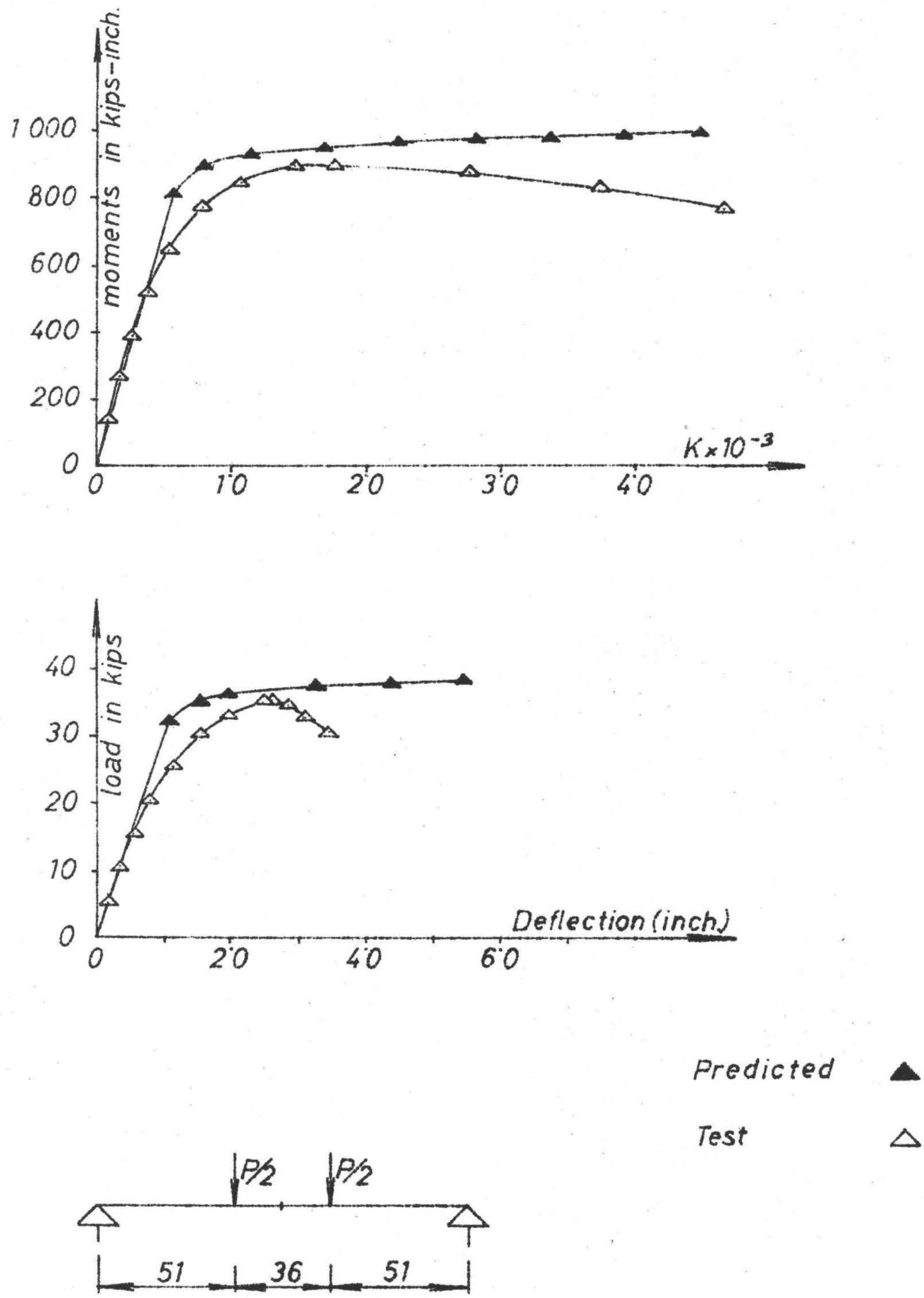

(4.26)

No. H.S.S.	R (in.)	S (in.)	Z (in.)	YS (ksi)	ET (ksi)	b/t
27 6.0 × 6.0 × .250	.500	10.11	11.93	60.5	167.	20.0

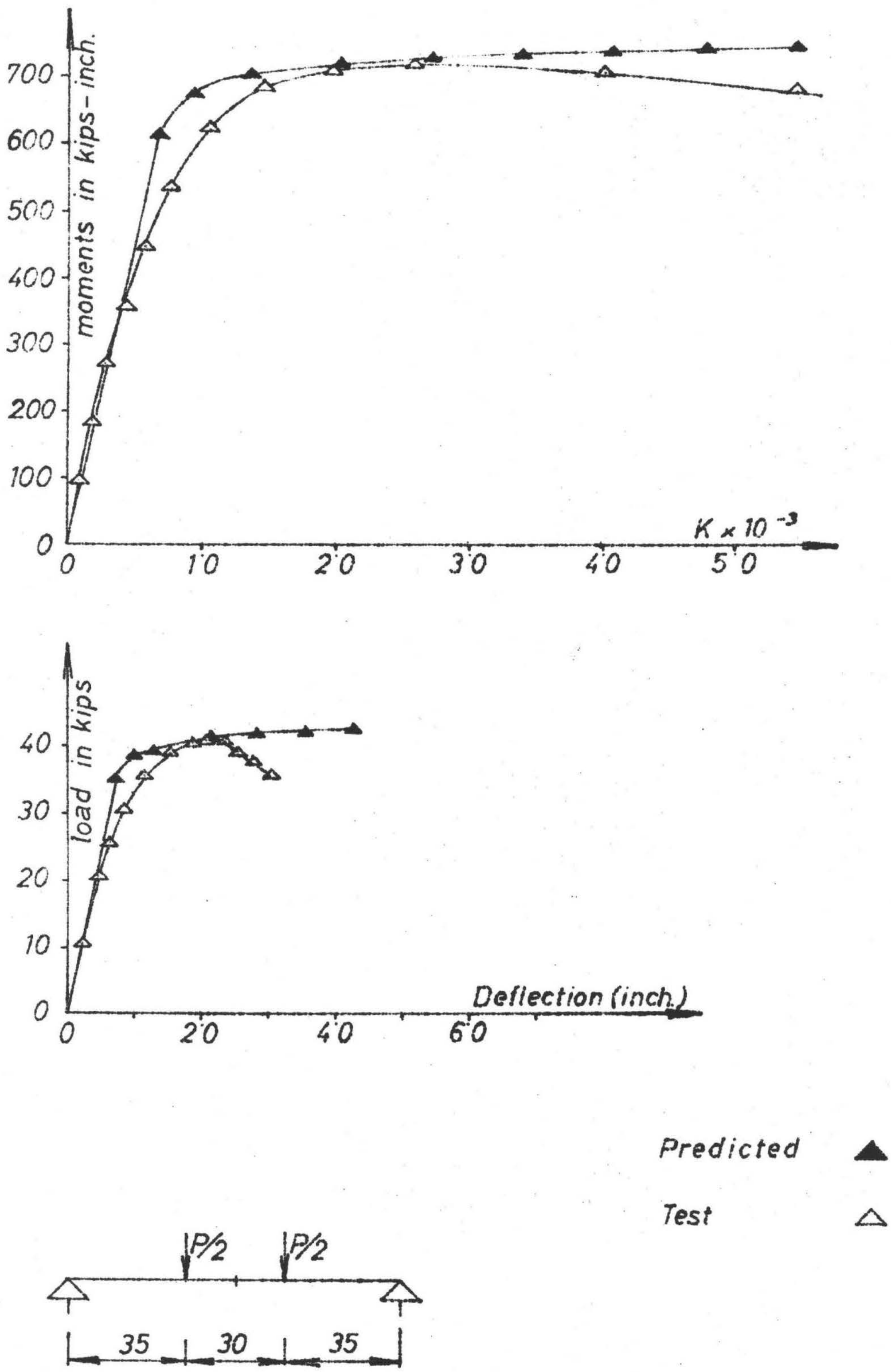

No.	H.S.S.	R (in.)	S (in.)	Z (in.)	YS (ksi)	ET (ksi)	b/t
(28)	4·0 × 4·0 × ·188	·282	3·35	3·97	51·0	660	18·3

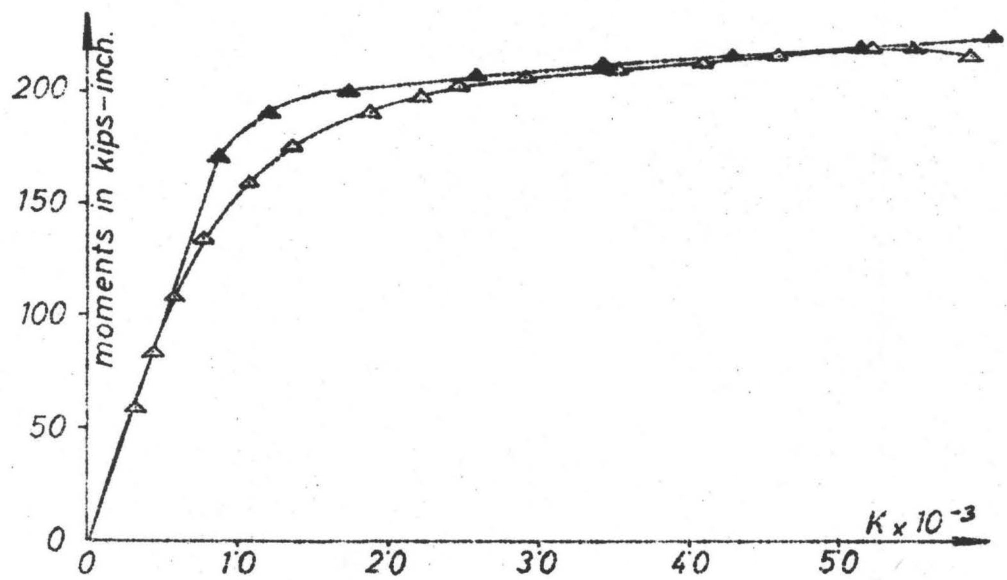

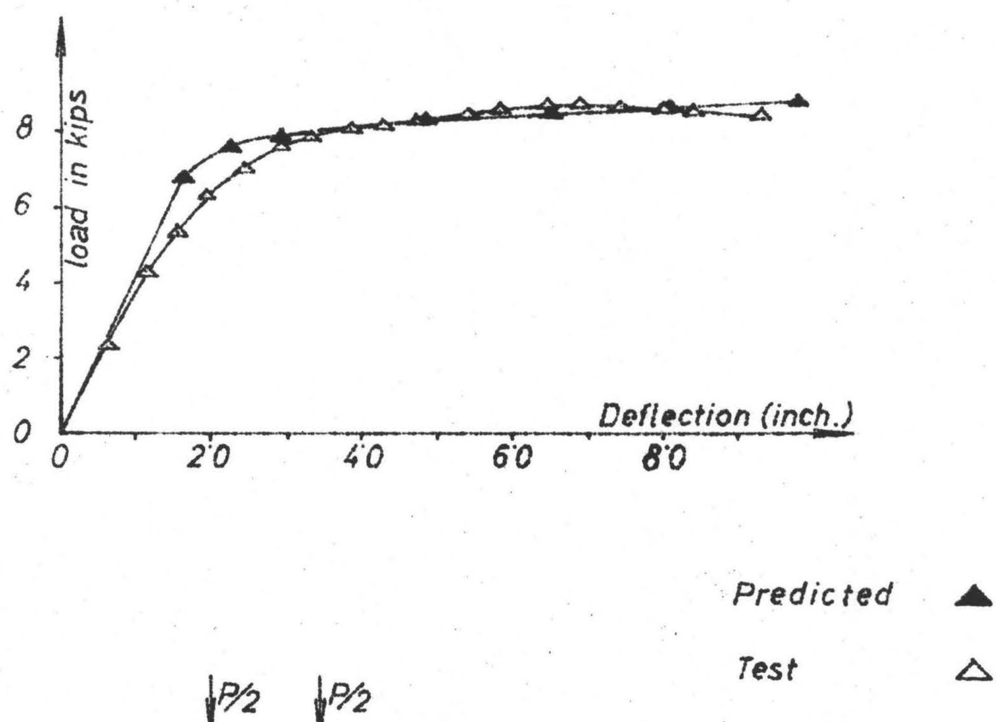

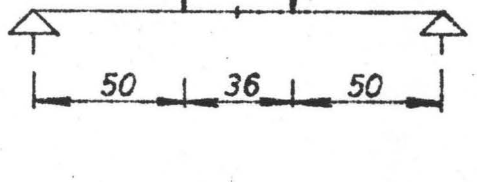

No.	H.S.S.	R (in.)	S (in.)	Z (in.)	YS (ksi)	ET (ksi)	b/t
29	3·5 O.D. × ·150	–	1·27	1·68	50·0	650·	22·3

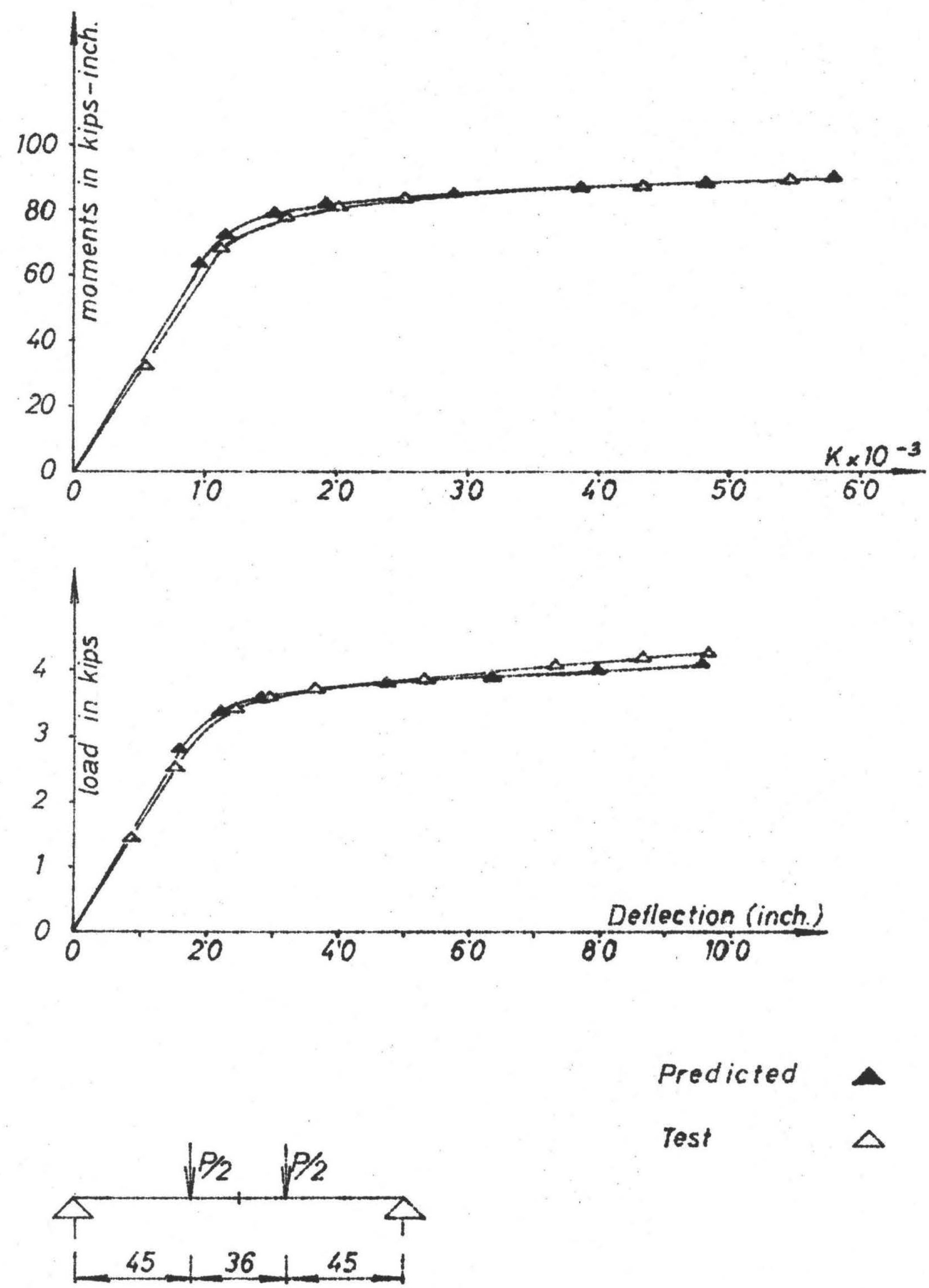

No L.B.

(4·29)

No.	H.S.S.	R (in.)	S (in.)	Z (in.)	YS (ksi)	ET (ksi)	b/t
30	4·0 O.D. × ·188	–	2·05	2·73	51·0	735·	20·3

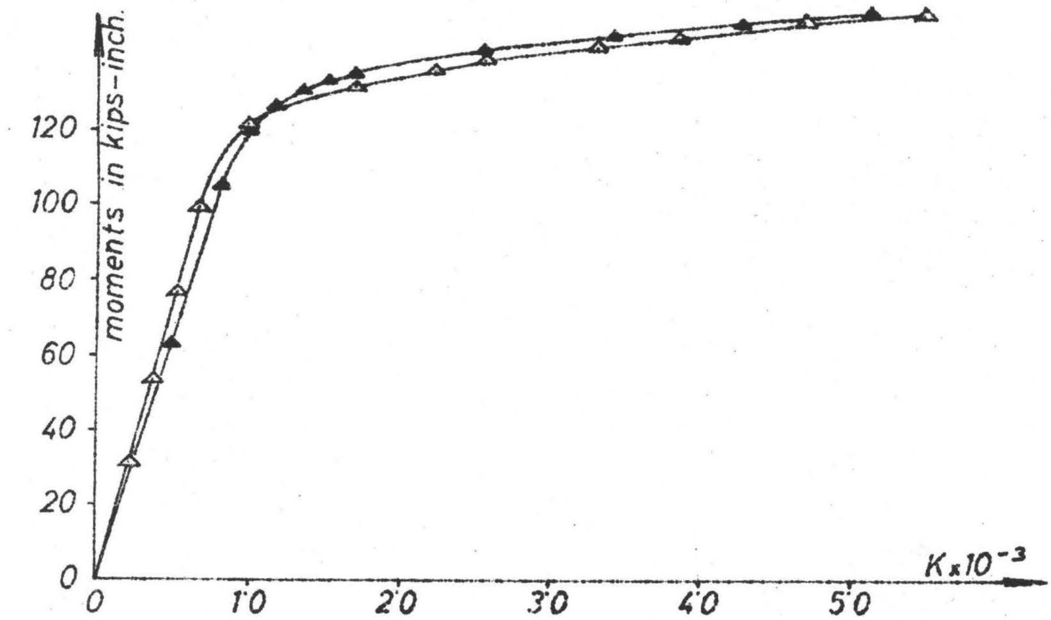

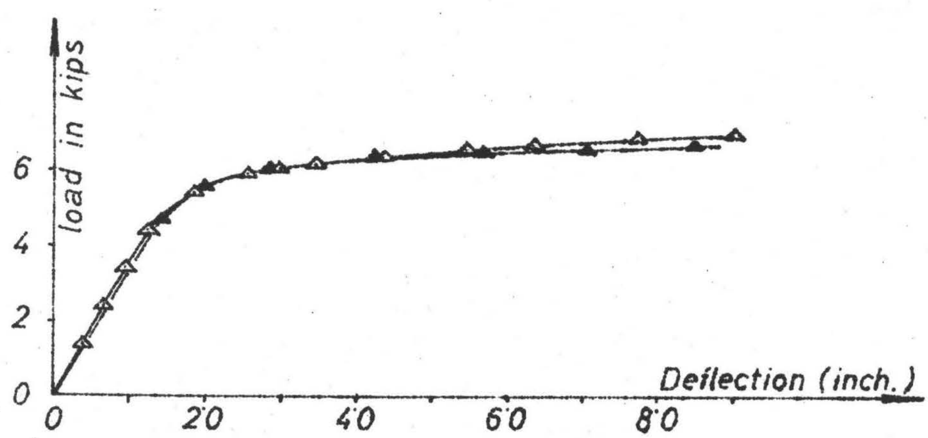

No L.B.

Predicted ▲

Test △

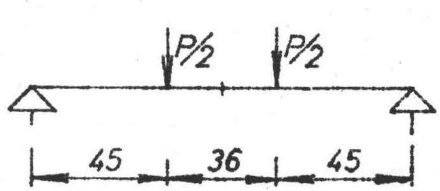

No.	H.S.S.	R (in.)	S (in.)	Z (in.)	YS (ksi)	ET (ksi)	b/t
31	4·5 O.D. × ·188	—	2·63	3·50	50·5	650·	23·0

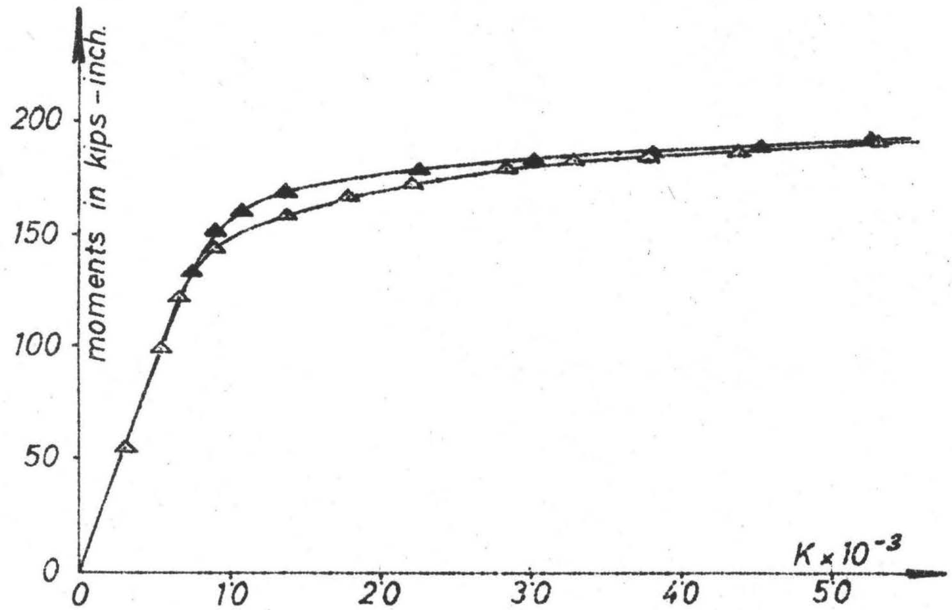

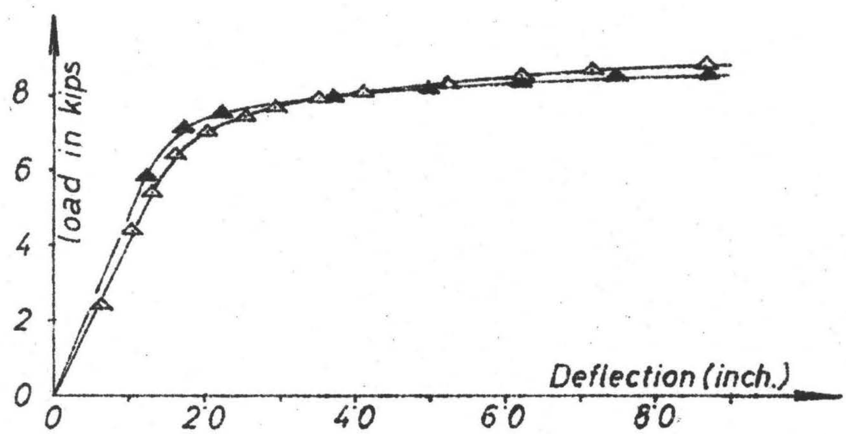

No L.B.

Predicted ▲

Test △

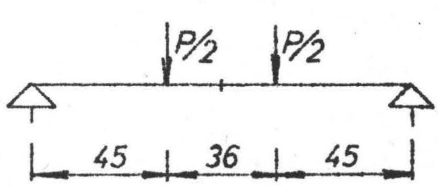

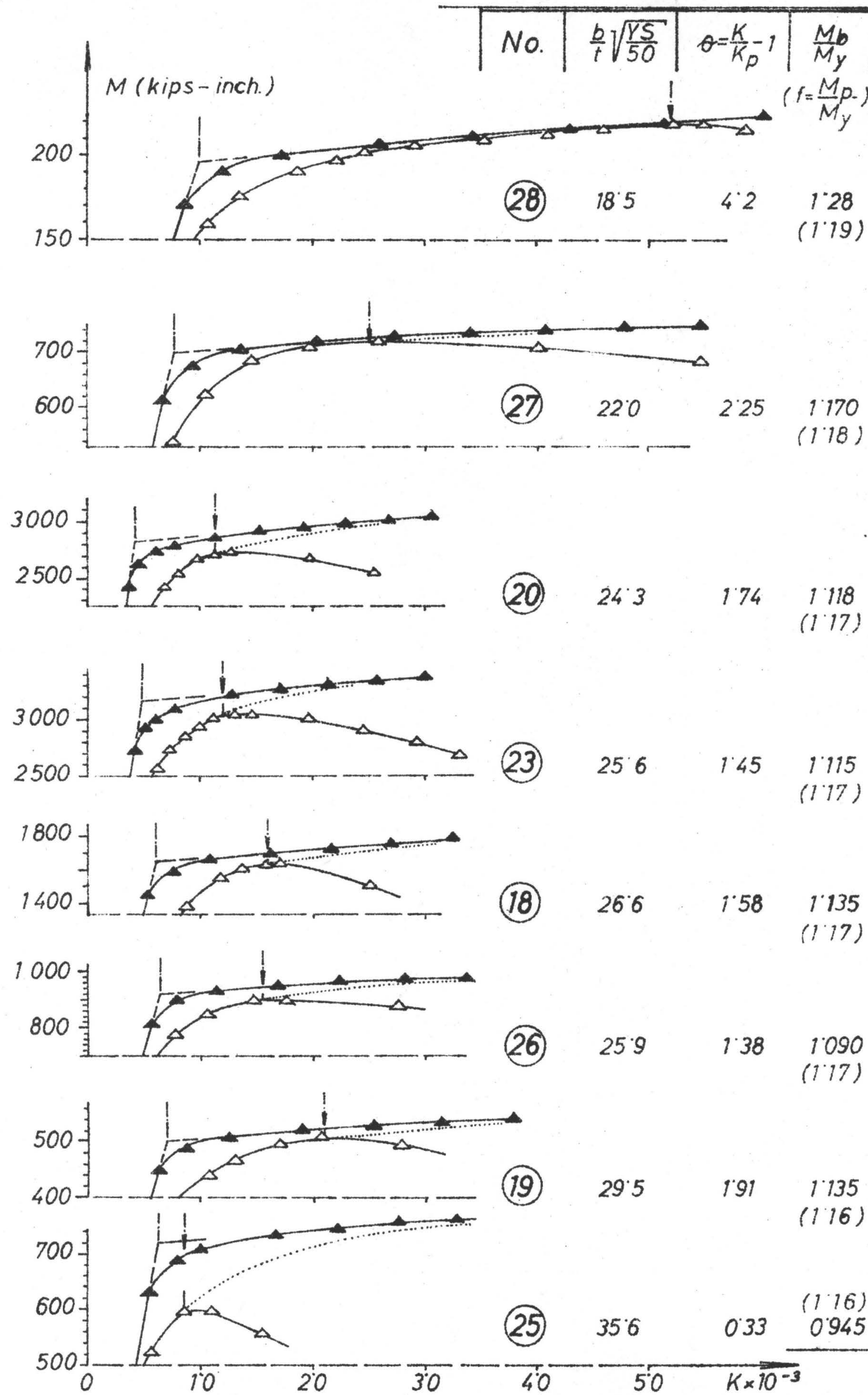

FIGURE 4·32 Rotation Capacities on Basis of Actual YS

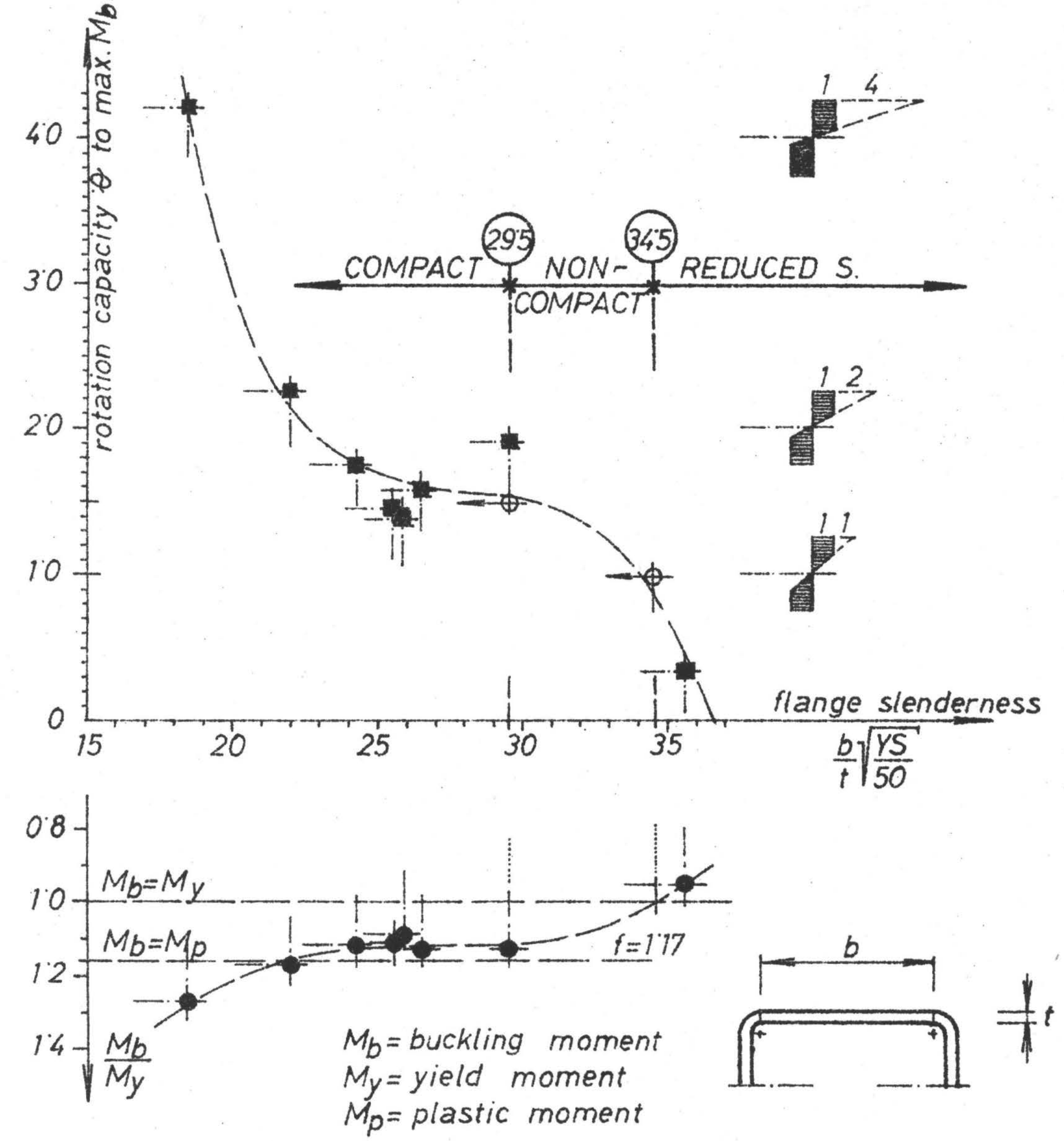

Non - Compact Sections :

$$\frac{b}{t}\sqrt{\frac{YS}{50}} \leqq 34.5 \qquad \frac{b}{t} \leqq \frac{245}{\sqrt{YS}}$$

Compact Sections in working stress design :

$$\frac{b}{t}\sqrt{\frac{YS}{50}} \leqq 29.5 \qquad \frac{b}{t} \leqq \frac{210}{\sqrt{YS}}$$

FIGURE 4.33 Limiting b/t Value for Working Stress Design

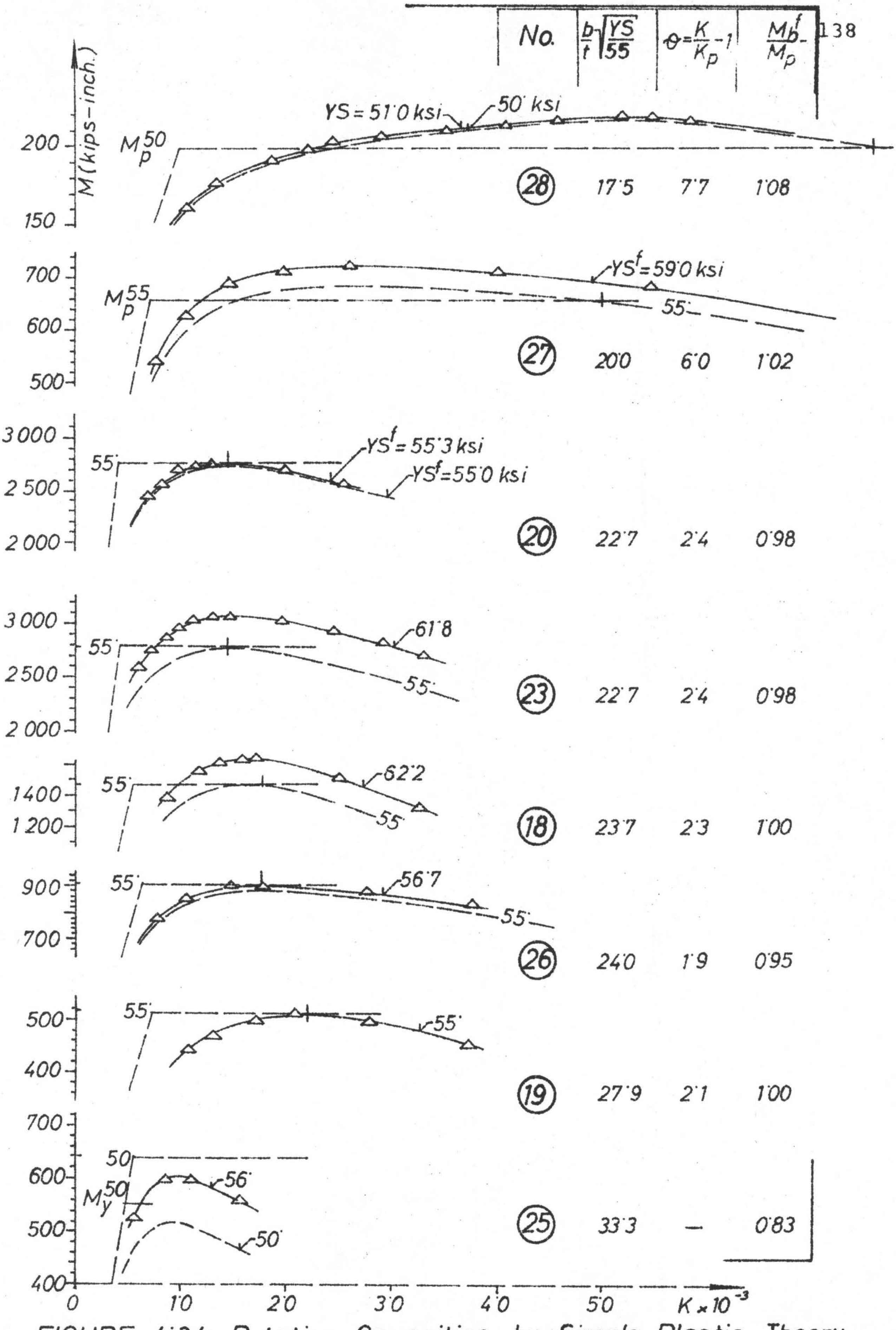

FIGURE 4·34 Rotation Capacities by Simple Plastic Theory

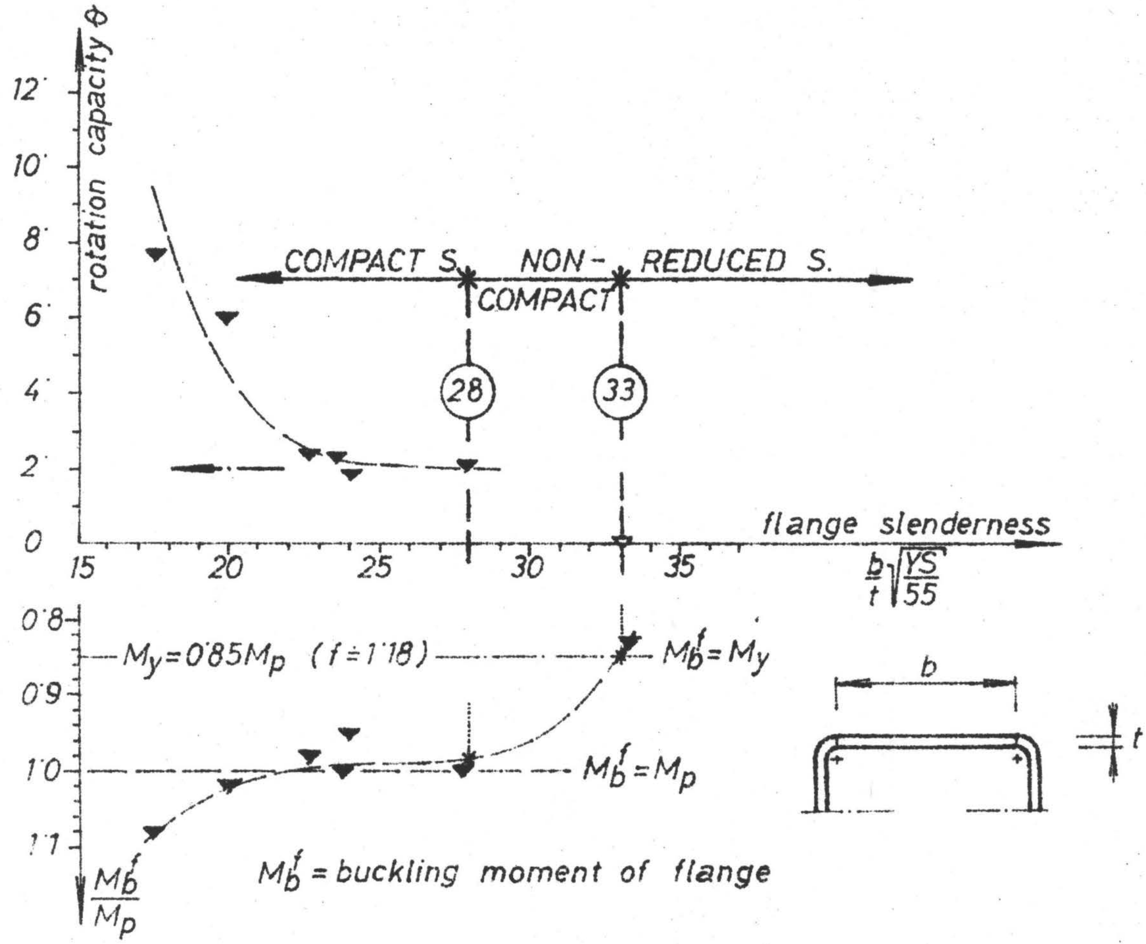

Non - Compact Sections :

$$\frac{b}{t}\sqrt{\frac{YS}{55}} \leqq 33 \qquad\qquad \frac{b}{t} \leqq \frac{245}{\sqrt{YS}}$$

Compact Sections in working stress design :

$$\frac{b}{t}\sqrt{\frac{YS}{55}} \leqq 28 \qquad\qquad \frac{b}{t} \leqq \frac{210}{\sqrt{YS}}$$

FIGURE 4·35 Limiting b/t Value for Working Stress Design

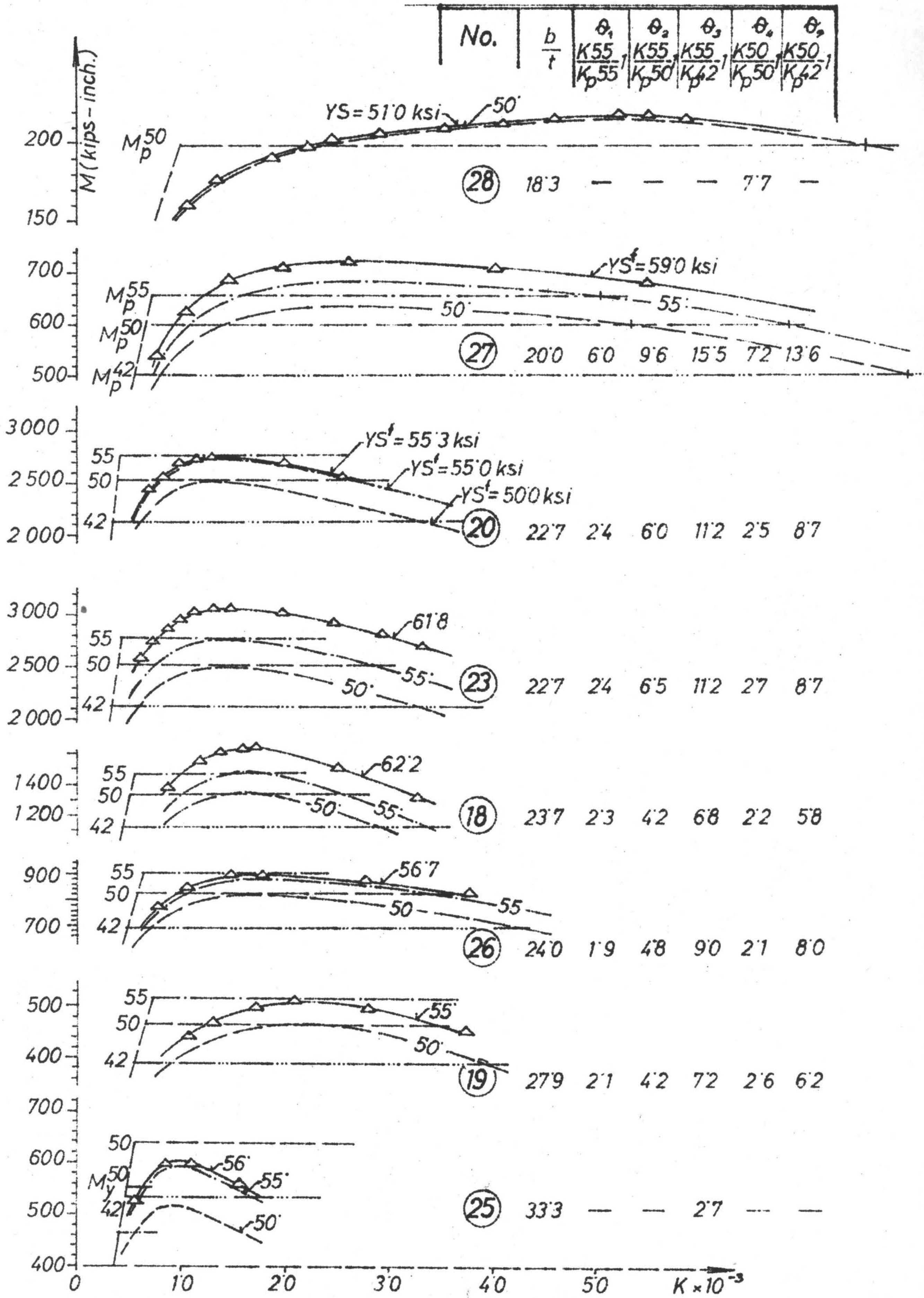

FIGURE 4·36 Rotation Capacities

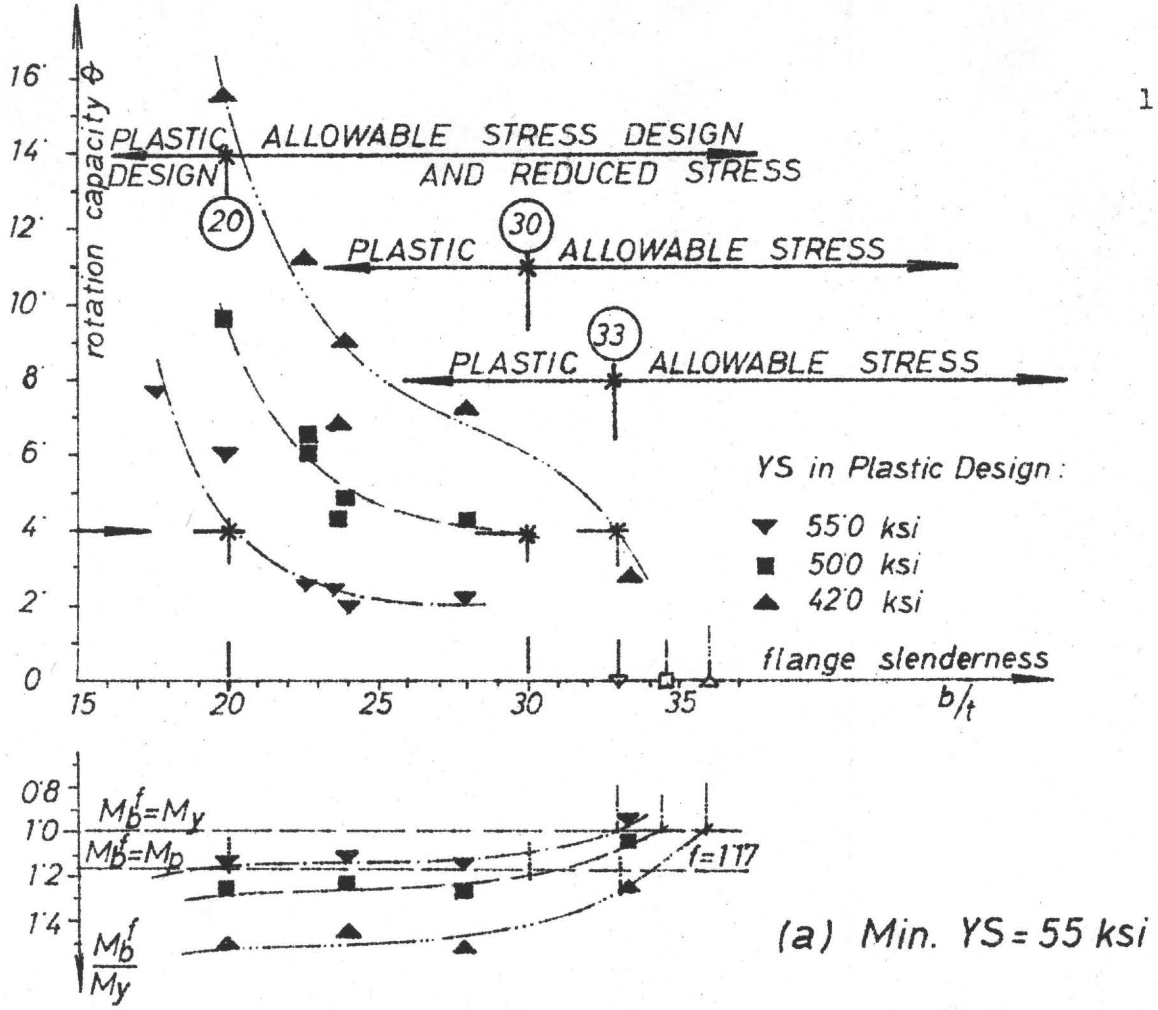

FIGURE 4·37 Limiting b/t Value for Plastic Design

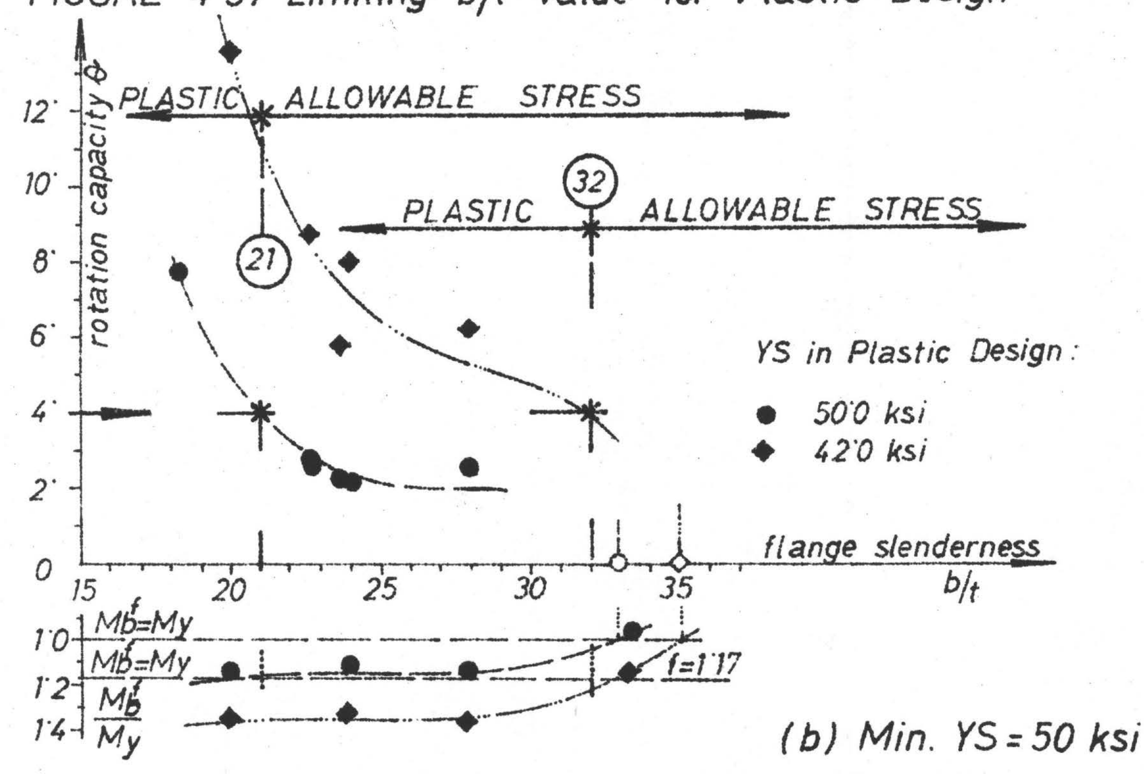

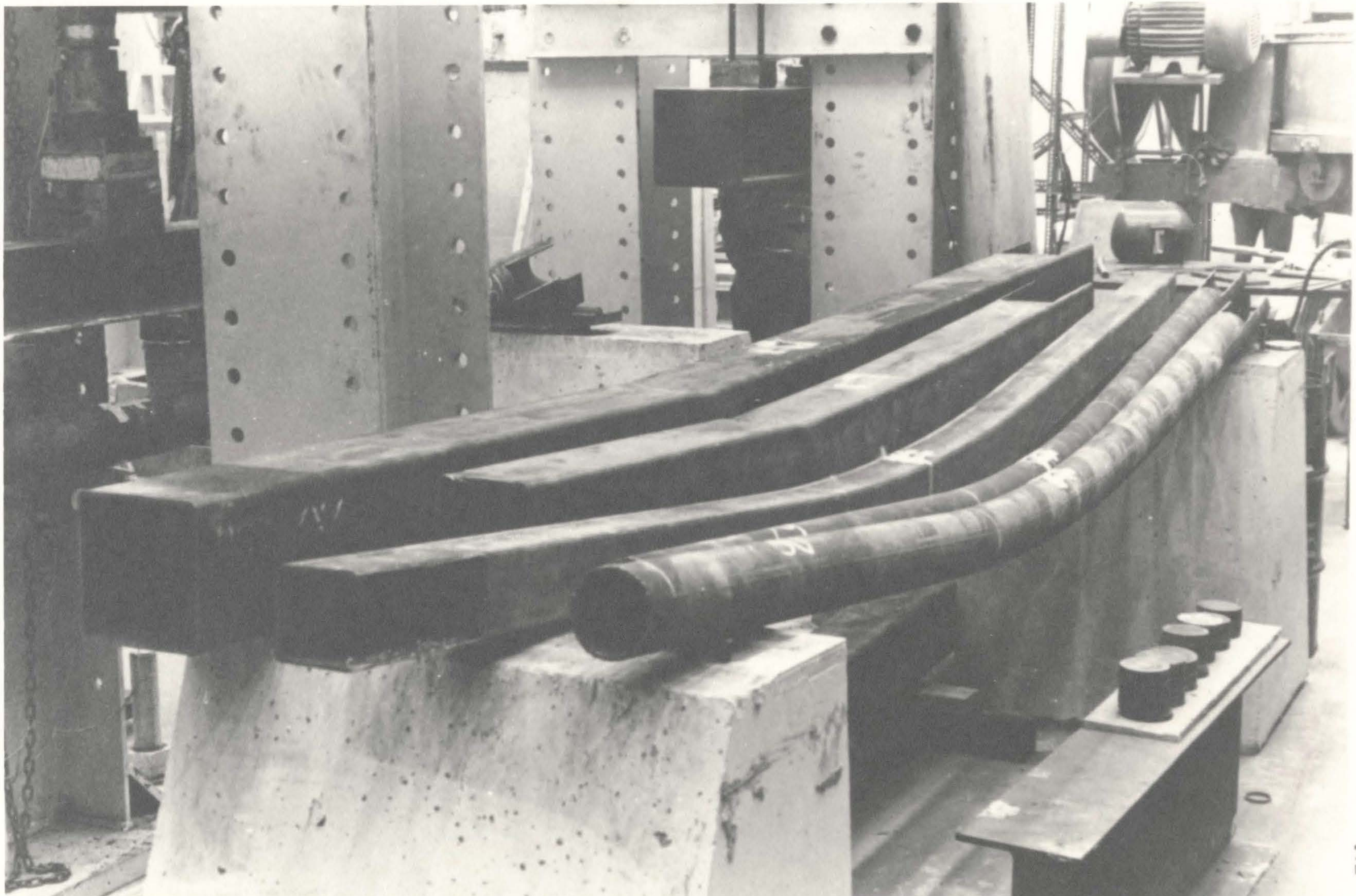

FIGURE 4.38 Local Buckling After Testing

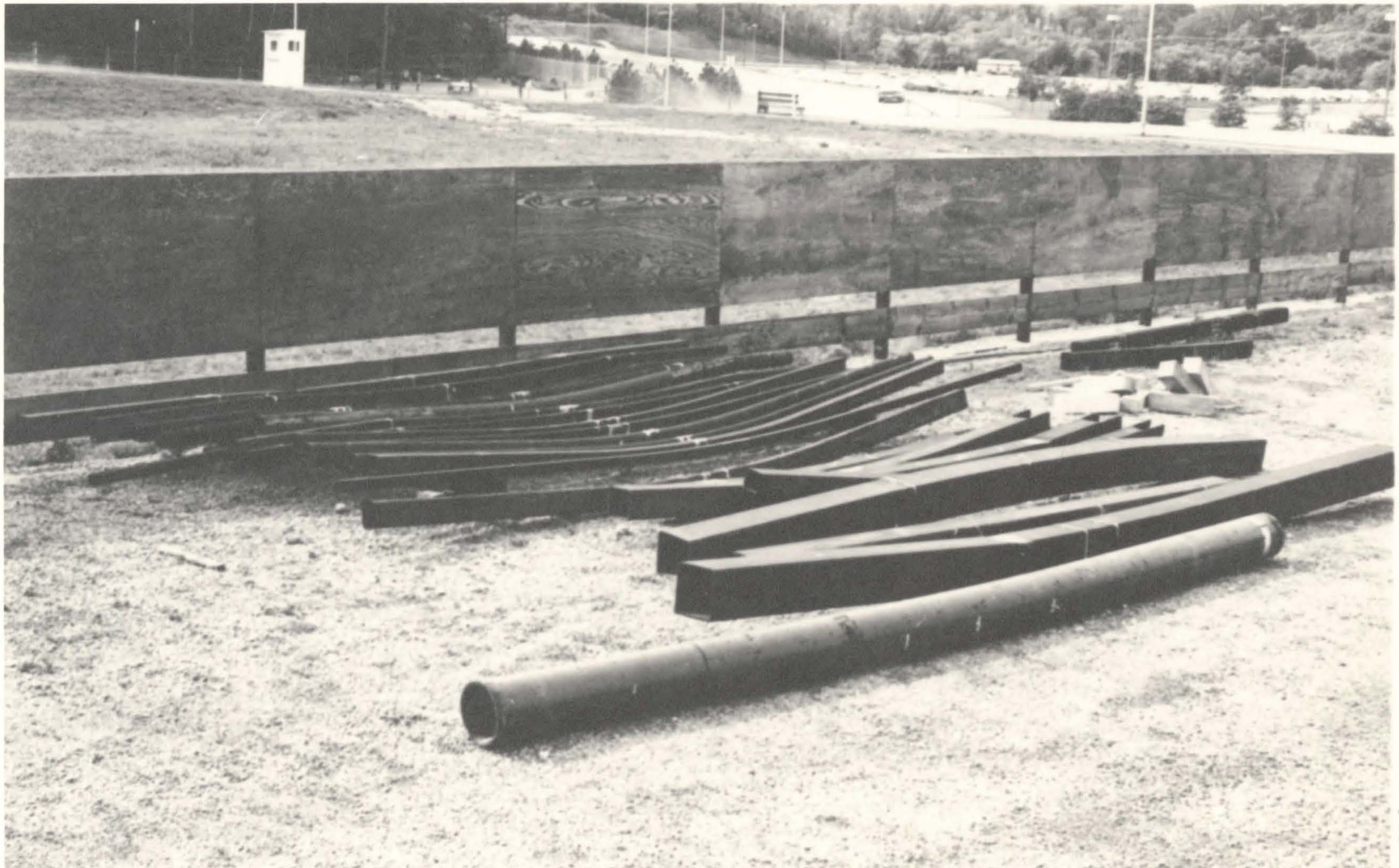

FIGURE 4.39 Series Sections After Testing

CHAPTER V

SUMMARY

This investigation was undertaken to attempt to relate the flange slenderness ratio (b/t) to the plastic rotation capacity of Hollow Structural Sections subjected to a moment gradient and constant moment. The rotation capacity is limited mainly by post-elastic buckling of the compression flange. In plastically designed structures it is assumed that any section at which a plastic hinge forms will sustain the full plastic moment until a collapse mechanism has formed.

The experimental program reported herein consisted of 31 tests on Hollow Structural Sections, having a range of b/t values from 5 to 34. This program was designed to simulate 2-point loading on a simple span beam or three span beam.

A wide range of rotation capacities was observed for the beams tested. As expected, the sections having slender flanges delivered smaller rotation capacities than did the stockier sections. Unloading was accompanied by local buckling of the compression flange.

The maximum rotation capacities required in practical structures have also been performed in Subsection 2.12(D). For plastically designed continuous beams it is recommended that the minimum plastic rotation capacity be 4 before the moment capacity drops below M_p. The limiting b/t value applicable to square and rectangular HSS for this recommended rotation cannot exceed the value of $150/\sqrt{YS}$. This is a more conservative requirement than is currently set forth in CSA Standard S16 where this ratio is $200/\sqrt{YS}$. In more complex structures with larger rotations, a load close to the ultimate can be attained with this plastic rotation capacity of 4 and therefore it can be considered satisfactory for design purposes.

In structures designed by the allowable stress method the "compact sections" have to reach the specified plastic moments while "non-compact sections" only need attain the yield moments without the requirement of minimum plastic rotation for a formation of mechanism.

The Canadian Standards Association[1] has defined a compact section as one in which the projecting elements of the compression flange shall have a width-to-thickness ratio less than $200/\sqrt{YS}$ and non-compact section less than $250/\sqrt{YS}$. This recommendation stated that for a section to qualify as a compact section in working stress design only this ratio would be changed from $200/\sqrt{YS}$ to $210/\sqrt{YS}$. On the basis of the current programme this recommendation appears to be adequate in fulfilling the necessary safety requirement for working stress design.

A further series of tests in the critical range of flange slenderness is proposed which would give a more exact limiting b/t value. It is expected that the results of that test series, in conjunction with the presently available test results, would provide a sufficient basis upon which to make specific design recommendations. Cognizance should be made, however, of the need to specify bearing stresses in relation to b/t and should be considered in an extension to this programme.

APPENDIX 1

COMPUTER PROGRAM FOR THE DETERMINATION OF MOMENT-CURVATURE AND LOAD-DEFLECTION RELATIONSHIPS

1.1 Introduction to the Program

The program is split into two main components:

(i) a main program for rectangular and round sections

(ii) a subroutine, SHAPE, for rectangular sections and a subroutine, ROUND, for round sections.

The load-deflection curve for a simple beam is computed from the expressions for deflection derived in Chapter 2.

The description of computer analysis is given in Subsection 4.11.

Names of Variables: The meaning of the variable names in the fortran program is explained in the program as well as in Subsection 4.11.

APPENDIX 1.2 General Flow Chart for Analysis of H.S.S.

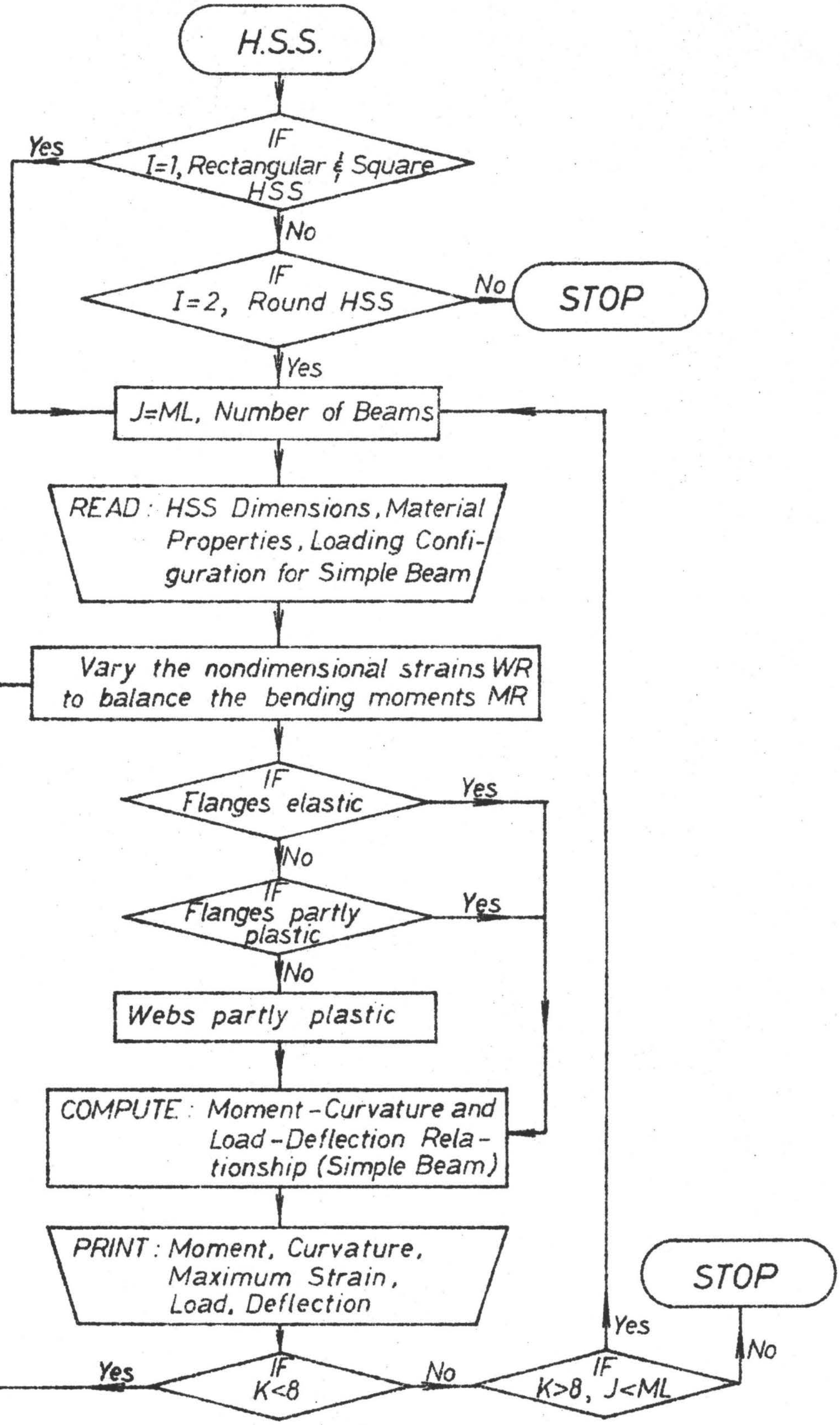

APPENDIX 1'3 Computer Program

```
      - -                                                          7L3E10.07
RUN(S)
SETINDF.
REDUCE.
LGO.
'         6400 END RECORD
      PROGRAM TST (INPUT,OUTPUT,TAPE5=INPUT,TAPE6=OUTPUT)
C     THE MOMENT - CURVATURE RELATIONSHIP FOR COMPACT HOLLOW SECTIONS.

C     NONDIMENSIONAL MOMENT - CURVATURE RELATIONSHIP RELATING
C     THE REDUCED MOMENT M/MY TO THIS REDUCED CURVATURE W/WY.

C     SUBROUTINE SHAPE FOR THE ELASTIC MODULUS S, PLASTIC MODULUS Z
C     AND THE SHAPE FACTOR F.

C     OUTSIDE DIMENSIONS - WIDTH B /IN INCHES/
C                        - DEPTH OF BEAM D /IN INCHES/
C     T IS THE WALL THICKNESS IN INCHES
C     R IS THE OUTSIDE RADIUS OF CORNERS IN INCHES

C     MR IS THE RATIO OF M/MY
C     WR IS THE RATIO OF W/WY

C     YIELD STRENGTH YS IN KSI
C     MODULUS OF ELASTICITY E IN KSI
C     STRAIN HARDENING MODULUS ET IN KSI

C     M IS MOMENT
C     W IS CORRESPONDING CURVATURE TO M
C     ST IS CORRESPONDING MAXIMUM STRAIN TO M

C     SE IS THE DISTANCE BETWEEN LOAD AND THE END OF BEAM
C     SM IS THE DISTANCE BETWEEN LOAD AND THE MIDDLE OF BEAM

      REAL MR,MY,M,MM,MS,MT
      READ(5,2)NECT
      DO 100 I =1,NECT
      READ(5,3)ML
      DO 100 J = 1,ML
      IF(I.EQ.2) GO TO 200
      READ(5,4)D,B,T,R,YS,E,ET,SE,SM
      GO TO 201
  200 READ(5,8)D,T,YS,E,ET,SE,SM
  201 CONTINUE
      WR = 0.2
      ER = E/ET
      IF(I.EQ.2) GO TO 150
      CALL SHAPE(D,B,T,R,S,Z,F)
      WRITE(6,50)D,B,T
      WRITE(6,60)S,Z,F
      WRITE(6,70)YS,E
      WRITE(6,72)R,ET
      WRITE(6,74)SE,SM
      WRITE(6,80)

C     A STRAIGHT ELASTIC PART
   10 IF(WR.GT.1.0) GO TO 20
      MR = WR
      GO TO 15

C     THE FLANGES ARE PLASTIC AND WEBS ARE ELASTIC
   20 U = D/(D-2.*T)
      IF(WR.GT.U) GO TO 30
```

```
      MR =WR*(1.-(B*D**2/(6.*S)))+(B*D**2/(4.*S))*(1.-1./(3.*WR**2))
      GO TO 15
C     THE FLANGES ARE PLASTIC AND THE WEBS ARE PARTLY ELASTIC
   30 IF(WR.GT.8.) GO TO 100
      MR = (F-T*D**2/(6.*S*WR**2))*(FR-1.)/FR+WR/FR
      GO TO 15
C     THE MAXIMUM ELASTIC STRAIN STY
   15 STY = YS/E
C     THE CORRESPONDING CURVATURE WY AND MOMENT MY
      WY = 2.*STY/D
      MY = YS*S
C     THE MOMENT M IN KIP-IN
      M = MR*MY
C     THE CURVATURE IN RAD
      W = WR*WY
C     THE STRAIN IN THE EXTREME FIBERS ST
      ST = W*D/2.
C     THE LOAD - DEFLECTION CURVE OF SIMPLE BEAM

      PE = 2.*MY/SE
      DF = (SF**2/3.+SF*SM+SM**2/2.)*WY
      PL = MR*PE
      DL = WR*DF

      WRITE(6,90)M,W,ST,PL,DL

      IF(WR.GT.2.) GO TO 38
      WR = WR+0.2
      GO TO 10
   38 WR = WR+1.0
      GO TO 10

  150 CALL ROUND(D,T,P,S,Z,F)
      WRITE(6,55)D,T
      WRITE(6,60)S,Z,F
      WRITE(6,70)YS,E
      WRITE(6,73)FT
      WRITE(6,74)SF,SM
      WRITE(6,80)

      R = D/2.
      A = 6.28*P*T
      V = A*D/(4.*S*(F-1.))
   35 X =  R/WR
C     A STRAIGHT ELASTIC PART
      IF(WR.GT.1.05) GO TO 32
      MR = WR
      GO TO 42
C     THE ELASTIC - PLASTIC PART
   32 UR = D/(D-2.*T)
      IF(WR.GT.UR) GO TO 25
      TV = 2.*SQRT(R**2-X**2)
      AO = 2.*TV*(R-X)/3.
      MR = F-(A/2.-AO)*X/(S*V)
      GO TO 42

   25 IF(WR.GT.8.) GO TO 100
      Y = X/SQRT(R**2-X**2)
      MR = (F-2.*R*T*X*ATAN(Y)/(S*V))*(FR-1.)/FR+WR/FR
      GO TO 42

   42 STY = YS/E
      WY = 2.*STY/D
      MY = YS*S
      M = MR*MY
      W = WR*WY
```

```
      ST = W*D/2.
C     THE LOAD - DEFLECTION CURVE OF SIMPLE BEAM
      PF = 2.*MY/SF
      DF = (SF**2/3.+SF*SM+SM**2/2.)*WY
      PL = MP*PF
      DL = WP*DF
      WRITE(6,90)M,W,ST,PL,DL
      IF(WP.GT.2.) GO TO 48
      WP = WP+0.2
      GO TO 35
   48 WP = WP+1.0
      GO TO 35
  100 CONTINUE
      STOP
    2 FORMAT(I5)
    3 FORMAT(I5)
    4 FORMAT(4F8.3,5F8.1)
    8 FORMAT(7F10.2)
   50 FORMAT(3X,15H HOLLOW SECTION,F9.3,3X,1HX,F9.3,3X,1HX,F9.3//)
   55 FORMAT(3X,14H ROUND SECTION,F9.3,1X,2HOD,2X,1HX,F6.3//)
   60 FORMAT(3X,11H ELASTIC S=,F5.2,5X,11H PLASTIC Z=,F5.2,5X,
     116H SHAPE FACTOR F=,F5.3//)
   70 FORMAT(3X,19H YIELD STRENGTH YS=,F5.2,1X,3HKSI,5X,
     125H MODULUS OF ELASTICITY E=,F7.1,1X,3HKSI/)
   72 FORMAT(3X,18H OUTSIDE RADIUS R=,F6.3,1X,2HIN,6X,20H TANGENT MODULU
     1S ET=,F7.1,1X,3HKSI//)
   73 FORMAT(36X,20H TANGENT MODULUS ET=,F7.1,1X,3HKSI//)
   74 FORMAT(3X,17H LOADING IN POINT,5X,4H SF=,F5.1,1X,5HINCH.,5X,
     14H SM=,F5.1,1X,5HINCH.//)
   80 FORMAT(4X,16H MOMENT (KIP-IN),4X,16H CURVATURE (RAD),8X,12H STRAIN
     1 (IN),8X,12H LOAD (KIPS),4X,16H DEFLECTION (IN)/)
   90 FORMAT(F20.2,2F20.6,2F20.2/)
      END
      SUBROUTINE SHAPE(D,B,T,R,S,Z,F)
C     DIMENSIONS OF HOLLOW SECTION T,A,D,R
C     ELASTIC MODULUS S
C     PLASTIC MODULUS Z
C     SHAPE FACTOR F
      S=T*((D-2.*R)**3/3.+(B*T**2)/3.+6.28*(2.*R-T)*(0.5*D-T)**2+
     1(B-2.*R)*(D-T)**2)/D
      Z=2.*T*((B-2.*R)*(D-T)*0.5+3.14*(R-0.5*T)*(0.5*D-T)+(0.5*D-R)**2)
      F = Z/S
      RETURN
      END
      SUBROUTINE ROUND(D,T,R,S,Z,F)
C     DIMENSIONS OF HOLLOW SECTION D,T
C     ELASTIC MODULUS S
C     PLASTIC MODULUS Z
C     SHAPE FACTOR F
      R = D/2.
      RV = D/2.-T
      P = (D-T)*0.5
      S = 3.14*(R**4-RV**4)/(4.*R)
      Z = 0.4244*3.14*(R**3-RV**3)
      F = Z/S
      RETURN
      END
         6400 END RECORD
    2
   10
  6.000    6.000    0.437    0.875    58.0 29600.0    320.0    30.0    38.0
  6.000    6.000    0.437    0.875    52.0 29600.0    320.0    30.0    38.0
  6.000    4.000    0.437    0.875    64.5 29600.0    307.0    30.0    38.0
  4.000    2.000    0.235    0.352    58.0 29600.0    528.0    30.0    38.0
  5.000    3.000    0.230    0.345    50.0 29600.0    683.0    30.0    38.0
  2.500    2.500    0.210    0.315    60.5 29600.0    333.0    30.0    38.0
 10.000   10.000    0.375    0.750    57.0 29600.0    250.0    60.0    48.0
 10.000   10.000    0.375    0.750    62.5 29600.0    250.0    72.0    36.0
```

10.000	6.000	0.500	1.000	58.0	29600.0	273.0	60.0	48.0
6.000	4.000	0.437	0.875	68.5	29600.0	307.0	30.0	38.0
4.000	4.000	0.250	0.375	53.5	29600.0	627.0	20.0	39.0
4.000	4.000	0.188	0.292	51.0	29600.0	660.0	50.0	18.0
6.000	6.000	0.250	0.500	60.5	29600.0	167.0	35.0	15.0
7.000	7.000	0.250	0.500	59.0	29600.0	194.0	51.0	18.0
7.000	7.000	0.188	0.376	57.0	29600.0	250.0	51.0	18.0
6.000	6.000	0.188	0.376	56.0	29600.0	357.0	36.0	32.0
8.000	8.000	0.312	0.624	63.7	29600.0	250.0	34.0	34.0
5.000	5.000	0.250	0.500	59.0	29600.0	250.0	34.0	38.0
7.000	7.000	0.312	0.624	60.5	29600.0	305.0	40.0	38.0

6

4.500	0.250	56.0	29600.0	674.0	30.0	38.0
10.750	0.500	41.5	29600.0	366.0	72.0	36.0
3.500	0.150	55.0	29600.0	656.0	30.0	38.0
3.500	0.150	50.0	29600.0	650.0	45.0	18.0
4.000	0.188	51.0	29600.0	735.0	45.0	18.0
4.500	0.188	50.5	29600.0	650.0	45.0	18.0

CD TOT 0230

APPENDIX 2

NOMENCLATURE

A_f	Area of flat part of the flange
A_c	Area of corner
b	Flat flange width
E	Modulus of elasticity
E_{st}	Strain-hardening modulus
F_y, YS	Yield stress
G_t	Tangent shear modulus
H	Hinge angle
$I = \frac{t^3}{12}$	Moment of inertia
K	Curvature
K_p	Curvature corresponding to M_p assuming ideally elastic material
ℓ, L	Length
ΔL	Hinge length
M	Moment
M_p	Plastic moment
M_b	Buckling moment
P	Load
P_y	Load at yield
P_u	Collapse load
t	Flange thickness
ε	Strain
M_y	Yield moment except as noted in Section 2.2

ε_y	Yield strain
θ	Inelastic hinge rotation (hinge capacity)
δ	Deflection
ν	Poisson's ratio
ϕ	End rotation
ϕ^F	Simple beam end rotation
σ	General stress quantity
σ_x, σ_y	Normal stresses in x and y directions
w	transverse deflection
υ_{xy}	Shear stress
τ	Ratio of strain-hardening to elastic modulus
σ_c	Buckling stress
$D = \dfrac{EI}{1-\nu^2}$	
ψ	Angle of rotation of the buckling plate
$\overline{\psi}$	Angle of rotation of the restraining web plate
M_y	Moment per unit length
$\overline{\xi}$	Coefficient of restraint of the restraining plate
ξ	Coefficient of restraint of the buckling plate
β	Ratio of length to width of the plate
$\overline{\beta}$	Limiting value of β for buckling
β_0	β for which σ_c reaches a minimum
p,q	Factors depending on ξ
k	Plate coefficient
$D' = \dfrac{Et_c^3}{12(1-\nu^2)}$	
t_c	Thickness of restraining web

λ	Length of the half wave of the buckling plate
ρ_1	Ratio of M_y to the rotation $\bar{\psi}$
r	Correcting coefficient of the effective width c
ν_x, ν_y	Coefficients of dilatation
γ	Shear strain
σ_e	Elastic buckling stress
σ_R	Residual compressive stress
σ_p	Effective proportional stress

$$\alpha = \frac{b}{\pi t}\sqrt{\frac{12F_y(1-\nu^2)}{kE}} \qquad \text{for } \alpha > \alpha_p$$

α_p	α at the proportional elastic limit
α_y	α at the point of strain-hardening

APPENDIX 3

LIST OF REFERENCES

(1) CSA - "Steel Structures for Buildings", Canadian Standards Association Standard S-16, 1965

(2) Bleich, F. - "Buckling Strength of Metal Structures", McGraw-Hill Book Company, Inc., New York, 1952

(3) Lay, M. G. and Galambos, T. V. - "Inelastic Steel Beams Under Uniform Moment", Proc. ASCE, Vol. 91, ST6, December 1965

(4) Haaijer, G. and Thurliman, B. - "Inelastic Buckling in Steel", Trans. ASCE, Vol. 125, Paper No. 3023, Part 1, 1960

(5) Haaijer, G. - "Plate Buckling in the Strain-Hardening Range", Trans. ASCE, Vol. 124, Paper No. 2968, 1959

(6) Lukey, A. F. and Adams, P. F. - "Rotation Capacity of Wide-Range Beams Under Moment Gradient", Department of Civil Engineering, Edmonton, Alberta, May 1967

(7) Smith, R. T. and Adams, P. F. - "Experiments on Wide-Flange Beams Under Moment Gradient", Department of Civil Engineering, Edmonton, Alberta, May 1968

(8) Beedle, L. S. - "Plastic Design of Steel Frames", New York, 1952, John Wiley & Sons, Inc.

(9) Driscoll, G. C. - "Rotation Capacity Requirements for Beams and Portal Frames", Ph.D. Dissertation, Lehigh University, 1958

(10) Roark, R. T. - "Formulas for Stress and Strain", 3rd edition, McGraw-Hill Book Co., New York, 1954

(11) Neal, B. G. - "The Plastic Methods of Structural Analysis", Chapman & Hall Ltd., London, 1965

(12) Kerfoot, R. P. - "Rotation Capacity of Beams", Lehigh University, Fritz Laboratory, Report No. 297 14, March 1965

(13) ASTM - "Mechanical Testing of Steel Products", American Society for Testing Materials, Standard A 370-65

(14) Beedle, L. S. - "Structural Steel Design", The Ronald Press Company, New York, 1964

(15) ASCE and WRC - "Commentary on Plastic Design in Steel", ASCE Manual of Engineering Practice No. 41, 1961

(16) Tombock, T. R. and Clark, T. W. - "Postbuckling Behaviour of Flat Plates", Journal of the Structural Division, Vol. 87, June 1961, pp. 17

(17) Thurlimann, B. - "New Aspects Concerning Inelastic Instability of Steel Structures", Journal of the Structural Division, Vol. 86, January 1960, pp. 99

(18) Johnson, A. L. and Winter, G. - "Behaviour of Stainless Steel Columns and Beams", Journal of the Structural Division, Vol. 92, No. ST5, October 1966, pp. 97-118

(19) McDermott, T. F. - "Plastic Bending of A514 Steel Beams", Journal of the Structural Division, Vol. 95, September 1969, pp. 1851